

J. A. "Buzz" Miller  
Senior Vice President  
Nuclear Development

Southern Nuclear  
Operating Company, Inc.  
40 Inverness Center Parkway  
Post Office Box 1295  
Birmingham, Alabama 35201

Tel 205.992.5754  
Fax 205.992.6165



APR 16 2007

Docket No.: 52-011

AR-07-0801

U.S. Nuclear Regulatory Commission  
Document Control Desk  
Washington, DC 20555-0001

Southern Nuclear Operating Company  
Vogtle Early Site Permit Application  
Response to Requests for Additional Information Letter No. 6 Involving Geology/Seismology

Ladies and Gentlemen:

By letter dated March 15, 2007, the U.S. Nuclear Regulatory Commission (NRC) provided Southern Nuclear Operating Company (SNC) with Request for Additional Information (RAI) Letter No. 6 on the Vogtle Early Site Permit (ESP) Application. The RAIs in that letter pertain to ESP application Part 2, Site Safety Analysis Report (SSAR), Section 2.4, *Hydrologic Engineering*, and Section 2.5, *Geology, Seismology and Geotechnical Engineering*. SNC's response to the RAIs pertaining to SSAR Section 2.5 is provided in the following Enclosures to this letter. SNC's response to the RAIs pertaining to SSAR Section 2.4 is provided letter AR-07-0639.

The SNC contact for this RAI response letter is J. T. Davis at (205) 992-7692.

D078

Mr. J. A. (Buzz) Miller states he is a Senior Vice President of Southern Nuclear Operating Company, is authorized to execute this oath on behalf of Southern Nuclear Operating Company and to the best of his knowledge and belief, the facts set forth in this letter are true.

Respectfully submitted,

SOUTHERN NUCLEAR OPERATING COMPANY



Joseph A. (Buzz) Miller

Sworn to and subscribed before me this 16 day of April, 2007

  
Glen H. Bui  
Notary Public

My commission expires: 05/06/08

JAM/BJS/dmw

Enclosures:

1. Response to March 15, 2007 RAI Letter No. 6 for the Vogtle ESP Application Involving Geology, Seismology and Geotechnical Engineering
2. CD of Electronic files

cc: Southern Nuclear Operating Company

Mr. J. B. Beasley, Jr., President and CEO (w/o enclosures)  
Mr. J. T. Gasser, Executive Vice President, Nuclear Operations (w/o enclosures)  
Mr. T. E. Tynan, Vice President - Vogtle (w/o enclosures)  
Mr. D. M. Lloyd, Vogtle Deployment Director (w/o enclosures)  
Mr. C. R. Pierce, Vogtle Development Licensing Manager (w/o enclosures)  
Mr. Donald P. Moore, Engineering Programs Consulting Engineer (w/o enclosures)  
Document Services RTYPE: AR01  
File AR.01.01.06

Nuclear Regulatory Commission

Mr. R. W. Borchardt, Director of Office of Nuclear Regulation (w/o enclosures)  
Mr. W. D. Travers, Region II Administrator (w/o enclosures)  
Mr. D. B. Matthews, Director of New Reactors (w/o enclosures)  
Ms. S. M. Coffin, AP1000 Manager of New Reactors (w/o enclosures)  
Mr. C. J. Araguas, Project Manager of New Reactors (plus five CDs)  
Mr. M. D. Notich, Environmental Project Manager  
Mr. G. J. McCoy, Senior Resident Inspector of VEGP (w/o enclosures)

Georgia Power Company

Mr. O. C. Harper, Vice President, Resource Planning and Nuclear Development (w/o enclosure)

Oglethorpe Power Corporation

Mr. M. W. Price, Chief Operating Officer (w/o enclosure)

Municipal Electric Authority of Georgia

Mr. C. B. Manning, Senior Vice President and Chief Operating Officer (w/o enclosure)

Dalton Utilities

Mr. D. Cope, President and Chief Executive Officer (w/o enclosure)

Bechtel Power Corporation

Mr. J. S. Prebula, Project Engineer (w/o enclosures)  
Mr. R. W. Prunty, Licensing Engineer (w/o enclosures)

**Southern Nuclear Operating Company**

**AR-07-0801**

**Enclosure 1**

**Response to March 15, 2007 RAI Letter No. 6**

**for the Vogtle ESP Application**

**Involving Geology, Seismology and Geotechnical Engineering**

## Section 2.5 Geology, Seismology, and Geotechnical Engineering

**2.5.1-1 Section 2.5.1.1.3.5 of the SSAR, under “Quaternary Surfaces and Deposits”, identifies a series of four abandoned fluvial terrace levels (i.e., Qty, Qtb, Qte, and Qto from youngest to oldest) that occur in the site area above Quaternary alluvium of the present-day flood plain of the Savannah River (SSAR Figure 2.5.1-29), and acknowledges that such features ideally can be used to evaluate Quaternary deformation.**

**a. Please indicate whether these terraces are regional in extent, or whether they only occur locally and mainly in the vicinity of the Pen Branch Fault.**

**b. Please provide information on the proposed origin of these fluvial terraces.**

Response:

Geomatrix (1993) mapped four abandoned fluvial terraces of the Savannah River, all of which extend well beyond the vicinity of the Pen Branch fault and are regional in extent. The Qty, Qtb, Qte, and Qto terraces are mapped for at least 20 mi upstream and 18 mi downstream (straight line distances) from the Vogtle ESP site (Geomatrix 1993).

The development of laterally extensive fluvial terraces is the result of the complex interaction of a number of variables. Regional fluvial terraces generally form as the result of a sequence of depositional and erosional events that are in turn the result of climatic, isostatic, and/or tectonic perturbations.

The development of a sequence of laterally extensive fluvial terraces along the Savannah River is characteristic of other major Piedmont-draining river systems. Similar sequences of laterally extensive fluvial terraces are found along other rivers, such as the Pee Dee River in South Carolina and the Cape Fear River in North Carolina (Geomatrix 1993). Moreover, at similar distances upstream from the modern coastline, the relative heights above local base level of terrace surfaces on the Savannah River are similar to those for both the Pee Dee and Cape Fear Rivers (Geomatrix 1993). The fact that the major fluvial terrace surfaces are correlative between major Piedmont-draining river systems suggests that these terraces form in parallel response to regional climatic and/or eustatic conditions, and are not the result of local tectonic perturbations.

The next revision to the ESP application will address as appropriate the information provided in this response.

**2.5.1-2 Section 2.5.1.1.3.5 of the SSAR, under “Quaternary Surfaces and Deposits”, states that terrace Qtb ranges from 8-13 m (26-43 ft) above the Savannah River surface at the Savannah River Site, and also indicates that terrace Qte shows a range in surface elevation from 17-25m (56-82 ft) above the Savannah River surface. Section 2.5.1.2.4.3 of the SSAR indicates a detectable resolution limit for observable deformation of terrace Qte of about 1m (3 ft) (pg 2.5.1-79), suggesting that less than 1m (3 ft) of warping or tilting of this terrace surface would not be detected.**

**a. Please provide information to address whether the elevation ranges noted above suggest tilting of terrace surfaces.**

**b. Please discuss implications of a deformation detection limit of about 1m (3 ft) for these fluvial terraces.**

Response:

Terrace surface elevations for the 100 to 250 ka Bush Field terrace (Qtb) range from 26 to 43 ft above the modern Savannah River in the VEGP site vicinity (Geomatrix 1993). The variability in Qtb terrace surface elevations is due to three main factors:

1. Terrace surface elevations typically decrease in a downstream direction, and the range of Qtb surface elevations reflects data collected from the entire 55-mi stretch of river mapped by Geomatrix (1993);
2. The Qtb deposits vary in thickness from approximately 29 to 49 ft, and have experienced varying degrees of erosion and dissection throughout the area mapped by Geomatrix (1993); and
3. Some of the deposits mapped as Qtb include slightly younger fill-cut terraces surfaces (unpub. data from Paul Nystrom, South Carolina Geological Survey, as described by Geomatrix 1993).

The second and third factors above indicate that the ranges in surface elevations reported by Geomatrix (1993) reflect greater variability than what would be measured across a single, well-preserved geomorphic surface.

Terrace surface elevations for the 350 ka to 1 Ma Ellenton terrace (Qte) range from 56 to 82 ft above the modern Savannah River in the VEGP site vicinity (Geomatrix 1993). Similar to the Qtb surface, this variability is primarily due to the large area of study and the eroded and dissected nature of the Qte deposits, which makes it difficult to discern the best-preserved remnants of the original terrace surface.

Using USGS 7.5-minute topographic maps with 10 ft contour intervals, Geomatrix (1993) constructed longitudinal profiles of terrace surfaces. By assuming that those terrace fragments with the highest elevations represent the best-preserved remnants of each terrace surface, they concluded that there is no observable tilting or deformation of the Qte terrace surface within a resolution of 7 to 10 ft within their study area.

Work performed for the Vogtle ESP application uses the 350 ka to 1 Ma Ellenton (Qte) terrace surface as a Quaternary strain marker to assess the presence or absence of evidence for tectonic deformation across the underlying Pen Branch fault. This work represents an improvement over previous studies for two main reasons:

1. Refinement in the location of the Pen Branch fault allowed for a more focused and investigation; and
2. Increased resolution of the variability in elevation of the best-preserved remnants of the Qte terrace surface overlying the Pen Branch fault. This increased resolution is the result of >2,600 survey data points.

A longitudinal profile of the Qte terrace surface in the study area provides evidence demonstrating the absence of tectonic deformation within a resolution of about 3 ft. This provides a much smaller deformation detection limit than previous studies, thereby providing greater confidence in the evidence demonstrating the lack of Quaternary deformation on the Pen Branch fault.

The next revision to the ESP application will address as appropriate the information provided in this response.

**2.5.1-3** Section 2.5.1.1.3.5 of the SSAR describes terrace Qty, positioned between the modern-day flood plain of the Savannah River and the next oldest overlying terrace (Qtb) as “minor and not laterally continuous.” Terrace Qty occurs along a stretch of the Savannah River that is relatively straight (SSAR Figure 2.5.1-29) where the river is incised, and appears to be mainly located southeast of the postulated surface trace of the Pen Branch Fault. Section 2.5.1.1.3.5 reports that terrace Qtb, immediately overlying Qty, is about 90,000 years old (Pleistocene) based on correlation, relative position, and morphology. Brooks and Sassaman (1990) suggested an age of 4,000 years for the modern-day flood plain. This information suggests that Qty, the lowest and youngest terrace, could be between 4,000 - 90,000 years old and therefore possibly Holocene in age.

**Considering origin, location, and approximate age of terrace Qty, please discuss the implications for possible Quaternary displacement on the Pen Branch Fault.**

Response:

The discontinuous Qty terrace surface of late Pleistocene to possible Holocene (?) age does not provide constraints for evaluating the potential for Quaternary displacement on the Pen Branch fault. The significantly older and more laterally continuous remnants of the 350 ka to 1 Ma (Geomatrix 1993) Ellenton terrace (Qte) provide a more robust datum to evaluate potential tectonic deformation of the Pen Branch fault. The most definitive evidence precluding Quaternary activity of the Pen Branch fault is based on a study of the Qte terrace at the Savannah River Site performed as part of the Vogtle ESP application. A longitudinal profile of the best-preserved remnants of the Qte surface provides evidence demonstrating the absence of tectonic deformation within a resolution of about 3 ft. The Qty terrace is significantly younger than the Qte terrace, and is therefore less useful as a Quaternary strain marker for evaluating the presence or absence of deformation.

The site area geologic map (SSAR Figure 2.5.1-29) shows Savannah River Quaternary terrace deposits as mapped by Geomatrix (1993). The Qty terrace is preserved as a series of relatively narrow, discontinuous remnants. The apparent spatial correlation between remnants of the Qty terrace and the Pen Branch fault is a function of the limited areal extent of SSAR Figure 2.5.1-29. Additional remnants of the Qty terrace are mapped by Geomatrix (1993) both upstream and downstream of the area shown in SSAR Figure 2.5.1-29, and these additional Qty remnants show no spatial correlation with the mapped locations of any postulated Quaternary faults.

The next revision to the ESP application will address as appropriate the information provided in this response.

**2.5.1-4** SSAR Figure 2.5.1-29 shows the Savannah River to be relatively straight in the site area in the vicinity of (i.e., southeast of) the proposed surface trace of the Pen Branch Fault. Section 2.5.1.2.1 of the SSAR describes the Savannah as incised at that location.

**Please provide information to address why the Savannah River is straight and incised at a position that appears to correspond with the location of the Pen Branch Fault “block” on the southeastern side of the fault.**

Response:

The Pen Branch fault projects across the Savannah River near the upstream limit of a linear segment of the channel in the vicinity of the VEGP site. The relatively straight portion of the river is incised along the southwestern margin of the floodplain to form the bluffs on the Georgia side of the river. While

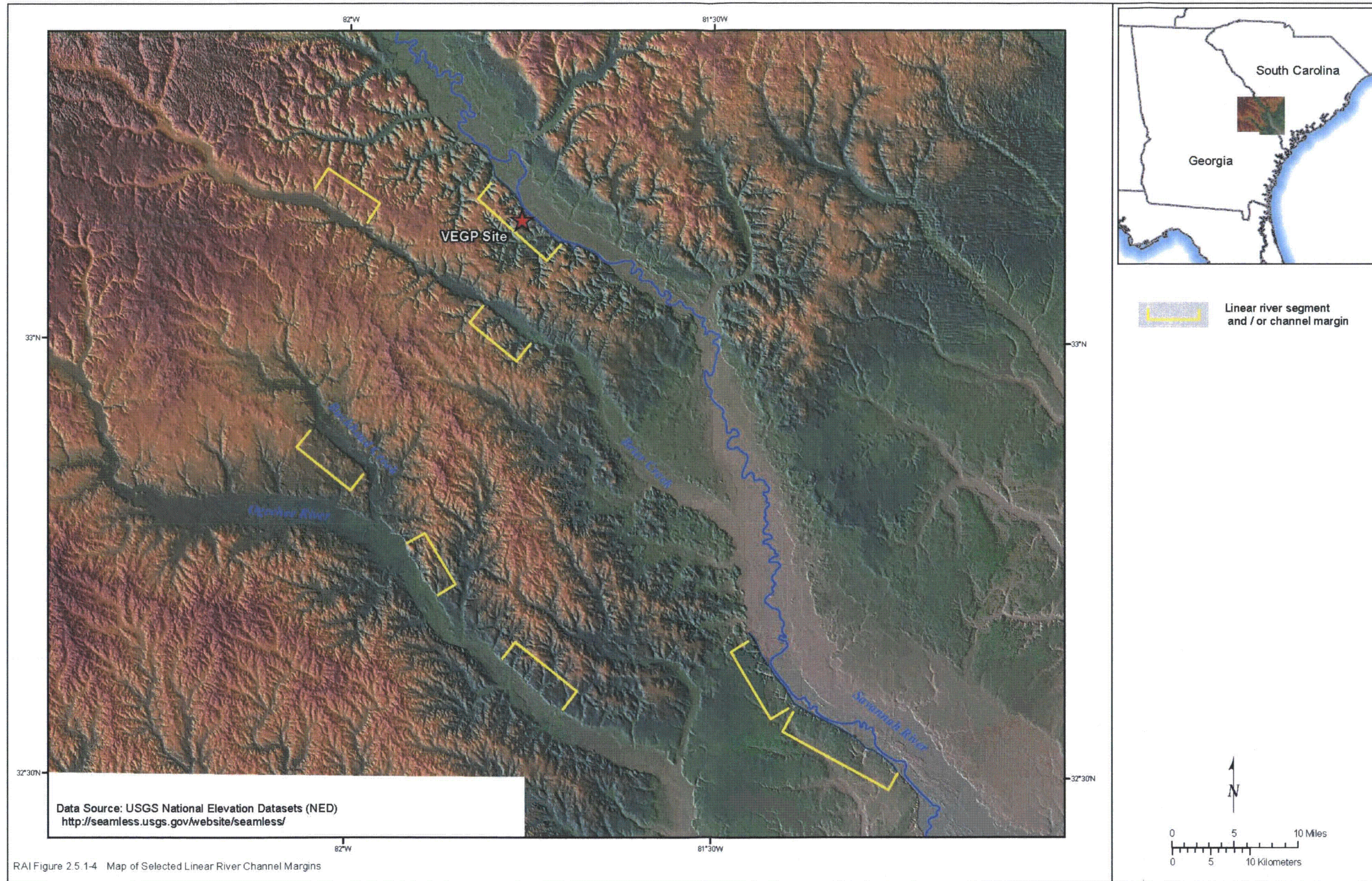
characteristics of rivers and channels can change or respond where they cross locations of tectonic activity, there are many other fluvial, geomorphic, eustatic, and other non-tectonic factors that control channel morphology and sinuosity.

It is not readily apparent what factors or combination of factors have produced the linear portion of the Savannah River in question. However, three observations preclude this straight segment of the river from being the result of recent movement of the Pen Branch fault:

The geomorphic surface of the 350 ka to 1 Ma Ellenton fluvial terrace along the Savannah River is undeformed to within a resolution of 3 ft. This observation is the best evidence precluding late Quaternary activity of the Pen Branch fault and establishing that this fault is non-capable. It is highly unlikely that changes in the modern river channel morphology at the fault would be the result of recent fault activity if the significantly older strain marker (Ellenton terrace surface) is preserved across the fault with no evidence of deformation.

Several other examples of linear and/or incised portions of rivers are present in the Coastal Plain within 50 mi of the VEGP site that are not associated with any mapped fault. As shown on the RAI Figure 2.1.5-4 following this response, this type of fluvial feature is not unique to the portion of the Savannah River adjacent to the VEGP site and downstream of the Pen Branch fault. Several linear and/or incised channel margins occur along the Savannah River, Brier Creek, Buckhead Creek, and Ogeehee River that are about 5 mi or greater in length (see RAI Figure 2.1.5-4 following this response). The occurrence of other linear portions of channel margins demonstrates that the morphology of the Savannah River adjacent to the VEGP site is not unique, but relatively common. These other linear reaches of river channels are not spatially associated with known mapped faults, strongly suggesting a non-tectonic origin for these types of features.

Although the Savannah River segment adjacent to the VEGP site appears to be "straight," micro-geomorphology along the river shows that young Holocene fluvial terraces indicate a meandering pattern as recently as 10 ka or younger. Localized remnant surfaces on the modern floodplain that formed as the result of paleochannel migration indicate that although the river at present appears relatively straight, it has meandered across the floodplain in recent time. Thus, the apparent "straight" segment of river near the VEGP site appears to be an ephemeral feature that changes or evolves through geologic time in response to changes in sediment load, discharge, eustatic base level change, etc.



**2.5.1-5** In Section 2.5.1.1.4.3, rocks of the Augusta and Modoc fault zones are described as containing both mylonitic (i.e., ductile) and brittle deformation fabrics. While the mylonitic fabric is clearly of Alleghanian age, there is no explanation of whether the brittle fabric is the result of late-stage Alleghanian deformation along these zones, either at shallower depths or lower slip rates; cross-cuts the mylonitic fabric and the product of later-stage folding or unloading rather than fault movement; or the result of a much younger, more recent episode of fault movement along the mylonitic zones.

**For both faults, please provide information on characteristics of the mylonitic and brittle fabrics (including textural, petrologic, structural, and orientation data or other evidence that may constrain age of the brittle deformation) which demonstrates that the brittle fabric likely did not form during a post-Alleghanian deformation event, e.g., during the Quaternary, or at least during the present-day stress regime.**

Response:

The southeast-dipping Augusta fault zone is characterized as a zone of quartzofeldspathic mylonites, ultramylonites, and blastomylonites with minor amphibolites, schists, and a variety of light-colored granitic veins (Maher 1987). The Augusta fault is exposed as a 250-m-thick ductile shear zone within the Martin Marietta Augusta quarry on the Georgia side of the Savannah River, the location that has provided the majority of structural and kinematic data.

Until Maher (1987) performed a detailed structural analysis of the fault zone rocks, the Augusta fault had been characterized variably as a thrust fault, a dextral strike-slip fault, a strain gradient with little displacement, and a possible listric normal fault within the early Mesozoic. The sense of movement of the fault zone is now constrained by regional context, mesoscopic structures, and microscopic textures. Maher (1987) notes five observations that indicate a hanging-wall-down, oblique sense of slip: (1) geometry and orientation of folded discordant granitic veins, (2) a sporadically developed lineation, (3) composite planar fabric (S and C surfaces), "mica fish", and (5) regional geologic relations. The significant normal component of slip during the Alleghanian collisional orogeny is seemingly contradictory, but extension on the Augusta fault (and others within the region) is consistent with a model involving gravitational collapse of a thickened crust, similar to examples from the Himalaya (Maher et al. 1994).

Geologic relations and the  $^{40}\text{Ar}/^{39}\text{Ar}$  cooling ages of Maher et al. (1994) suggest that extensional movement on the Augusta fault zone initiated about 274 Ma. Maher et al. (1994) constrains Augusta fault extension as occurring late in the Alleghanian phase and well after initiation of Alleghanian crustal shortening in the Valley and Ridge and Blue Ridge.

Some discontinuous silicified breccias occur along the Augusta fault zone east of the Savannah River, and minor brittle faults utilizing the mylonitic fabric also occur in the Augusta quarry and have striae subparallel to the mylonitic lineation (Maher 1987). The brittle striae and faults record the same sense and direction of shear as the mylonitic fabric, indicating Alleghanian movement on the Augusta fault occurred during transition from ductile to brittle conditions (Maher 1987; Maher et al. 1994).

Alleghanian extensional events have been interpreted for not only the Augusta fault, but also the Goat Rock, Modoc, and Towaliga fault zones, suggesting that extension played a significant role in the development of the Appalachians. Maher et al. (1994) suggest that the new geochronology indicates Piedmont normal faulting is not solely Mesozoic, but includes late Alleghanian episodes.

The Modoc fault zone is a northwest-dipping, several-km-wide ductile shear zone that experienced significant granitic sheet intrusion, prograde metamorphism, and penetrative strain during the Alleghanian (Snoke et al. 1980; Secor et al. 1986a; Secor et al. 1986b; Secor 1987). Mylonitic rocks are common within the zone, although the intensity of mylonitization varies widely (Bramlett et al. 1982). Regional relationships and structures within the zone reflect predominantly dextral motion with a northwest-side-down normal component, related to early Alleghanian extension (Sacks and Secor 1990). Geochronologic data from Dallmeyer et al. (1986) indicate movement occurred between 315 and 290 Ma, during the Alleghanian Lake Murray deformation, D<sub>2</sub>.

Recent exposures created for the construction of Saluda Dam on Lake Murray exposed a portion of the Modoc fault zone where four Paleozoic ductile deformational events are recognized. The D<sub>4</sub> deformation is recognized as an east-northeast-striking zone at least 20 km wide, and it shows a transition from ductile to brittle behavior, which correlates with retrograde mineral assemblages in D<sub>4</sub> faults in the Modoc zone (Howard et al. 2005). Brittle features observed in the Saluda Dam foundation are interpreted to be the result of a readjustment from differential loading and unloading, as well as tectonic movement associated with latest Alleghanian deformation and initial Triassic rifting (McCarney et al. 2005).

Several lines of evidence suggest that the brittle fabrics associated with the Augusta and Modoc fault zones are either late Alleghanian or early Mesozoic age and do not represent Quaternary reactivation in the modern stress regime. These include (1) similar kinematics of the brittle and ductile fabrics, (2) observed normal components of brittle slip are incompatible with the modern stress regime, and (3) the observed mineralization of some brittle fabrics (silicified breccias and zeolite and epidote growth) exposed at the surface are not able to form under the modern geologic and hydrothermal conditions.

The next revision to the ESP application will address as appropriate the information provided in this response.

Additional References Not Cited in SSAR Section 2.5.1:

Howard, C.S., Charleton, J.E., and McCarney, K.J., New geologic synthesis of the Dreher Shoals and Carolina Terranes, Lake Murray and Saluda Dam, Columbia, SC: Geological Society of America Abstracts with Programs, v. 37, no. 2, p. 36, 2005.

McCarney, K.J., Charleton, J.E., and Howard C.S., Brittle features mapped along a shear zone at Saluda Dam, central South Carolina: Geological Society of America Abstracts with Programs, v. 37, no. 2, p. 5, 2005.

Sacks, P.E. and Secor, D.T., Delamination in collisional orogens: *Geology*, v. 18, p. 999-1002, 1990.

AR-07-0801  
Enclosure 1  
RAI Response

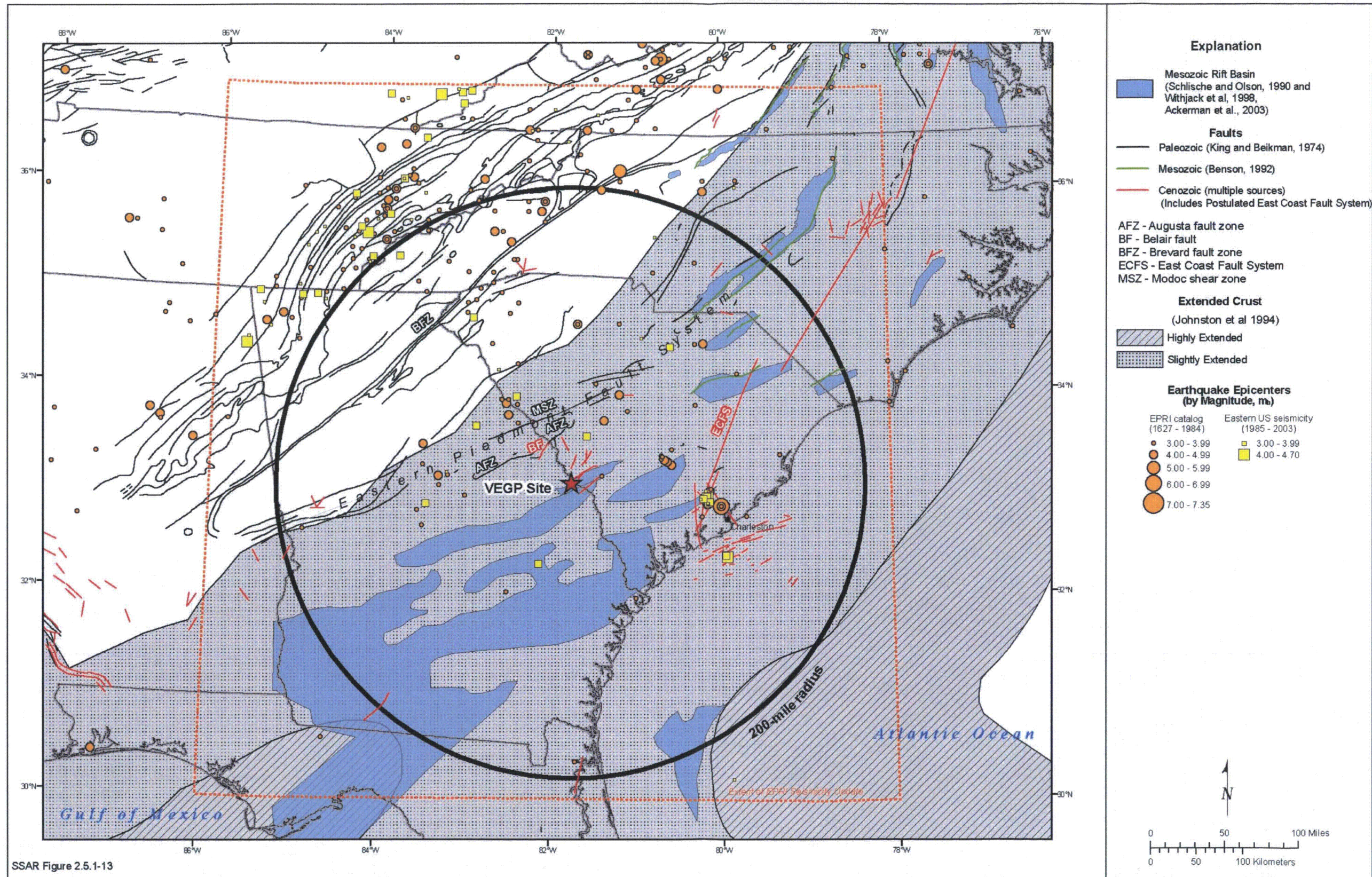
**2.5.1-6 For faults listed under “Other Paleozoic Faults” in SSAR Section 2.5.1.1.4.3, the Central Piedmont Suture and the Eastern Piedmont Fault System are not shown in Figure 2.5.1-14.**

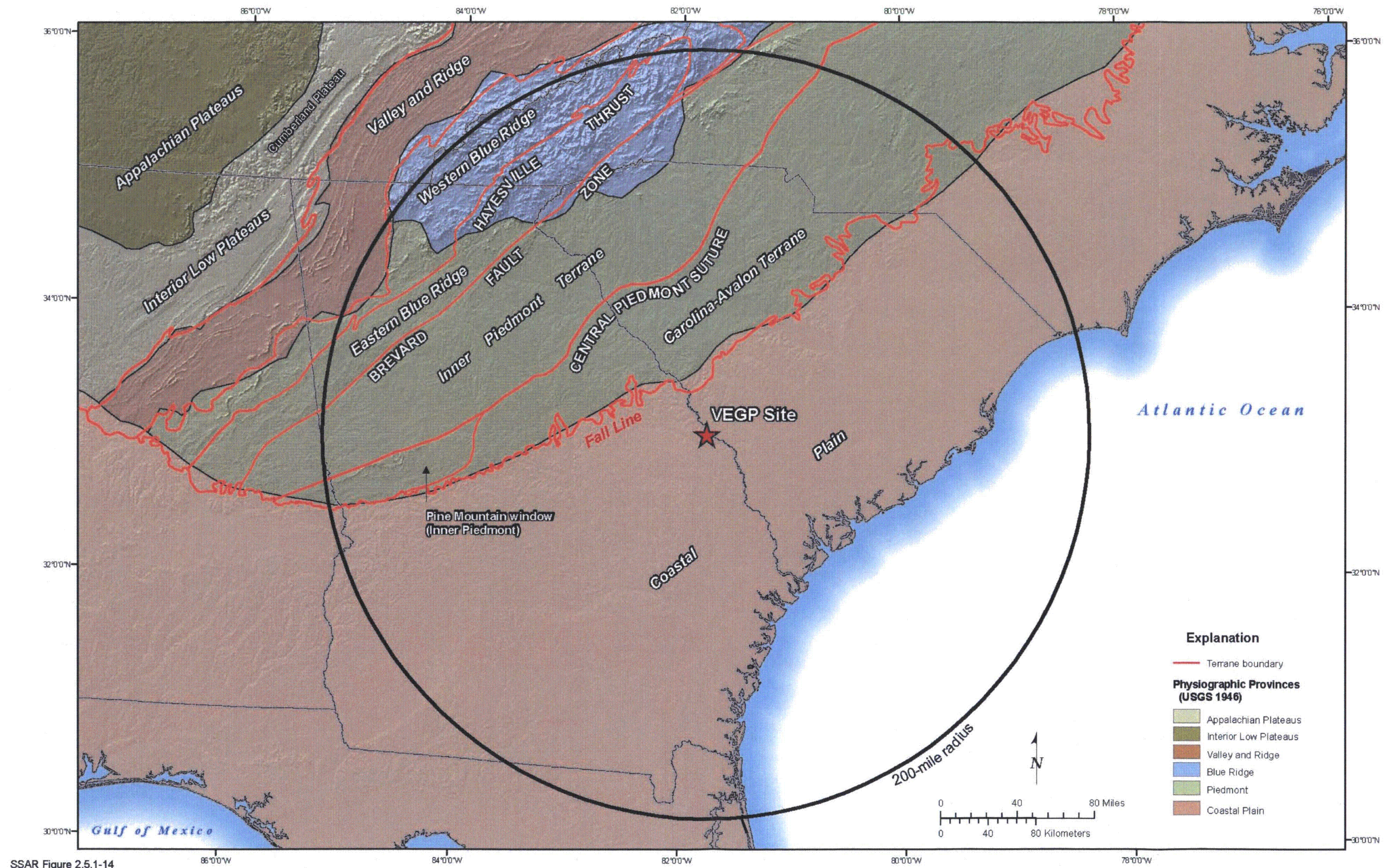
**Please correct Figure 2.5.1-14 to include these two faults since others listed are shown therein.**

Response:

The reviewer is correct. The Central Piedmont suture and the Eastern Piedmont fault system are discussed in the text, but are not labeled on figures. This will be corrected in next revision of the ESP application.

The Eastern Piedmont fault system will be labeled on SSAR Figure 2.5.1-13 and the Central Piedmont suture will be labeled on SSAR Figure 2.5.1-14, as shown on the revised figures following this response. References to these figures in the text will be changed accordingly.





SSAR Figure 2.5.1-14

**2.5.1-7 In Section 2.5.1.1.4.3, the Grenville Front is not described under “Regional Geophysical Anomalies and Lineations”, although it is listed among the features occurring within 200 mi of the VEGP site and shown in SSAR Figure 2.5.1-12.**

**Please describe this regional feature, including whether or not is considered to be a potential seismic source, and provide a basis for the conclusion.**

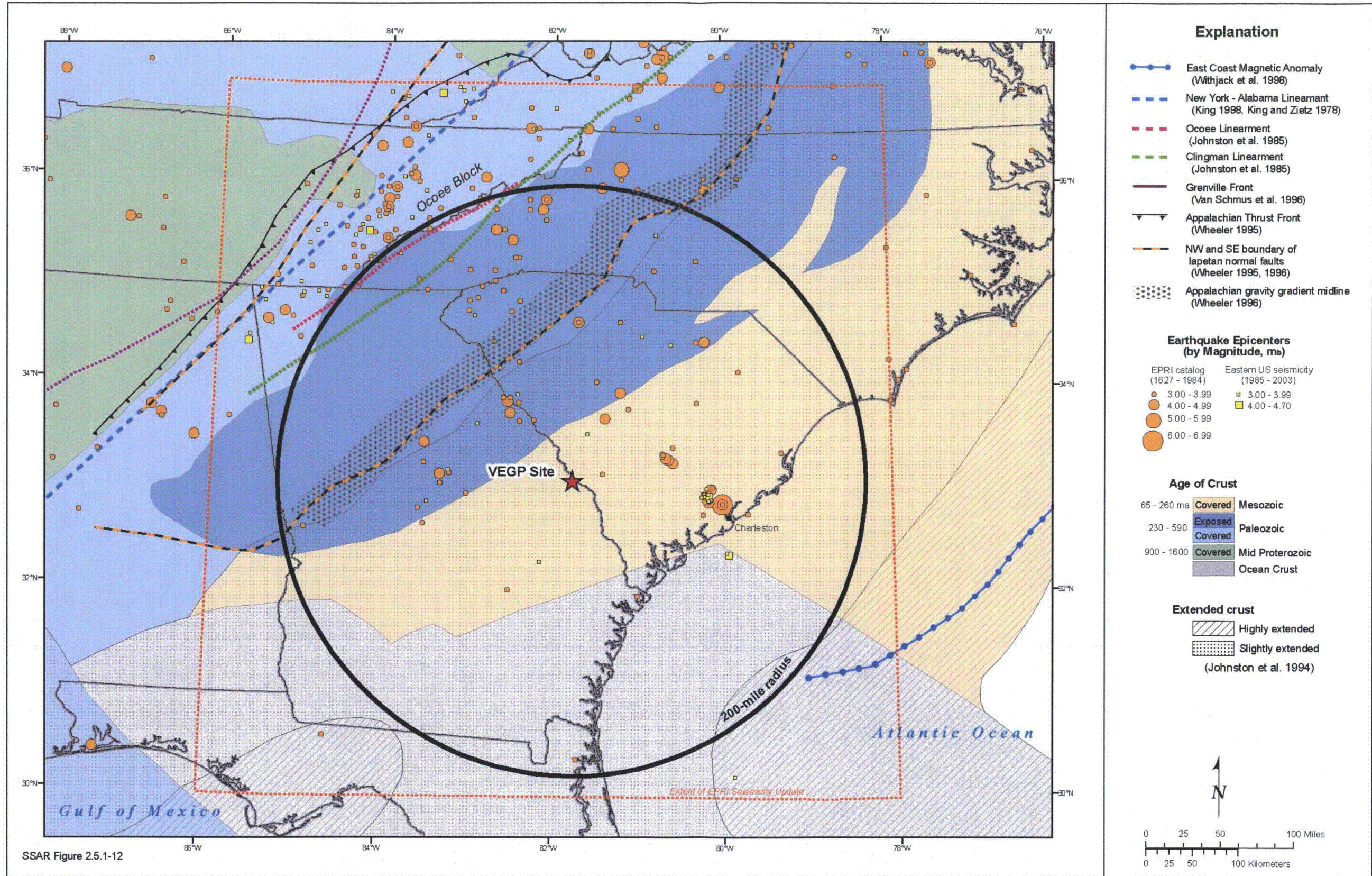
Response:

The Grenville Front was erroneously listed under “Regional Geophysical Anomalies and Lineations” as a feature occurring within 200 mi of the VEGP site. The Grenville Front, which is described under section 2.5.1.1.4.1 (Plate Tectonic Evolution of the Appalachian Orogenic Belt at the Latitude of the Site Region), is located beyond the 200 mi site region and was not shown on SSAR Figure 2.5.1-12. The “Grenville Craton – Eastward Extent” of Ebel and Tuttle (2002) was shown on SSAR Figure 2.5.1-12, which is taken from Wheeler’s (1996) representation of the southeast boundary of the intact Iapetan margin and does not represent the Grenville Front. SSAR Figure 2.5.1-12 has been revised (as shown following this response) to eliminate any confusion by showing the Grenville Front and changing the name of the Ebel and Tuttle (2002) feature to the original name given by Wheeler (1996).

The southeast and northwest boundaries of Iapetan normal faults shown in the revised SSAR Figure 2.5.1-12 (following this response) define the extent of the Iapetan margin of the craton containing normal faults that accommodated extension during the late Proterozoic to early Paleozoic rifting of the Iapetan Ocean. Wheeler (1996) defined the southeast boundary as the southeastern limit of the intact Iapetan margin, which is nearly coincident with the Appalachian gravity gradient in the southeastern US. The Iapetan normal faults are concealed beneath Appalachian thrust sheets that overrode the margin of the craton during the Paleozoic. A few of these Iapetan faults are thought to be reactivated and responsible for producing earthquakes in areas such as eastern Tennessee; Giles County, Virginia; and Charlevoix, Quebec (Bollinger and Wheeler 1988, Wheeler 1996).

The southeast margin of the Iapetan normal faults shown on SSAR Figure 2.5.1-12 does not represent a potential seismic source since it does not represent a discrete crustal discontinuity or tectonic structure. The linear feature shown in the SSAR Figure 2.5.1-12 (following this response) represents the southeastern extent of the intact Iapetan margin (with a location uncertainty of 30 to 35 km), and therefore, the southeastern limit of potentially seismogenic Iapetan faults (Wheeler 1996).

The next revision to the ESP application will address as appropriate the information provided in this response.



**2.5.1-8** Of the six regional geophysical anomalies and lineaments listed in SSAR Section 2.5.1.1.4.3, information is presented to explain why the East Coast and Blake Spur magnetic anomalies are not considered as potential seismic sources. Discussions of the New York-Alabama, Clingman, and Ocoee lineaments do not indicate whether or not they could be potential seismic sources. Also, locations of the Clingman and Ocoee Lineaments and the Ocoee Block are not illustrated in Figure 2.5.1-12, and earthquakes interpreted by Wheeler (1996) as occurring within the Ocoee block in the “modern” tectonic setting were not quantified with regard to the age of faulting with which these earthquakes were associated. (SSAR Section 2.5.1.1.4.6 includes a discussion of the Eastern Tennessee Seismic Zone in which seismic events have occurred that are related to the Ocoee block.)

**a. Please correct Figure 2.5.1-12 to include the Clingman and Ocoee Lineaments and the Ocoee Block.**

**b. Please indicate the age of the “modern” tectonic setting with regard to whether faults in that setting are potential seismically capable structures to be considered for the VEGP site, and explain whether or not these three lineaments are specifically considered to be potential seismic sources and provide the basis for the conclusion.**

Response:

The Clingman and Ocoee lineaments and the Ocoee block are discussed in the text, but are not labeled on SSAR Figure 2.5.1-12. This will be corrected in the next revision of the ESP application. The revised SSAR Figure 2.5.1-12 is as shown in RAI 2.5.1-7.

The modern tectonic setting of the east coast of the United States is that of a passive continental margin. In general, tectonic stress in the central and eastern United States is characterized by northeast-southwest-directed horizontal compression. This stress is likely the result of ridge-push force associated with the Mid-Atlantic ridge, transmitted to the interior of the North American plate by the elastic strength of the lithosphere. As a result of their orientations roughly parallel to the regional structural grain, the New York-Alabama, Clingman, and Ocoee lineaments are potential seismic sources.

Along with the New York-Alabama lineament, the Clingman and Ocoee lineaments bound a block of crust responsible for the majority of earthquakes in the Eastern Tennessee seismic zone. The proximity of these lineaments to current seismicity therefore suggests the possibility that they are potential seismic structures. Most focal mechanism nodal planes within the Eastern Tennessee seismic zone, however, are not parallel to these northeast-trending geophysical anomalies.

The New York-Alabama, Clingman, and Ocoee lineaments were known to the six EPRI ESTs in 1986. Five of the six EPRI ESTs included source zones specifically designed to capture one or more of these lineaments (e.g., Bechtel’s source #25- Tennessee Segment of the New York-Alabama lineament; Rondout’s source #13- New York Alabama Lineament; Weston Geophysical’s source #24- New York-Alabama-Clingman lineaments; Woodward-Clyde Consultants source #31- Blue Ridge Combination). The sixth team, Dames & Moore, did not explicitly discuss the New York-Alabama, Clingman, and Ocoee lineaments (EPRI 1986, 1989). No new information has been published since 1986 on these geophysical lineaments that would cause a significant change in the EPRI seismic source model.

The next revision to the ESP application will address as appropriate the information provided in this response.

**2.5.1-9 Section 2.5.1.1.4.3 describes Regional Mesozoic Tectonic Structures and states that normal faults which “bound Triassic basins may be listric into the Paleozoic detachments faults (Dennis et al., 2004) or may penetrate through the crust as high-angle faults.” The distinction between these basin-bounding faults being listric or penetrating through the crust as high-angle faults is crucial to their potential for generating large-magnitude earthquakes.**

**a. Please discuss the evidence related to whether or not these structures could extend through the crust to depths where large-magnitude earthquakes commonly nucleate.**

**b. Please explain how the distinction between listric and high-angle fault geometries is treated in the probabilistic seismic hazard analysis (PSHA), and explain how the difference between the two geometries would affect hazard at the site. Alternatively, cross-reference a SSAR section that provides the explanation.**

Response:

Data constraining the down-dip geometry of faults that bound Mesozoic basins are equivocal. Seismic reflection data, borehole studies, gravity and magnetic signatures, and geologic mapping have all been used to characterize these faults, but different studies have depicted these faults as both listric (e.g., Crespi 1988; Manspeizer and Cousminer 1988; Dennis et al. 2004) and as high-angle features (e.g., Wentworth and Mergner-Keefer 1983; Schlische 2003). The on-going debate over the down-dip geometry of these features pre-dates the seismic source characterizations of the original EPRI ESTs (EPRI 1986). No new information has been published since 1986 on these features that would cause a significant change in the EPRI seismic source model, therefore the distinction between listric and high-angle geometries is not explicitly treated in the PSHA.

The effects of these two possible geometries on hazard at the site are highly uncertain, but both geometries can potentially produce moderate- to large-magnitude earthquakes on seismogenic structures. High-angle faults that extend through the crust are potentially the loci of moderate to large earthquakes because they penetrate to seismogenic depths. Earthquake magnitude is primarily a function of fault plane area. Listric features potentially have far greater fault plane area than high-angle features, especially if they sole into a regional detachment that extends to seismogenic crustal depths. However, if listric structures are thin-skinned and limited to the upper few km of crust, they may have no seismogenic potential. Because of the uncertainty regarding their geometry, the EPRI ESTs used area sources instead of individual fault sources to represent these basin-bounding faults in the PSHA (EPRI 1986).

Additional References Not Cited in SSAR Section 2.5.1:

Crespi, J.M., Using balanced cross sections to understand early Mesozoic extensional faulting, *in* A.J. Froelich and G.R. Robinson Jr. (eds.), *Studies of the Early Mesozoic Basins of the Eastern United States*, U.S. Geological Survey Bulletin no. 1776, p. 220-229, 1988.

Manspeizer, W. and Cousminer, H.L., Late Triassic-early Jurassic synrift basins of the U.S. Atlantic margin, *in* R.E. Sheridan and J.A. Grow (eds.), *The Atlantic Continental Margin*, vol. 1-2 of *The Geology of North America*, Geological Society of America, Boulder CO, p. 197-216, 1988.

Schlische, R.W., Progress in Understanding the structural geology, basin evolution, and tectonic history of the eastern North America rift system, *in* P.M. LeTourneau and P.E. Olsen (eds.), *The Great Rift Valleys of Pangea in Eastern North America--Volume 1--Tectonics, Structure, and Volcanism*, Columbia University Press, New York, p. 21-64, 2003.

**2.5.1-10 Section 2.5.1.1.4.3 discusses the Belair Fault and indicates that this structure is likely a tear fault or lateral ramp in the hanging wall of the Augusta fault zone. Age constraints on last movement of the Belair Fault are sometime between post-late Eocene and pre-26,000 years ago (Prowell, 2005). Thus, the Belair Fault is one of the few structures in the region with interpreted evidence of late Cenozoic movement (SSAR Figures 2.5.1-3 and 2.5.1-13). If the Belair is a tear fault or lateral ramp associated with the Augusta fault zone, then movement on the Belair may be related to movement on the larger, regional-scale Augusta fault.**

**Please explain how the inference of possible Cenozoic movement on the Belair Fault and its possible association with the Augusta fault zone might affect seismic hazard at the Vogtle site.**

Response:

Mapping and structural analysis by Bramlett et al. (1982) indicate that the Belair fault likely formed as a lateral ramp or tear associated with the Augusta fault when these faults when displacement on these faults initiated during the Paleozoic Alleghanian orogeny . The timing and sense-of-slip for the most-recent movements on the Belair and Augusta faults, however, demonstrate that these two structures have not reactivated as a single tectonic element in Cenozoic or younger time. Prowell et al. (1975) and Prowell and O'Connor (1978) document Cenozoic, brittle, reverse slip on the Belair fault. Quaternary slip on the Belair fault is allowed but not demonstrated by the available data (Crone and Wheeler 2000). In contrast, the latest movement on the Augusta fault, as demonstrated by brittle overprinting of ductile fabrics, exhibits a normal sense-of-slip and is constrained to have occurred in late Alleghanian time during the transition from brittle to ductile conditions (Maher 1987; Maher et al. 1994).

The brittle overprinting on the Augusta fault is consistent with the ductile normal sense of slip. In contrast, the Belair fault exhibits a reverse sense-of-slip during its Cenozoic reactivation. Therefore, different slip histories and opposite senses of dip-slip for the Belair and Augusta faults demonstrate that these two faults have not been reactivated as a single structure during the Cenozoic.

The next revision to the ESP application will address as appropriate the information provided in this response.

**2.5.1-11** Figure 2.5.1-19 of SSAR Section 2.5.1.1.4.4 is important for illustrating what is known or inferred about which liquefaction features may be related to the 1886 Charleston earthquake as opposed to other past earthquake events, and for correlating geographic proximity of individual liquefaction features with each other and with proposed sources.

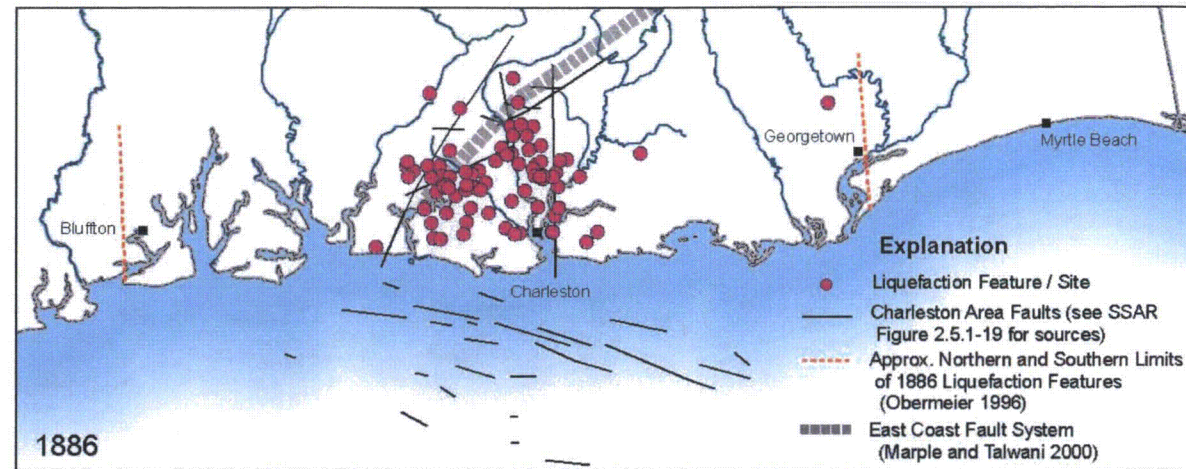
**Please provide new figures that clearly distinguish the liquefaction features related to the 1886 Charleston earthquake from each of the proposed paleoliquefaction events A,B,C',E,F' (C' to include C and D events from Talwani and Schaeffer, 2001 and F' to include F and G events, also from Talwani and Schaeffer, 2001). These figures should outline the areal extent of the features associated with each event, how they correlate with areal coverage of 1886 features, and their proximity to the regional tectonic structures shown in SSAR Figure 2.5.1-19.**

Response:

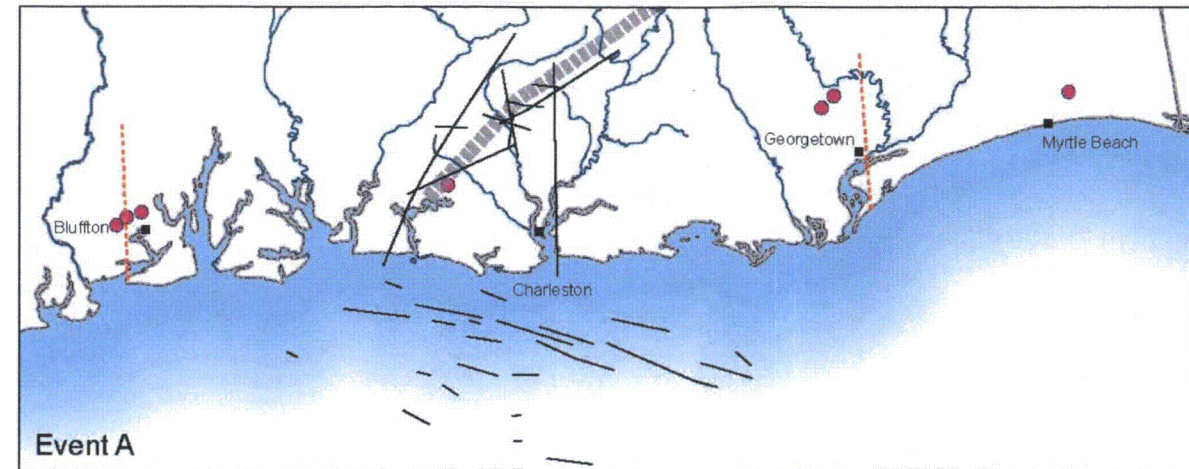
RAI Figure 2.5.1-11 following this response depicts the geographic distributions of liquefaction features associated with the 1886 earthquakes and each of the proposed prehistoric Charleston seismic source earthquakes. SSAR Figure 2.5.1-19 differentiates between 1886 liquefaction features and those features that pre-date 1886, but does not show the geographic distribution of liquefaction sites for each event in the prehistoric record.

RAI Figure 2.5.1-11 shows the liquefaction features associated with the 1886 Charleston earthquake, as well as the liquefaction sites associated with each of the proposed paleoliquefaction events (Events A, B, C', E, and F'). An important observation from RAI Figure 2.5.1-11 is that the spatial distributions of paleoliquefaction sites for Events A, B, C', E, and F' closely approximate the spatial distribution of 1886 liquefaction features.

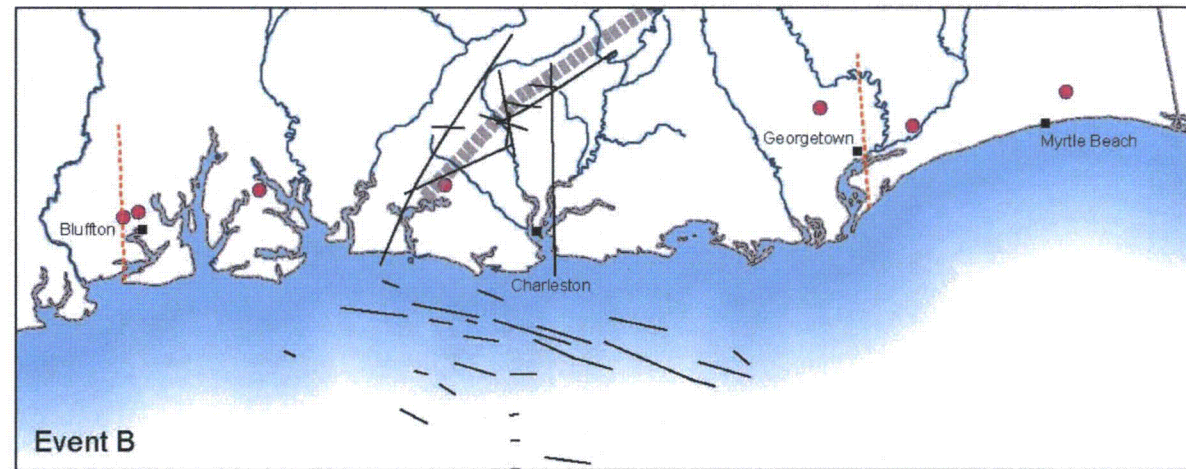
The next revision to the ESP application will address as appropriate the information provided in this response.



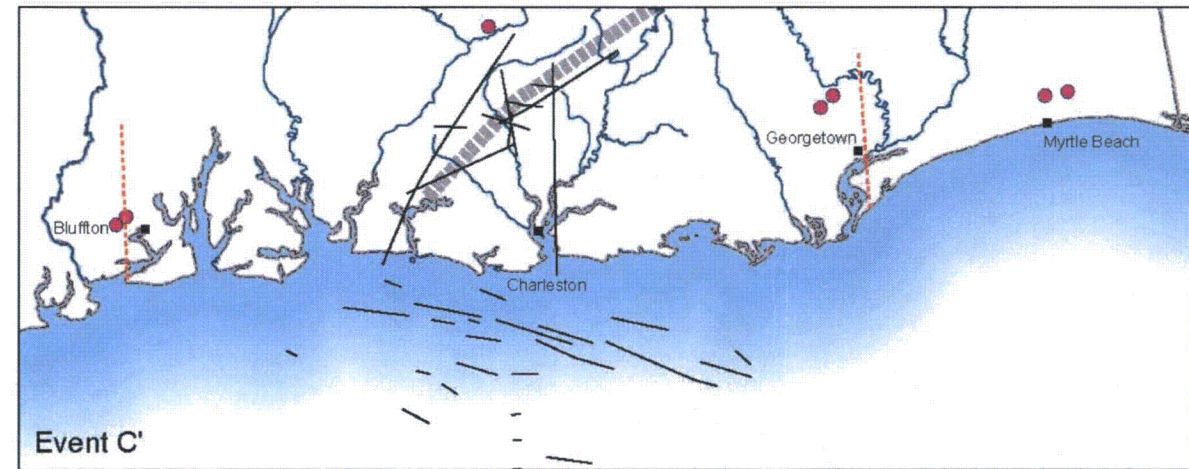
Source: Amick et al. (1990)



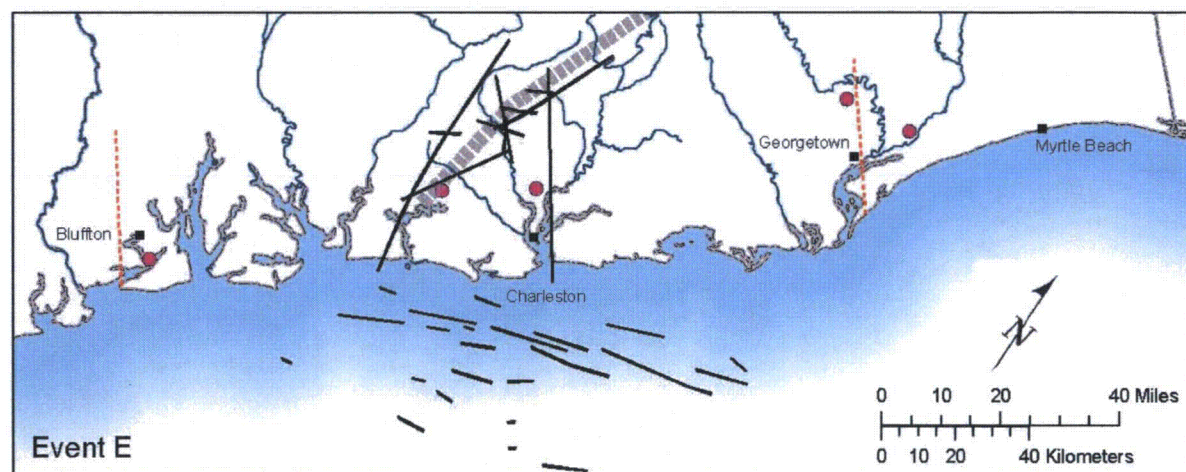
Source: Talwani and Schaeffer (2001)



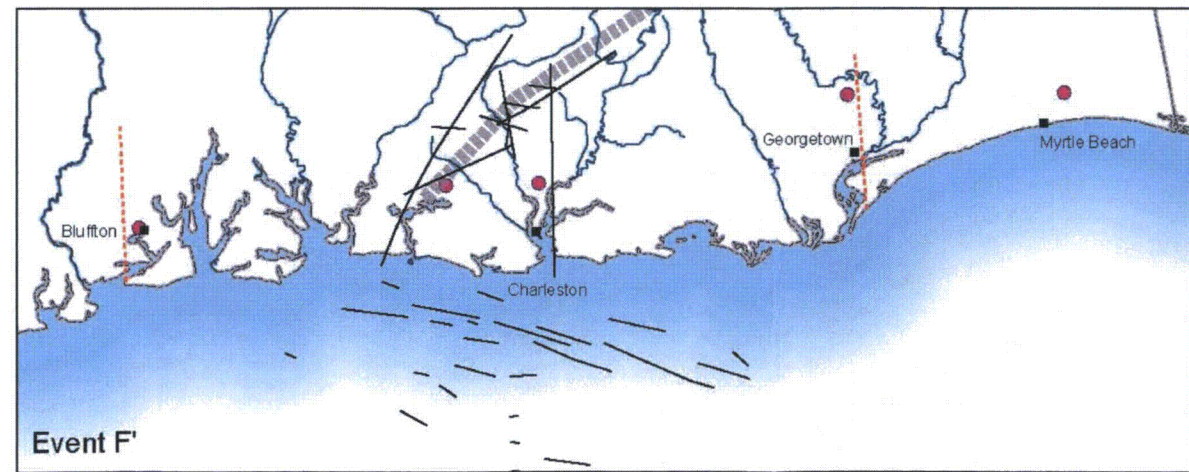
Source: Talwani and Schaeffer (2001)



Source: modified after Talwani and Schaeffer (2001)



Source: Talwani and Schaeffer (2001)



Source: modified after Talwani and Schaeffer (2001)

RAI Figure 2.5.1-11

Geographic Distribution of Liquefaction Features Associated with Charleston Earthquakes

**2.5.1-12 SSAR Section 2.5.1.1.4.4 discusses Charleston Tectonic Features and cites Figure 2.5.1-18. The isoseismal contour lines for the 1886 Charleston earthquake in this figure are attributed to Bollinger (1977), but this reference is not included in the list of references for Section 2.5.1.**

**Please include Bollinger (1977) in the list of references cited.**

Response:

The reviewer is correct. Bollinger (1977) is cited as a source for SSAR Figure 2.5.1-18, but the citation for this reference does not appear in the list of references. This will be corrected and following reference will be incorporated into SSAR Section 2.5.1 in the next revision to the ESP application:

**(Bollinger 1977)** Bollinger, G.A., Reinterpretation of the intensity data for the 1886 Charleston, South Carolina, earthquake: in Studies Related to the Charleston, South Carolina, Earthquake of 1886- A Preliminary Report (D. W. Rankin, ed.): U.S. Geological Survey Professional Paper 1028, p. 17-32, 1977.

**2.5.1-13 SSAR Section 2.5.1.1.4.4 states that it describes all the faults that occur within the meizoseismal area for the 1886 Charleston earthquake, but appears to exclude the Gants and Drayton Faults.**

**Please provide a description of these two faults since they are shown in SSAR Figures 2.5.1-19 and 2.5.1-20.**

Response:

The reviewer is correct. The Gants and Drayton faults appear on SSAR Figures 2.5.1-19 and 2.5.1-20 (and in SSAR Table 2.5.2-10), but are not discussed in the text. This will be corrected in the next revision of the ESP application by adding the following descriptions of these features:

**Drayton Fault** – The Drayton fault is imaged on onshore seismic reflection lines and was known to the six EPRI ESTs at the time of EPRI (1986). The Drayton fault is mapped as a 5.5-mi-long, apparently northeast-trending, high-angle, reverse fault in the meizoseismal area of the 1886 Charleston earthquake (**Hamilton et al. 1983**) (Figures 2.5.1-19 and 2.5.1-20). The Drayton fault terminates upward at approximately 2,500 ft below the ground surface within a Jurassic-age basalt layer (**Hamilton et al. 1983**), precluding significant Cenozoic slip on this fault.

**Gants Fault** – The Gants fault is imaged on onshore seismic reflection lines and was known to the six EPRI ESTs at the time of EPRI (1986) as a possible Cenozoic-active fault. The Gants fault is mapped as a 5.5-mi-long, apparently northeast-trending, high-angle, reverse fault in the meizoseismal area of the 1886 Charleston earthquake (**Behrendt et al. 1981; Hamilton et al. 1983**) (Figures 2.5.1-19 and 2.5.1-20). The Gants fault displaces vertically a Jurassic-age basalt layer by about 150 ft at approximately 2,500 ft below the ground surface (**Hamilton et al. 1983**). Overlying Cretaceous and Cenozoic beds show apparent decreasing displacement with decreasing depth (**Hamilton et al. 1983**), indicating likely Cenozoic activity, but with decreasing displacement on the Gants fault during the Cenozoic.

**2.5.1-14 SSAR Section 2.5.1.1.4.5 discusses faults postulated for the Savannah River Site (SRS) by Cumbest et al. (1998) which are illustrated in SSAR Figure 2.5.1-22. The density of faults shown in this figure suggests there may be faults at the VEGP site which have not yet been identified.**

**Please address the issue of why density of faults on the eastern side of the Savannah River around the SRS is much greater than that currently shown for the VEGP site on the western side of the river, and the implication for seismic hazard at the ESP site.**

Response:

There are a greater number of faults recognized east of the Savannah River because the Savannah River Site has been the focus of several decades of subsurface exploration and research over a much larger area than the VEGP site. However, the availability of high quality, high resolution seismic reflection profile data that completely traverse the VEGP site from north to south (normal to regional geologic structural grain) and that image the complete Coastal Plain stratigraphic section from the top of basement to shallow levels, collected as part of the Vogtle ESP project, make the existence of any unrecognized faults at the VEGP site unlikely. In comparison, the Savannah River Site is 300 square miles in area and has more than 200 linear miles of seismic reflection data. Although the faults shown on the Savannah River Site are larger in number, considering the difference in area between the Savannah River Site and the VEGP site, the fault densities are comparable. It should also be noted that the resolution and signal-to-noise ratio of the VEGP seismic profile that traverses the site (VEGP-4) is significantly better than almost all of the seismic reflection data available for SRS. The absence of previously unrecognized faults in the VEGP seismic reflection data indicate that faulting at the VEGP site and in the site area has been adequately characterized and that there are no unknown faults that would affect seismic hazard at the site.

The next revision to the ESP application will address as appropriate the information provided in this response.

**2.5.1-15 SSAR Section 2.5.1.1.4.5 on SRS Tectonic Features does not summarize pertinent information collected from the SRS that was used to define fault traces at the SRS and draw the conclusion, presented in SSAR Sections 2.5.1.2.4 and 2.5.3.1.3, that no faults, in particular the Pen Branch, are capable features at the VEGP site.**

**a. Please provide a concise summary of definitive data collected at the SRS, including direct evidence from borings and seismic profiles, which demonstrate that the Pen Branch Fault is not a capable structure at the SRS.**

**b. Please compare data collected and analyses performed for the SRS to demonstrate the most recent movement on the Pen Branch fault with data and analyses employed to make this determination for the VEGP site, leading to the conclusion that the Pen Branch Fault is not a capable structure at the VEGP site.**

Response:

SSAR Section 2.5.3 of the ESP lists several lines of direct and indirect evidence based on previous studies at the Savannah River Site that substantiate the non-capability of the Pen Branch fault. The data, results, and conclusions for these Savannah River Site studies are summarized in the Confirmatory Drilling Project Final Report (Stieve et al. 1994). In addition, Moos and Zoback (2001) report regional stress orientations. Specifically these data are:

- Faulting deforms sediments no younger than Eocene in age. The data for this conclusion are based on 18 closely spaced Savannah River Site drill holes that allowed construction of a map of the base of the Upland Formation above the fault. Additional support for this conclusion is based on geologic mapping and data from 20 auger holes in the Long Branch, South Carolina 7.5-minute quadrangle (Nystrom et al. 1994; auger holes located off of, but adjacent to, the Savannah River Site, on strike with the Pen Branch fault), which showed no evidence for faulting.
- Seismic reflectors as shallow as 0.04 s on CONOCO high-resolution seismic reflection profile 2EXP show no clear fault-related deformation (Chapman and DiStefano 1989; Stieve et al. 1994).
- Savannah River Quaternary fluvial terraces are not deformed across the fault trace (resolution 7 to 10 ft; Geomatrix 1993). This is based on longitudinal profiles along two Savannah River terraces.
- Regional principal stress orientations based on stress-induced wellbore breakouts and hydraulically induced fracturing show that the maximum horizontal stress is parallel to the regional orientation of the Pen Branch fault, which make “strike-slip faulting unlikely” and “reverse faulting essentially impossible” (Moos and Zoback 2001). The most-recent deformation observed for this fault in Tertiary sediments is reverse faulting.

The Vogtle ESP Pen Branch fault terrace study documented that no fault-related deformation could be discerned on the 350 ka to 1 Ma Ellenton (Qte) terrace above the fault trace within a resolution of 3 ft. The resolution of this study compared to the previous studies make it by far the most definitive evidence for the non-capability of the Pen Branch fault both at the Savannah River Site and the VEGP site.

The next revision to the ESP application will address as appropriate the information provided in this response.

**2.5.1-16 Section 2.5.1.2.4 discusses faults in the site area that involve deformation of basement rocks. The Steel Creek fault is not considered to be a capable tectonic source, but this conclusion is not substantiated.**

**Please provide information and references that support the conclusion that the Steel Creek Fault is not a capable tectonic source.**

Response:

The Steel Creek fault is an approximately 10-mi-long, steeply northwest-dipping, southeast-side-down reverse fault that terminates to the northeast on the Savannah River Site (Domoracki 1994). The Steel Creek fault is subparallel to, and southeast of, the Pen Branch fault. Together the Pen Branch and Steel Creek faults form the boundaries of an uplifted block of Triassic basement, indicating that the Steel Creek fault is genetically associated with, and probably an antithetic feature to, the Pen Branch fault. The orientation of the Steel Creek fault is similar to that of the southeast-dipping Pen Branch fault relative to the maximum horizontal compressive stress field (Moos and Zoback 2001), thereby making both the Steel Creek and Pen Branch faults unfavorably oriented to be reactivated in a reverse or strike-slip sense.

Geomatrix (1993) addressed the potential capability of the Steel Creek fault in conjunction with the Pen Branch fault. This study concluded that there is no discernible warping or faulting of Quaternary fluvial terraces due to the Steel Creek fault within a resolution of 7 to 10 ft.

The next revision to the ESP application will address as appropriate the information provided in this response.

**2.5.1-17 In the brief history of the Pen Branch Fault presented in SSAR Section 2.5.1.2.4.1, there is no reference to the suggestion of Hanson et al. (1993) that possible rejuvenation of drainage along traces of the Pen Branch and Steel Creek Faults on the SRS may suggest either local tectonic uplift along these faults or non-tectonic geologic or geomorphic processes.**

**Please discuss this suggestion of possible displacement along the Pen Branch Fault in relation to potential implications for the VEGP site.**

Response:

Studies of Savannah River Site Quaternary fluvial terraces overlying the surface projection of the Pen Branch fault performed by Geomatrix (1993) demonstrate the lack of evidence for vertical tectonic deformation of the terrace surfaces within a resolution of 7 to 10 ft. A higher-resolution study performed for the VEGP ESP application provides evidence demonstrating the absence of tectonic deformation within a resolution of about 3 ft for the 350 ka to 1 Ma Ellenton (Qte) terrace surface. The results of these studies provide the most-reliable evidence demonstrating the lack of Quaternary deformation on the Pen Branch fault.

In addition to their fluvial terrace investigation, Geomatrix (1993) performed various other morphometric analyses of the Savannah River Site. These analyses included calculation of drainage densities and frequencies, regional slope, stream-gradient indices, and estimations of drainage basin morphometry. Geomatrix (1993) noted drainage density highs and possible small topographic residuals and complexities in longitudinal profiles near the Pen Branch fault. Although these morphometric signatures may be attributed to possible long-term tectonic effects, Geomatrix (1993, p. 58) states "these features may derive entirely or in part from other [non-tectonic] geologic factors and geomorphic processes."

Savannah River Quaternary fluvial terrace surfaces represent the most-reliable strain markers with which to test for the possibility of tectonic deformation. Geologic mapping and a high-resolution topographic survey of the Qte surface provides the most definitive evidence for the non-capability of the Pen Branch fault both at the Savannah River Site and the VEGP site.

**2.5.1-18 SSAR Section 2.5.1.2.4.2 states that the Pen Branch Fault at the VEGP site is made up of two specific fault segments trending N45° E and N34° E with a dip of 45° SE. Cumbest et al. (2000) reported a N46° - 66° E range in strike of the Pen Branch Fault at the SRS.**

**Please discuss whether or not either fault segment at the VEGP site is favorably oriented to experience slip in response to the existing regional stress field defined by Moos and Zoback (2001).**

Response:

Moos and Zoback (2001) determined a maximum horizontal compressive stress oriented N50° to 70°E, with a local perturbation at intermediate depths (3,000 to 3,700 ft) at which the maximum horizontal stress was oriented N33°E. Assuming an average orientation of the maximum horizontal stress as N60°E, then planes oriented at N45°E and N34°E and dipping 45°SE would form angles to the maximum horizontal stress of approximately 10° and 20°, respectively. These orientations are not parallel to the maximum horizontal stress, and therefore these planes would experience some resolved shear stress. However, Ramsey and Huber (1987, Figure E.6 page 671) show that these small, 10° to 20° angles would, at most, experience about 1/3 to less than 1/2 the resolved stress on favorably oriented planes (i.e., at 45° to the maximum horizontal stress). Moos and Zoback (2001) state that at shallow depths the stress

magnitudes only approach the frictional strength of favorably oriented reverse faults (i.e., 45°). Therefore, the stress magnitudes at other orientations will be well below those necessary for activation in the modern-day stress field. Also, the more northerly orientation of the Pen Branch fault segments at the VEGP site make them less favorably oriented to the intermediate depth stress perturbation of N33°E for strike-slip or reverse movement.

**2.5.2-4 Regulatory Guide 1.165 describes the necessity of updating the Electric Power Research Institute (EPRI) and Lawrence Livermore National Laboratory seismic sources and using the Senior Seismic Hazard Analysis Committee (SSHAC) recommendation to implement a probabilistic seismic hazards assessment (PSHA). SSAR Section 2.5.2.2.2.4 describes the updated Charleston seismic source model (UCSS). Please justify your rationale for using the SSHAC Level 2 methodology for the UCSS update. In addition, please describe the implementation of the SSHAC Level 2 methodology. Specifically, how were the experts' opinions integrated into the development of the final UCSS model? How were any conflicting opinions between the experts dealt with, and how does the final source model represent the informed consensus of the community beyond those selected for the UCSS update?**

**In addition, please justify the adequacy of a Level 2 study for the update of Charleston seismic source zone, rather than a level 3 or 4 study?**

Response:

Methods used to update the Charleston seismic source follow guidelines provided in Regulatory Guide 1.165 (NRC 1997). For the VEGP ESP study, a Senior Seismic Hazard Analysis Committee (SSHAC) Level 2 study was performed to incorporate current literature and data and the understanding of experts into an update of the Charleston seismic source model. SSHAC (1997) outlines this methodology and provides guidance on incorporating uncertainty and the use of experts in PSHA studies. The intent of the SSHAC process is to represent the range of current understanding of seismic source parameters by the informed technical community.

SSHAC (1997) describes four levels of study (Levels 1 through 4), in increasing order of sophistication and effort. The choice of the level of a PSHA is driven by two factors: (1) the degree of uncertainty and contention associated with the particular project, and (2) the amount of resources available for the study (SSHAC 1997). SSHAC (1997, Table 3-1) suggests that a Level 2 study is appropriate for issues with "significant uncertainty and diversity," and for issues that are "controversial" and "complex." In a SSHAC Level 2 study, a Technical Integrator (TI) is responsible for reviewing data and literature and contacting experts who have developed interpretations or who have specific knowledge of the seismic source. The TI interacts with experts to identify issues and interpretations, and to assess the range of informed expert opinion. In Level 3 studies, the TI goes a step further by bringing together experts and focusing dialog and interaction between them in order to evaluate relevant issues. In Level 4 studies, a Technical Facilitator/Integrator (TFI) is responsible for aggregating the judgments of a panel of experts to develop a composite distribution of the informed technical community. In a meeting held on July 7, 2005, VEGP ESP Technical Advisory Group (TAG) members Dr. Martin Chapman, Dr. Robert Kennedy, Dr. Carl Stepp, and Dr. Robert Youngs agreed that a Level 2 study is appropriate for updating the Charleston seismic source model.

The SSHAC Level 2 process utilizes an individual, team, or company to act as the TI. For the VEGP ESP update to the Charleston seismic source model, the TI was a team of six William Lettis & Associates, Inc. (WLA) personnel (Scott Lindvall, Ross Hartleb, William Lettis, Jeff Unruh, Keith Kelson, and Steve Thompson). This TI team (1) compiled and reviewed all new information developed since 1986

regarding the 1886 Charleston earthquake and the seismic source that may have produced this earthquake; (2) compared this new information with information available prior to 1986 and the EPRI EST assessments of the Charleston seismic source; (3) contacted researchers familiar with recent and ongoing studies of the Charleston seismic source; and (4) integrated this information to develop an updated characterization of the Charleston seismic source that captures the composite representation of the informed technical community. Mr. Lindvall directed efforts of the TI team. Dr. Hartleb compiled available literature and data and facilitated data review by the team members through overseeing the development of a GIS database. Dr. Lettis, Dr. Unruh, Mr. Kelson, and Dr. Thompson worked with Mr. Lindvall and Dr. Hartleb to critically review and evaluate the available data and to develop the updated Charleston source model.

Specific activities performed during the SSHAC Level 2 study included:

- Review of published literature, data, and maps, with a focus on post-EPRI data (c. 1986)
- Review of the EPRI source model to understand the intent of each EST's modeling of the Charleston source.
- Interviews with experts and researchers familiar with geologic/seismologic data and recent characterizations of the Charleston seismic source. The following experts were consulted:
  - Dr. David Amick, SAIC
  - Dr. Martin Chapman, Virginia Polytechnic Institute
  - Dr. Chris Cramer, U.S. Geological Survey
  - Dr. Art Frankel, U.S. Geological Survey
  - Dr. Arch Johnston, Center for Earthquake Research and Information, University of Memphis
  - Dr. Richard Lee, Los Alamos National Laboratory
  - Dr. Joe Litehiser, Bechtel Corporation (original team leader of the 1986 Bechtel EST)
  - Dr. Stephen Obermeier, U.S. Geological Survey (retired)
  - Dr. Pradeep Talwani, University of South Carolina
  - Dr. Robert Weems, U.S. Geological Survey

These experts were asked a series of questions pertaining to key issues regarding the Charleston seismic source. This was not a formal process of expert interrogation to obtain from each expert all of the specific parameters and weights to be used in the model. Instead, we allowed the experts to speak to their own areas of expertise. It was then the TI's responsibility to combine these responses with data from the published literature to capture the range of expert opinion and judgment regarding parameters and weights to be used in the UCSS model.

- Update the Charleston seismic source based on published information and data (e.g., seismicity) and knowledge of current researchers. This activity included a two-day workshop held on September 13-14, 2005 to develop the UCSS model at the WLA office in Valencia, California after several weeks of literature and data review. The workshop included the TI team, who integrated Charleston area data and expert interpretations, discussed uncertainties and conflicting expert interpretations, and developed UCSS geometries and the logic tree.
- Update the 1986 EPRI ESTs' seismic source models with the updated assessment of the Charleston seismic source. A meeting was held at Bechtel's San Francisco office on September 15, 2005, with Joe Litehiser (Bechtel) and Robin McGuire (Risk Engineering, Inc.; PSHA analyst) and two members of the TI team (Lindvall and Lettis) to determine how the UCSS would be integrated into the EPRI source models for each EST.
- Recalibration and reanalysis of radiocarbon ages and timing of Charleston area paleoliquefaction episodes to develop a quantitative estimate of recurrence.

A Technical Advisory Group (TAG) panel was convened in April 2006 in Frederick, Maryland to critically review the UCSS model and to provide feedback regarding the process and the results of the study. TAG members Chapman, Kennedy, Stepp, and Youngs were in attendance. In addition, Dr. Carl Stepp and Dr. Martin Chapman reviewed written copies of the Engineering Report describing the UCSS and provided written comments on, and approval of, the document.

The UCSS model represents a composite of the TI's assessment of the interpretations of informed expert opinion regarding the Charleston seismic source. The UCSS model source parameters for geometry, Mmax, and recurrence of Mmax reflect the TI's assessment of the range of expert interpretations.

**2.5.2-5** In SSAR Sections 2.5.1.1.4.6 and 2.5.2.2.1 the range of  $M_{max}$  values developed by each EST are given as  $m_b$ . Please provide a table for converting values of  $m_b$  to  $M_w$  by the equations used for the SSAR.

Response:

RAI Table 2.5.2-5 below will be incorporated into SSAR Section 2.5.2 in the next revision to the ESP application:

RAI Table 2.5.2-5 Conversion between body-wave ( $m_b$ ) and moment ( $M_w$ ) magnitudes<sup>1</sup>.

<b>Convert</b>	<b>To</b>	<b>Convert</b>	<b>To</b>
<b><math>m_b</math></b>	<b><math>M_w</math></b>	<b><math>M_w</math></b>	<b><math>m_b</math></b>
4.00	3.77	4.00	4.28
4.10	3.84	4.10	4.41
4.20	3.92	4.20	4.54
4.30	4.00	4.30	4.66
4.40	4.08	4.40	4.78
4.50	4.16	4.50	4.90
4.60	4.24	4.60	5.01
4.70	4.33	4.70	5.12
4.80	4.42	4.80	5.23
4.90	4.50	4.90	5.33
5.00	4.59	5.00	5.43
5.10	4.69	5.10	5.52
5.20	4.78	5.20	5.61
5.30	4.88	5.30	5.70
5.40	4.97	5.40	5.78
5.50	5.08	5.50	5.87
5.60	5.19	5.60	5.95
5.70	5.31	5.70	6.03
5.80	5.42	5.80	6.11
5.90	5.54	5.90	6.18
6.00	5.66	6.00	6.26
6.10	5.79	6.10	6.33
6.20	5.92	6.20	6.40
6.30	6.06	6.30	6.47
6.40	6.20	6.40	6.53
6.50	6.34	6.50	6.60
6.60	6.49	6.60	6.66
6.70	6.65	6.70	6.73
6.80	6.82	6.80	6.79
6.90	6.98	6.90	6.85
7.00	7.16	7.00	6.91
7.10	7.33	7.10	6.97
7.20	7.51	7.20	7.03
7.30	7.69	7.30	7.09
7.40	7.87	7.40	7.15
7.50	8.04	7.50	7.20
		7.60	7.26
		7.70	7.32
		7.80	7.37
		7.90	7.43
		8.00	7.49

<sup>1</sup> Average of relations given by Atkinson and Boore (1995), EPRI (1993), and Frankel and others (1996).

**2.5.2-6 SSAR Section 2.5.2.2.1 summarizes the EPRI source zones that include the site, and the Mmax values and weights that each EPRI Earth Science Team (EST) assigned to these source zones. Mmax values of the zones have a weighted mean of about Mw 6.0. Mmax values of Mw 7.5 and larger were assigned low probabilities that average 0.08. In contrast, the USGS national seismic-hazard maps utilize an Mmax that is based on (1) A.C. Johnston's (1994, EPRI) survey of large earthquakes worldwide in areas that are tectonically similar to the U.S. east of the Rockies, and on (2) L. Kanter's (1994, EPRI) final assessments of the tectonic setting of each earthquake. The 1996, 2002, and 2007 USGS national hazard maps use Mmax of Mw 7.5 with high weights for the area that includes the site.**

**a. Please explain whether or not the Johnston (1994) findings, the final versions of the Kanter (1994) assessments, and USGS's use of them as support for high Mmax, constitute new information that requires an update of the 1989 EPRI PSHA, and why.**

**b. Please explain why you believe that an Mmax value of Mw 7.5 with a weight of 0.5 or larger is not warranted.**

Response:

The final versions of the Johnston (1994) and Kanter (1994) assessments (included in Volume 1 of the Johnston et al. 1994 study) and the USGS's use of them in the national hazard maps does not constitute new information that requires an update of the EPRI seismic source model for the following reasons:

1. Initial results of the Johnston et al. (1994) study were available to the EPRI SOG ESTs. The study was initiated specifically for use by the ESTs in their development of the EPRI SOG seismic source model. As stated in the introduction to the Johnston et al. (1994) volume, "Part of the focus of the early phase of this work was the evaluation of existing methods for assessing maximum earthquakes and preliminary development of new methods for use by the earth science teams in the EPRI-SOG seismic hazard analysis for the Central and Eastern United States (CEUS)" (Coppersmith 1994; Chapter 1 of Johnston et al. 1994).
2. Final results of the Johnston et al. (1994) study generally support the initial findings of the study. Johnston et al. (1994) also conclude that, "The results of this study lend support to preliminary indications from this work (Coppersmith et al. 1987) that were used in the assessments of maximum magnitude for seismic source zones in the EPRI SOG seismic hazard methodology." Both Coppersmith et al. (1987) and Johnston (1994; Chapter 4 in Johnston et al. 1994) report that  $M \geq 7$  earthquakes are found only in Mesozoic or younger extended crust. Therefore, the ESTs were aware that the largest observed earthquakes in Stable Continental Regions (SCR) are concentrated in extended crust, similar to the passive margin along the eastern seaboard.
3. Final results of the Kanter (1994; Chapter 2 of Johnston et al. 1994) tectonic interpretation of SCR distinguish the Eastern Seaboard (#218) domain as extended crust and the Piedmont (#223), Valley and Ridge (#224), and Grenville (#226) domains to the west as non-extended crust. While these formal domain names and interpretations were not available to the ESTs, the basic knowledge that the Atlantic passive margin represented extended Mesozoic crust and that the world's largest observed earthquakes were limited to this type of crust was known to the ESTs. It should be noted that the North Anna site is located within Kanter's (1994) Piedmont (#223) domain in non-extended crust; and, thus, large magnitude earthquakes are not expected in this domain.

4. A statistical analysis performed by Cornell (1994; Chapter 5 of Johnston et al. 1994) shows that many extended crustal domains have maximum observed magnitudes smaller than **M7**, such that the mean maximum magnitude is not significantly different than for non-extended crust. This suggests that extended crust in some areas has maximum magnitudes less than **M7**, or that the “observed” historical data in the database are still too few to draw statistically significant results, despite the underlying premise of the Johnston et al. (1994) study to substitute “space for time.”
5. Recent updates in the estimate of moment magnitude from intensity data for large SCR earthquakes indicate significant uncertainty in the estimate of maximum magnitude, and generally, have decreased magnitude estimates. For example, Johnston (1996) assigned moment magnitude estimates of **M8.1**, 8.0 and 7.8 for the three 1811-1812 New Madrid earthquakes, and **M7.3** for the 1886 Charleston earthquake. More recently, these moment magnitude estimates have been downgraded to **M7.2** to 7.3, 7.4 to 7.5, and 7.1 for the New Madrid sequence (Bakun and Hopper 2004; Hough et al. 2000), and **M6.9** for the Charleston earthquake (Bakun and Hopper 2004). These and other magnitude revisions may influence the statistical results of the Johnston et al. (1994) study. This uncertainty must be taken into consideration when using the Johnston et al. (1994) study to evaluate whether or not there has been a significant change to the EPRI SOG source characterization.
6. The USGS use of the Johnston (1994) and Kanter (1994) studies (both in Johnston et al. [1994]) to justify the selection of a high **Mmax** is not clearly presented in the published documentation of the USGS source model (Frankel et al. 1996, 2002). For example, the only discussion in Frankel et al. (1996) regarding the selection of **M7.5** as the **Mmax** for the extended crust outboard of the craton is “this large **Mmax** was motivated by the magnitude of the Charleston event (**M7.3**; Johnston 1996), since the workshop participants felt such a large event could not be ruled out in other areas of the extended crust.” Johnston et al. (1994) was cited in Frankel et al. (1996) as the justification for separating the craton and extended crust zones. The 2002 update to the USGS model cited Johnston et al. (1994) as the basis for revising the **Mmax** for the “inboard” craton zone from **M6.5** to **M7.0**, but no mention of the extended crust **Mmax** appeared in Frankel et al. (2002).

The boundary separating extended and non-extended crust in the USGS source model (Frankel et al. 2002) lies west of the boundary defined by Kanter (1994) and represents the northwestern limit of the Iapetan margin of Wheeler (1995). While the USGS source model includes a more recent interpretation of the location of extended crust based on the late Proterozoic to early Paleozoic Iapetan extension (Wheeler 1995), it is not clear why Kanter (1994) did not interpret the older portion of the crust as extensional, since the basic information regarding the earlier extensional period was known to her. In fact, she describes the Iapetan rifting episode as follows: “During the late Proterozoic and continuing into the earliest Paleozoic, rifting occurred along the eastern and southern margin of North America, eventually leading to a passive margin (p. 2-67).” She also notes that this older passive margin is covered by the Appalachian crust: “During the Paleozoic a series of arc and continental collisions added a belt of Paleozoic crust to the late Proterozoic passive margin along the eastern edge of North America (p. 2-68).” Therefore, the difference in the northwestern boundary of extended crust between Kanter (1994) and Wheeler (1995) is primarily due to different interpretations as opposed to new geologic or seismologic data.

There is considerable uncertainty in the assessment of  $M_{max}$  for the CEUS, as well as the identification and classification of crustal domains that are capable of generating different  $M_{max}$  magnitudes. Seismic source models for PSHAs should incorporate a range of uncertainty in model parameters, including  $M_{max}$ . We believe that an  $M_{max}$  value of  $M7.5$  with a weight of 0.5 or larger is not warranted for the Paleozoic and Mesozoic crust of North America for the following reasons:

1. The USGS  $M_{max}$  zones have incorporated the interpretation that the Iapetan margin (Wheeler 1995, 1996) should be classified as “extended crust” as opposed to the Kanter (1994) interpretation that the Piedmont, Valley and Ridge, and Grenville domains represent non-extended crust. In the CEUS, Kanter (1994) confines extended crust to Mesozoic and younger extended crust. These differing interpretations reflect uncertainty in how the informed technical community has classified crustal domains. The site region includes both Mesozoic extended crust and older crust of the Piedmont, Blue Ridge, and Valley and Ridge provinces.
2. Although a primary observation from the Johnston et al. (1994) study is that large magnitude ( $M > 7$ ) earthquakes are confined to Mesozoic and younger extended crust, this observation by itself does not mean that all Mesozoic and younger crust is capable of producing large magnitude earthquakes. The observation rightfully focuses attention on the Mesozoic and younger crust in which there is a need to identify geologic, tectonic, seismologic, or geophysical features as potential sources of large magnitude earthquakes, as was done by the EPRI ESTs.
3. Even though the final Johnston (1994) study has placed less emphasis on discriminating between different ages of extended crust, events larger than  $M7$  have only been observed in extended crust of Mesozoic age or younger. Therefore, in Paleozoic or older extended crust, there should be a greater degree of uncertainty and a lower range of  $M_{max}$  values assigned to this type of crust which has yet to record an earthquake larger than  $M7$ .
4. Magnitude estimates of historic large earthquakes from Charleston and New Madrid have been reevaluated and more recent assessments have suggested smaller magnitudes. In the case of Charleston, a magnitude estimate of  $M7.3$  for the 1886 earthquake (Johnston 1996) was influential in shaping the  $M7.5$   $M_{max}$  value assigned to the extended margin zone for the USGS model (Frankel et al. 1996). A recent study by Bakun and Hopper (2004) provides a best estimate of  $M6.9$  for the 1886 event and suggests that  $M_{max}$  distributions should include magnitudes less than  $M7.5$ .

The next revision to the ESP application will address as appropriate the information provided in this response.

**2.5.2-7 SSAR Section 2.5.2.2.2.3 (page 2.5.2-16) states that the results of the Lawrence Livermore National Laboratory Trial Implementation Project (TIP) study are not explicitly included in the SSAR because the study was as much “a test of the methodology as a real estimate of seismic hazard”. Please clarify why you believe the TIP was more of a test of the methodology rather than a real estimate of the seismic hazard. Please provide more detail explaining why the TIP results were not used.**

Response:

The purpose of the Lawrence Livermore National Laboratory Trial Implementation Project (TIP) study was to “test and implement the guidelines developed by the Senior Seismic Hazard Analysis Committee (SSHAC) developed under FIN L2503 (NRC 1997)” (Savy et al. 2002, p. 1). To test the SSHAC PSHA methodology, the TIP study focused on seismic zonation and earthquake recurrence models for the Watts Bar site in Tennessee and the VEGP site. The TIP study includes information and discussions regarding seismic hazard assessment for the VEGP site, and for this reason we thoroughly reviewed the report.

The TIP study focuses primarily on implementing the Senior Seismic Hazard Advisory Committee (SSHAC) PSHA methodology (SSHAC 1997), however, and was designed to be as much of a test of the methodology as a calculation of seismic hazard. For example, as part of the test of the methodology, Committee members were asked to present opposing arguments, regardless of whether they agreed with the position they were asked to present. As a disclaimer, Kevin Coppersmith prefaced his discussion of the Pen Branch fault with the following statement:

“The following white paper—much like a lawyers (*sic*) legal argument—presents a particular position and seeks only to support that position. I have intentionally tried to present an unbalanced case, giving only lip service to counter arguments...Further, I have done a poor job of citing references and providing supporting data to many of my arguments.” (p. A-51)

The TIP study provides useful discussions, including speculations regarding the Charleston seismic source, seismic hazards of the South Carolina–Georgia region, and Eastern Tennessee. However, the TIP study focuses primarily on methodology. The process-oriented focus of the TIP study is also illustrated in the report presentation, which is very thorough on methodology, but significantly lacking in presenting a summary of seismic source model parameters. For these reasons, the TIP study results are not explicitly incorporated into the VEGP ESP application.

The next revision to the ESP application will address as appropriate the information provided in this response.

**2.5.2-8 SSAR Section 2.5.2.2.2.4.1 states that the characteristics of the 1886 Charleston earthquake, and the greatest density of prehistoric liquefaction features, taken together “show that future earthquakes having magnitudes comparable to the Charleston earthquake of 1886 most likely will occur within the area defined by Geometry A. A weight of 0.7 is assigned to Geometry A ...” (page 2.5.2-18). Additionally, Figure 2.5.2-9 indicates no likelihood that an 1886-sized earthquake has occurred inland from the coastal region, except along Geometry C, and then only with a probability of 0.1.**

**a. Please summarize the age, liquefaction susceptibility, and geographic distribution of liquefiable deposits in the zone 50 km (31 miles) - 150 km (93 miles) inland from the coast, and explain whether this information supports a negligible probability of large inland earthquakes.**

**b. Please reconcile a negligible probability of large inland earthquakes, as indicated in Figure 2.5.2-9, with the discovery of prehistoric liquefaction features as much as 100 km (62 miles) inland in fluvial deposits of the**

**Edisto River (Obermeier, 1996, in McCalpin, J., ed., "Paleoseismology", Fig. 7.6; same figure is Fig. 11 in Engineering Geology, 1996, v. 44, p. 1-76).**

Response:

Liquefaction susceptibility is a function of numerous variables including, but not limited to, sediment grain size and sorting, degree of compaction and/or cementation, deposit thickness, depth below ground surface, degree of saturation, and sediment age. Obermeier (1996) suggested South Carolina Coastal Plain deposits older than about 250 ka have negligible potential for liquefaction due to the effects of chemical weathering. Obermeier (1996) observed that, in general, the region within 30 mi (~50 km) of the coast is highly susceptible to liquefaction. The liquefiable deposits of the about 100 ka Princess Anne Formation, however, are mapped greater than 65 mi inland (McCartan et al. 1984).

Numerous liquefaction features caused by the 1886 Charleston earthquake and paleoliquefaction features from prehistoric Events A, B, C', E, and F' are distributed along a 115 mi stretch of coastal South Carolina from Bluffton in the south to Georgetown in the north. The inland extent of 1886 liquefaction is less well-constrained. Seeber and Armbruster (1981, as presented in Talwani and Schaeffer's [2001] Figure 1) described poorly documented, contemporary accounts of liquefaction as far inland as Columbia (about 100 mi inland). Amick et al. (1990) described 1886 liquefaction features at four sites along the Edisto River as much as 60 mi inland (their sites #117, 119, 120, and 121; shown on SSAR Figures 2.5.1-18, 2.5.1-19, 2.5.2-7, 2.5.2-8, and 2.5.2-9). Obermeier (1996), however, described these same four sites as prehistoric. When we asked about this discrepancy, Dr. Stephen Obermeier (U.S. Geological Survey, retired) stated that it is likely that both 1886 liquefaction features and paleoliquefaction features are preserved inland along the Edisto River (pers. comm., April 4, 2007).

Amick et al. (1990) determined that their liquefaction site #117 is located in deposits of Holocene age. Sites #119, 120, and 121 are located in the Princess Anne Formation, estimated at 100 ka (McCartan et al. 1984). The presence of liquefaction (paleoliquefaction?) features in 100 ka and younger sediments is in accordance with Obermeier's (1996) 250 ka age limit of liquefiable deposits. Regardless of whether the Edisto River liquefaction features are the result of the 1886 earthquake or an earlier earthquake, the inland extent of liquefaction as measured from the meizoseismal area is about equidistant to the extent of liquefaction from the 1886 and prehistoric earthquakes as measured up and down the coast from the meizoseismal area.

Three of the source geometries for the updated Charleston seismic source model (Geometries A, B, and B') are elongated northeast-southwest to represent the orientation of the regional structural grain. The fourth geometry (Geometry C) represents the areal extent of the postulated southern segment of the East Coast fault system (Marple and Talwani 2000). There is no structural, geomorphic, paleoseismic (other than the cited sparse liquefaction data), or historic (i.e., 1886) evidence to suggest a source zone geometry that trends northwest-southeast or extends significantly inland from the 1886 meizoseismal area. The sparse liquefaction features along the Edisto River cited by Seeber and Armbruster (1981), Amick et al. (1990), and Obermeier (1996) likely reflect strong ground shaking in deposits susceptible to liquefaction, and not a localized, inland source. Like the South Carolina Department of Transportation source model (Chapman and Talwani 2002), the updated Charleston seismic source model presented in the VEGP ESP application incorporates only the seaward-most of the four Edisto River liquefaction sites (Amick et al.'s [1990] site #117). The U.S. Geological Survey's (Frankel et al. 2002) Charleston seismic source model extends about 10 mi farther inland to include two of the four Edisto River liquefaction sites.

The next revision to the ESP application will address as appropriate the information provided in this response.

Additional Reference Not Cited in SSAR Section 2.5.2:

McCartan, L., Lemon E.M. Jr., and Weems, R.E., Geologic map of the area between Charleston and Orangeburg, South Carolina: U. S. Geological Survey miscellaneous investigations series map I-1472, 1:250,000 scale, 1984.

**2.5.2-9 SSAR Section 2.5.2.2.4.3 suggests that the liquefaction features attributed to a single large, prehistoric earthquake might actually have been produced by several moderate-magnitude earthquakes that are closely spaced in time (page 2.5.2-26). Please determine whether Talwani or Obermeier have data on sizes of prehistoric liquefaction craters, and whether these or any related data might constrain the possible magnitudes of the prehistoric earthquakes.**

Response:

Magnitudes of prehistoric earthquakes can be estimated based on the sizes and/or geographic distribution of paleoliquefaction features. For the Charleston seismic source, it is possible to compare historical and prehistoric liquefaction effects. Data describing the size and spatial distribution of paleoliquefaction features suggest at least some prehistoric earthquakes were of similar magnitude to the 1886 Charleston earthquake.

Obermeier (1996) noted “almost all craters that predate 1886 have a morphology and size comparable to the 1886 craters” (p. 345). Liquefaction craters formed during prehistoric events at about 600 and about 1,250 years BP (likely Talwani and Schaeffer’s [2001] events B and E) are at least as widely distributed throughout coastal South Carolina as are 1886 liquefaction features. Moreover, the sizes of individual craters formed during the 600 and 1,250 yr BP events are at least as large as those formed during the 1886 earthquake, both in the vicinity of Charleston and farther away (Obermeier 1996). These observations suggest that some prehistoric earthquakes have been at least as large as the 1886 earthquake.

Talwani and Schaeffer (2001) estimated the magnitudes of prehistoric Charleston area earthquakes based on the spatial distribution and areal extent of paleoliquefaction sites. Talwani and Schaeffer (2001) did not use a rigorous method in their estimation of the magnitudes of past events, but instead they used a simple approach by which all past liquefaction episodes interpreted as having spanned a region comparable in size to the 1886 liquefaction field were assigned **M 7+**, and all past liquefaction episodes interpreted as having spanned a smaller areal extent were assigned **M 6+**.

Additional related studies include those by Hu et al. (2000a, 2000b), Leon (2003), and Leon et al. (2005). Hu et al. (2000a, 2002b) used the event chronology as interpreted by Talwani and Schaeffer (2001) and the energy-stress method to estimate magnitudes of past Charleston area earthquakes. For earthquakes that produced liquefaction features over extended areas centered near Charleston, Hu et al. (2002b) estimated magnitudes of **M 6.8 to 7.8**, and they estimated magnitudes of **M 5.5 to 7.0** for earthquakes that produced liquefaction over more limited areas.

Leon (2003) and Leon et al. (2005) also estimated the magnitudes of past Charleston area earthquakes using the event chronology as interpreted by Talwani and Schaeffer (2001), but the Leon (2003) and Leon et al. (2005) method takes into account the effects of sediment age on the liquefaction potential of those sediments. Using the magnitude-bound method, Leon et al. (2005) estimated magnitudes of **M** 6.9 to 7.1 for earthquakes that produced liquefaction features over extended areas, and **M** 5.7 to 6.3 for earthquakes that produced liquefaction over more limited areas. Using the energy-stress method, Leon et al. (2005) estimated magnitudes of **M** 5.6 to 7.2 for earthquakes that produced liquefaction features over extended areas, and **M** 4.3 to 6.4 for earthquakes that produced liquefaction over more limited areas.

In summary, given the large uncertainties in working with the paleoliquefaction record and methods for estimating magnitudes from these data, the magnitude ranges estimated for prehistoric Charleston earthquakes are broad. Nevertheless, these studies suggest that at least some prehistoric earthquakes have been comparable in magnitude to the 1886 earthquake.

The next revision to the ESP application will address as appropriate the information provided in this response.

Additional References Not Cited in SSAR Section 2.5.2:

Hu, K., Gassman, S.L., and Talwani, P., In-situ properties of soils at paleoliquefaction sites in the South Carolina coastal plain, *Seismological Research Letters*, v. 73, no. 6, p. 964-978, 2002a.

Hu, K., Gassman, S.L., and Talwani, P., Magnitudes of prehistoric earthquakes in the South Carolina coastal plain from geotechnical data, *Seismological Research Letters*, v., 73, no. 6, p. 979-991, 2002b.

Leon, E., Effect of aging of sediments on paleoliquefaction evaluation in the South Carolina coastal plain, unpub. Ph.D. dissertation, University of South Carolina, 181p., 2003.

Leon, E., Gassman, S.L., and Talwani, P., Effect of soil aging on assessing magnitudes and accelerations of prehistoric earthquakes, *Earthquake Spectra*, v. 21, no. 3, p. 737-759, 2005.

Obermeier, S., Liquefaction-induced features, *in* "Paleoseismology," J. McCalpin (ed.), Academic Press, San Diego, p. 331-396, 1996.

**2.5.2-10 SSAR Section 2.5.2.2.4.3 states that liquefaction from the 1886 Charleston earthquake is preserved in geologic deposits at numerous locations and that liquefaction deposits from earlier earthquakes are preserved in the region.**

**For each of the pre-1886 events please summarize the number of liquefaction features and sites that have been documented, the areal extent of liquefaction (i.e., how many square kilometers), how many dates have been collected, and how well the features correlate from one site to the next.**

Response:

In this response we provide the number and geographic distribution of liquefaction sites, the number of radiocarbon samples constraining event ages, and the degree of correlation between liquefaction sites for the 1886 and prehistoric Charleston earthquakes. The figure following RAI 2.5.1-11 response illustrates the distribution of liquefaction features and sites. Before addressing these specific questions, however, we provide a brief overview of the methods used in the VEGP ESP application to constrain the timing of Charleston seismic source paleoliquefaction events. For reference, SSAR Table 2.5.2-13 provides a comparison of age constraints on Charleston paleoliquefaction events from Talwani and Schaeffer (2001) and from the VEGP ESP application.

Talwani and Schaeffer (2001) used calibrated radiocarbon ages with 1-sigma error bands in order to define the timing of past liquefaction episodes in coastal South Carolina. The standard in paleoseismology, however, is to use calibrated ages with 2-sigma (95.4% confidence interval) error bands (e.g., Sieh et al. 1989; Grant and Sieh 1994). Likewise, in paleoliquefaction studies, in order to more accurately reflect the uncertainties in radiocarbon dating, the use of calibrated radiocarbon dates with 2-sigma error bands (as opposed to narrower 1-sigma error bands) is advisable (Tuttle 2001). Talwani and Schaeffer's (2001) use of 1-sigma error bands may lead to over-interpretation of the paleoliquefaction record such that more episodes are interpreted than actually occurred. In recognition of this possibility, the conventional radiocarbon ages presented in Talwani and Schaeffer (2001) were recalibrated and reported with 2-sigma error bands in the VEGP ESP application. The broader age ranges with 2-sigma error bands were then used to obtain broader age ranges for paleoliquefaction events in the Charleston area.

Talwani and Schaeffer (2001) distinguish three classes of radiocarbon dates. "Contemporary" radiocarbon samples are those collected from within liquefaction feature deposits and are interpreted as having been incorporated into the deposit during or shortly after formation. Contemporary ages provide the best estimate of the age of liquefaction feature formation. "Minimum" and "maximum" radiocarbon samples are those collected from stratigraphically above and below the liquefaction feature, respectively. For each event summarized below, we provide the total number of radiocarbon dates (contemporary, minimum, and maximum) used to constrain the event.

Paleoearthquakes were distinguished based on grouping paleoliquefaction features that have contemporary radiocarbon samples with overlapping calibrated ages. The event ages were then defined by selecting the age range common to each of the samples. For example, an event defined by overlapping 2-sigma sample ages of 100 to 200 cal yr BP and 50 to 150 cal yr BP would have an event age of 100 to 150 cal yr BP. We consider the "trimmed" ages to represent the ~95% confidence interval, with a "best estimate" event age as the midpoint between the ~95% age range.

The 2-sigma analysis identified six earthquakes (including 1886) in the data presented by Talwani and Schaeffer (2001). As noted by that study, events C and D are indistinguishable at the 95% confidence interval, and together they compose Event C'. Additionally, our 2-sigma analysis suggests that Talwani and Schaeffer's (2001) events F and G may have been a single, large event, which we name Event F'.

One important difference between our results and those of Talwani and Schaeffer (2001) is that their three events C, D, and F are inferred to be smaller, moderate-magnitude events. In the analysis performed for the VEGP ESP application, these moderate earthquakes are grouped into more regionally extensive, large-magnitude events C' and F'. As a result, all earthquakes in the 2-sigma analysis represent large,  $M_{\max}$  events.

August 31, 1886 Charleston Earthquake. Numerous liquefaction features caused by the 1886 Charleston earthquake are distributed along a 115 mi stretch of coastal South Carolina from Bluffton in the south to Georgetown in the north (Obermeier 1996) (see figure following RAI 2.5.1-11 response). The inland extent of liquefaction is less well constrained. Seeber and Armbruster (1981, as presented in Talwani and Schaeffer's [2001] Figure 1) described poorly documented, contemporary accounts of liquefaction as far inland as Columbia (about 100 mi inland). Amick et al. (1990) described 1886 liquefaction features up to 60 mi inland along the Edisto River, but Obermeier (1996) describes these same features as prehistoric.

Event A. Talwani and Schaeffer (2001) document Event A paleoliquefaction features at seven sites distributed along 150 mi of coastal South Carolina from Bluffton in the south to Myrtle Beach in the north (see figure following RAI 2.5.1-11 response). A total of twelve radiocarbon ages collected from these seven sites constrain the timing of Event A.

Event B. Talwani and Schaeffer (2001) document Event B paleoliquefaction features at seven sites distributed along 150 mi of coastal South Carolina from Bluffton in the south to Myrtle Beach in the north (see figure following RAI 2.5.1-11 response). A total of twenty-five radiocarbon ages collected from these seven sites constrain the timing of Event B.

Event C'. Talwani and Schaeffer (2001) document Event C' paleoliquefaction features at seven sites distributed along 150 mi of coastal South Carolina from Bluffton in the south to Myrtle Beach in the north (see figure following RAI 2.5.1-11 response). A total of twenty-two radiocarbon ages collected from these seven sites constrain the timing of Event C'.

Talwani and Schaeffer (2001) include an alternative scenario in which their Event C' is divided into two smaller-magnitude, localized earthquakes (their Events C and D). The two-sigma reanalysis of Talwani and Schaeffer's (2001) age data performed for the VEGP ESP application suggests that their Events C and D were likely a single, large event (Event C'). The incorporation of a single, large Event C' into the updated Charleston seismic source model is, in effect, a conservative approach. The moderate-magnitude ( $\sim M 6$ ) earthquakes C and D would be eliminated from the record of large ( $M_{\max}$ ) earthquakes in the updated Charleston seismic source model, thereby increasing the calculated  $M_{\max}$  recurrence interval and lowering the hazard without sufficient justification. For these reasons the updated Charleston seismic source model uses a single, large Event C' (instead of separate, smaller Events C and D).

Event E. Talwani and Schaeffer (2001) document Event E paleoliquefaction features at five sites distributed along 130 mi of coastal South Carolina from Bluffton in the south to Georgetown in the north (see figure following RAI 2.5.1-11 response). A total of twenty-one radiocarbon ages collected from these five sites constrain the timing of Event E.

Event F'. The two-sigma reanalysis of Talwani and Schaeffer's (2001) age data performed for the VEGP ESP application suggests that their Events F and G were likely a single, large event (Event F'). The incorporation of a single, large Event F' into the updated Charleston seismic source model is, in effect, a conservative approach, for reasons outlined above for Event C'.

Talwani and Schaeffer (2001) document Event F' paleoliquefaction features (their Events F and G features) at five sites distributed along 150 mi of coastal South Carolina from Bluffton in the south to Myrtle Beach in the north (see figure following RAI 2.5.1-11 response). A total of eleven radiocarbon ages collected from these five sites constrain the timing of Event F'.

The next revision to the ESP application will address as appropriate the information provided in this response.

Additional References Not Cited in SSAR Section 2.5.2:

Grant, L.B. and Sieh, K., Paleoseismic evidence of clustered earthquakes on the San Andreas fault in the Carrizo Plain, California, *Journal of Geophysical Research*, v. 99, n. B4, p. 6819-6841, 1994.

Obermeier, S., Liquefaction-induced features, *in* "Paleoseismology," J. McCalpin (ed.), Academic Press, San Diego, p. 331-396, 1996.

Seeber, L. and Armbruster, J. G., The 1886 Charleston, South Carolina earthquake and the Appalachian detachment, *Journal of Geophysical Research*, v. 86, no. B9, p. 7874-7894, 1981.

Sieh, K., Stuiver, M., and Brillinger, D., A more precise chronology of earthquakes produced by the San Andreas fault in southern California, *Journal of Geophysical Research*, v. 94, n. B1, p. 603-623, 1989.

Tuttle, M.P., The use of liquefaction features in paleoseismology: lessons learned in the New Madrid seismic zone, central United States, *Journal of Seismology*, v. 5, p. 361-380, 2001.

**2.5.2-11 SSAR Section 2.5.2.2.2.4.3 states that paleoliquefaction Event C is defined by features north of Charleston while Event D is defined by sites south of Charleston. Events C and D are combined as a single large event C'.**

**Please provide any information on liquefaction features, geographically located between these two areas, that have similar radiocarbon ages which supports your characterization of these events as a single large event rather than two separate events. Provide justification that there is enough paleoliquefaction data to support a single large event C' from a single source.**

Response:

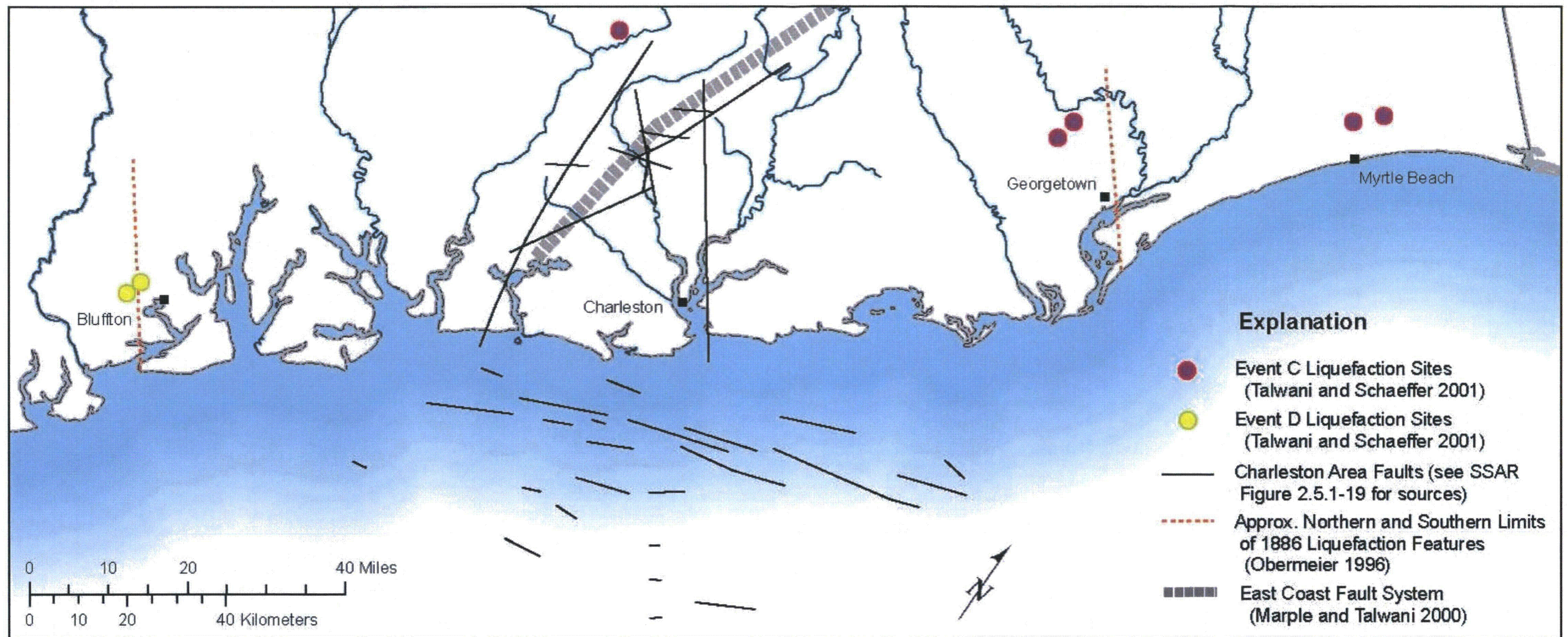
The geographic distributions of paleoliquefaction sites and the 1-sigma age estimates for Events C and D suggest these events may be separate, moderate magnitude (~M 6) events (Talwani and Schaeffer 2001). The liquefaction sites for Events C and D are localized and show no spatial overlap, and therefore do not provide definitive geographic evidence for combining these events into a single, large Event C' (see RAI Figure 2.5.2-11 following this response). However, Talwani and Schaeffer (2001) also interpret another scenario in which Events C and D may be the same event (Event C'). Using 2-sigma age ranges for radiocarbon dates performed in the VEGP ESP study, Events C and D are indistinguishable based on timing alone.

The decision to include a single, large magnitude Event C' (instead of smaller magnitude, localized Events C and D) into the updated Charleston seismic source model used in the VEGP ESP application is based on three reasons:

1. The two-sigma reanalysis of Talwani and Schaeffer's (2001) age data performed for the VEGP ESP application indicates that the age data constraining the timing of Events C and D overlap one another and therefore the two events are indistinguishable. This observation is consistent with the interpretation of a single, large Event C'.
2. The incorporation of a single, large Event C' into the updated Charleston seismic source model is, in effect, a conservative approach. In developing a recurrence interval for large, characteristic earthquakes in the updated Charleston seismic source model, it was desirable to include the possibility that Events C and D represent a single, large earthquake. Talwani and Schaeffer's (2001) moderate-magnitude ( $\sim M 6$ ) earthquakes C and D would be eliminated from the record of large ( $M_{max}$ ) earthquakes in the updated Charleston seismic source model, thereby increasing the calculated  $M_{max}$  recurrence interval and lowering the hazard without sufficient justification.
3. The distribution of paleoliquefaction sites for Event C' is very similar to the coastal extent of liquefaction features from the 1886 earthquake. Moreover, the distribution and number of paleoliquefaction sites for Event C' are very similar to those for Events A and B, the two best-documented prehistoric events (see figure following RAI 2.5.1-11 response).

For these three reasons the updated Charleston seismic source model uses a single, large magnitude Event C' (instead of separate, moderate magnitude Events C and D).

The next revision to the ESP application will address as appropriate the information provided in this response.



RAI Figure 2.5.2-11, Liquefaction Sites for Events C', C, and D

**2.5.2-12 SSAR Section 2.5.2.2.4.3 describes the calculation of two average recurrence intervals covering two different time intervals, which are used as two recurrence branches on the logic tree. Please justify in greater detail your rationale for the weighting of the two recurrence branches on the logic tree.**

**In addition, please justify your use of these two scenarios rather than another case study (for example, ten large-magnitude earthquakes occurring at approximately regular intervals during the past 5,000 years), including its impact on the hazard calculation you could have considered.**

Response:

The calculation of average recurrence intervals for Charleston seismic source  $M_{\max}$  earthquakes performed for the VEGP ESP application is based largely on paleoliquefaction data compiled by Talwani and Schaeffer (2001). Using these data, two average recurrence intervals covering two different time intervals were calculated. The first recurrence interval is based on the most-recent ~2,000-yr record of paleoliquefaction events and is given a 0.80 weight in the logic tree. The second recurrence interval is based on the entire ~5,000-yr record of paleoliquefaction events and is given a 0.20 weight in the logic tree. The entire ~5,000-yr record and the ~2,000-yr subset were used to calculate separate recurrence intervals in order to capture varying degrees of confidence expressed by experts regarding the relative completeness of different portions of the geologic record.

The relative weighting of these two branches of the logic tree is based on a SSHAC level 2 assessment of completeness of the geologic record of paleoliquefaction events over these two time intervals. Earthquakes in the paleoliquefaction record do not occur at regular intervals, and this may be the result of “temporal clustering of seismicity, fluctuation of water levels, or their evidence having been obliterated” (Talwani and Schaeffer 2001; p. 6640). Talwani and Schaeffer (2001) consider the paleoliquefaction record to be complete for the past 2,000 yrs. Moreover, Prof. Pradeep Talwani (University of South Carolina, pers. comm. 9/8/05) and Dr. Steve Obermeier (U.S. Geological Survey [retired], pers. comm. 9/2/05) consider the 2,000-yr record to represent a complete portion of the paleoseismic record. For these reasons, the average recurrence interval calculated for the most-recent ~2,000 yr portion of the paleoseismologic record is given a relatively high weight of 0.80.

The degree of completeness for the entire ~5,000-yr record of paleoliquefaction events is uncertain. It is possible that all paleoliquefaction events in this time period have been preserved and recognized in the geologic record. Alternatively, it is possible that events are missing from the ~5,000-yr record. Average  $M_{\max}$  recurrence interval calculated from the entire ~5,000-yr record is greater (i.e., larger average inter-event time) than that calculated for the ~2,000-yr record. The decision to give less weight (0.20) to this recurrence estimate is therefore conservative.

We also considered other scenarios from which to calculate earthquake recurrence, but ultimately decided not to incorporate those that included non-conservative assumptions. For example, Talwani and Schaeffer (2001) include a scenario in which their events C and D are moderate-magnitude, local earthquakes. These moderate-magnitude earthquakes would be eliminated from the record of large ( $M_{\max}$ ) earthquakes, thereby increasing the calculated recurrence interval. This and other permutations of the paleoliquefaction record (and resulting recurrence intervals) could be included, but, if based on non-conservative assumptions, would increase the recurrence interval and lower the hazard without sufficient justification.

The given example of “ten large-magnitude earthquakes occurring at approximately regular intervals during the past 5,000 years” was not included in the model because: (1) it is permissible only if events are assumed to be missing from the geologic record, and (2) the resulting recurrence interval would be very similar to the branch of the logic tree using the ~2,000-yr paleoliquefaction record.

**2.5.2-13 SSAR Section 2.5.2.4.4 states that "the new interpretation of the Charleston source indicates that a source of the large earthquakes in the Charleston area exists with weight 1.0..." Although the UCSS update of the Charleston source zone covers a fairly large area, the weighting and source geometries give the largest hazard only inside Zone A (either 0.9 (A, B, B') or 1.0 (A, B, B', C)), which is a relatively small zone. In view of this result, provide justification for the UCSS source geometries and weighting scheme and define what is meant by the "Charleston area".**

Response:

As part of the VEGP ESP application, a SSHAC level 2 committee characterized source parameters of the Charleston seismic source. This committee assessed that the preponderance of evidence strongly supports the conclusion that the seismic source for the 1886 and prehistoric Charleston earthquakes is stationary in space. In other words, the source area that produces 1886 Charleston-type large-magnitude earthquakes is likely relatively restricted in area.

The updated Charleston seismic source model includes four potential geometries (A, B, B', and C) to represent the source area for the Charleston seismic source zone. The greatest weight is given to a localized zone (Geometry A) that completely incorporates the 1886 earthquake Modified Mercalli Intensity (MMI) X isoseismal (Bollinger 1977), the majority of identified Charleston meizoseismal-area tectonic features and inferred fault intersections, and the majority of reported 1886 liquefaction features. Outlying liquefaction features are excluded because liquefaction occurs as a result of strong ground shaking that may extend well beyond the areal extent of the tectonic source. Data describing the size and spatial distribution of paleoliquefaction features suggest prehistoric earthquakes (Events A, B, C', E, and F') were of similar magnitude and location to the 1886 Charleston earthquake, which produced liquefaction at significant distances northeast and southwest from the meizoseismal area. Lower weights are given for source geometries that envelop specific postulated tectonic features (i.e., Geometry C for the southern segment of the East Coast fault system), or for broader areal distributions that also envelop the localized zone to allow for greater uncertainty in the location and lateral extent of a fault that may have produced the 1886 Charleston earthquake.

The term “Charleston area” as used in the third sentence of the first paragraph of Section 2.5.2.4.4 is vague and the following wording is proposed for the next revision of the ESP application:

The new interpretation of the Charleston source (see Section 2.5.2.2.2) indicates that a unique source of large earthquakes exists with weight 1.0 and that large magnitude events occur with a rate of occurrence unrelated to the rate of smaller magnitudes.

The next revision to the ESP application will address as appropriate the information provided in this response.

**2.5.2-14 SSAR Section 2.5.2.2.2.4.1 states that the width of Geometry B is 80 km (50 miles). However, SSAR Figure 2.5.2-9 shows the width of Geometry B to be approximately 100 km (62 miles). Please provide the actual dimensions of Geometry B used for the UCSS.**

Response:

The reviewer is correct. The width of UCSS geometry B is 100 km as pointed out by the reviewer, not 80 km as stated in Section 2.5.2.2.2.4.1. This is a typographical error that will be corrected in the next revision of the ESP application.

**2.5.2-15 As stated in SSAR Section 2.5.2.2.2.4.1, the offshore Helena Banks fault zone was detected by multiple seismic reflection profiles. Please explain why the two seismic events (mb 3.5 and 4.4) in 2002, which occurred in the vicinity of the Helena Bank fault system, cannot be positively correlated with the fault zone, and did not demonstrate recent activity for the fault zone. Could the seismicity symbolize the reactivation of the Helena Bank fault zone?**

Response:

In 2002, two earthquakes ( $m_b$  3.5 and 4.4) occurred off the coast of South Carolina in the vicinity of the Helena Banks fault zone in an area previously devoid of seismicity. Whereas we cannot entirely rule out the possibility that the Helena Banks fault zone produced these two earthquakes, neither can we positively correlate these two earthquakes with the Helena Banks fault for the following three reasons:

1. Large uncertainty in the location of these events. Small offshore earthquakes like those in question are typically difficult to locate accurately given the asymmetric distribution of recording stations relative to the hypocenters (the instrumentation is confined to land). Positional uncertainties for earthquakes in the updated EPRI catalog are not stated, but it is likely that the horizontal uncertainties for the two 2002 offshore South Carolina earthquakes are on the order of a few miles. For this reason it is not possible to attribute these small earthquakes to any fault or faults within the Helena Banks fault zone.
2. Events do not define a swarm or lineament of seismicity that can be used to define orientation and/or geometry of any causative fault. The two 2002 earthquakes occurred in approximately the same location, therefore making it difficult to deduce an orientation for the causative fault (if, in fact, the two earthquakes were produced by the same feature).
3. Lack of focal mechanisms. Focal mechanisms, when available, can be used to help define fault orientation and sense-of-slip on the causative fault. Focal mechanisms for the events in question, however, are not available.

The lack of detailed information on these two 2002 offshore earthquakes (poor location, no focal mechanisms) and the lack of additional seismic activity in this offshore area, make it difficult to assign the Helena Banks fault zone as the causative fault. It is possible that the two 2002 earthquakes indicate reactivation of the Helena Banks fault zone, but the fact that these events cannot be positively correlated to the fault suggests otherwise. There are numerous faults in the central and eastern United States located close to a few or more poorly located, small earthquakes, but this simple and very limited spatial association has not typically led researchers to positively correlate them to specific faults and classify these faults as reactivated seismogenic structures.

**2.5.2-16 SSAR Section 2.5.2.2.2.5 discusses the Eastern Tennessee Seismic Zone (ETSZ). Please provide, electronically, the geographic coordinates defining the geometry of the Eastern Tennessee Seismic Zone (ETSZ) seismic source zones and associated seismicity parameters (including Mmax magnitude distributions) for each EPRI-SOG EST.**

Response:

None of the EPRI-SOG teams specifically defined a zone identified as “Eastern Tennessee Seismic Zone.” Each EPRI-SOG team did define one or more zones that encompass seismicity in eastern Tennessee and, in most cases, surrounding regions. These zones were as follows:

<u>Team</u>	<u>Zone number</u>	<u>Zone name</u>
Bechtel:	24	Bristol trends
	25	NY-AL lineament
	25A	NY-AL lineament (alternative)
Dames & Moore	04	Appalachian fold belt
	4A	Kinds in Appalachian fold belt
Law Engineering	17	Eastern basement
Rondout	13	So. NY-AL lineament
	25	So. Appalachians
	27	TN-VA border
Weston Geophysical	24	NY-AL Clingman
Woodward-Clyde	31	Blue Ridge comb.
	31A	Blue Ridge comb. (alternative)

The geometries for these 12 sources are included in an electronic file in Enclosure 2 to this letter labeled “252-16\_geom.txt”. Also, the maximum magnitude distributions for these sources are included in an electronic file in Enclosure 2 to this letter labeled “252-16\_mmax.xls.” We understand from a telephone conference call conducted with the NRC on March 9, 2007, that associated seismicity parameters will not be required because they are specified by degree cell within each source, and this information would be voluminous.

**2.5.2-17 SSAR Section 2.5.2.2.2.5 discusses the Eastern Tennessee Seismic Zone (ETSZ). Please justify in greater detail your rationale for not updating the ETSZ as characterized by the EPRI ESTs. In addition, please discuss how the Mmax magnitude distributions developed by each EST compare with more recent Mmax estimates by the USGS hazard model (Frankel et al. 2002) and Bollinger (1992).**

**SSAR Section 2.5.2.2.2.5 states that the ETSZ does not contribute significantly to the hazard at the VEGP site. Please explain whether and how this would change if the EST’s source zones representing the ETSZ were assigned a single Mmax of Mw 7.5. Alternatively, explain why you believe an Mmax value of Mw 7.5 with a weight of 0.5 or higher is not warranted for the ETSZ.**

Response:

The reasons for not revising the EPRI ETSZ source characterizations for the Vogtle ESP are summarized as follows:

- (1) The majority of seismicity that defines the ETSZ is beyond the 200-mi site region. The Clingman and Ocoee geophysical lineaments that define the southeastern boundary of the Ocoee block and the bulk of ETSZ seismicity lie about 170 mi and 195 mi, respectively, northwest of the VEGP site. The USGS representation of the ETSZ (Frankel et al. 1996, 2002) lies about 200 mi northwest of the VEGP site.
- (2) The revision of the Charleston seismic source recurrence from a few thousand years in the EPRI SOG model to several hundred years (based on paleoliquefaction evidence) has increased the relative contribution of the Charleston source to the VEGP site. The increase in hazard contribution from the Charleston source serves to decrease the relative contribution of more distant sources such as the ETSZ.
- (3) The largest recorded earthquake within the ETSZ is about “magnitude 4.6” (Chapman et al. 2002). The recent Fort Payne, AL earthquake of April 29, 2003 that occurred near the southwestern limit of ETSZ seismicity was also a magnitude 4.6. Unlike other zones of significant seismicity in the CEUS, there is no historic or prehistoric evidence for large magnitude events occurring in the eastern Tennessee area. Seismic sources that model earthquake activity in Charleston and New Madrid have been assigned large  $M_{max}$  values both by EPRI ESTs and more recent PSHA studies, because of the occurrence of large historical earthquakes. In addition, these areas also exhibit abundant evidence for prehistoric, large magnitude earthquakes in the form of paleoliquefaction features. Evidence documenting large earthquakes in the geologic record has yet to be found in the eastern Tennessee area. While the lack of evidence for past large events in ETSZ does not preclude large events from occurring in the future, this fact should influence the weighting of the  $M_{max}$  distribution. It is therefore logical that the  $M_{max}$  distribution for the ETSZ should have lower weights assigned to the largest magnitudes, in contrast to the Charleston and New Madrid sources, where there is a high confidence that those sources are capable of producing large events since they have occurred in the past.
- (4) The EPRI SOG maximum magnitude distributions for the ETSZ span the range of more recent assessments.

More recent estimates of maximum magnitudes for the ETSZ include Bollinger (1992) and the USGS source models for the national hazard maps (Frankel et al. 2002). In developing a source model for the Savannah River Site (SRS), Bollinger (1992) used three methods to estimate maximum magnitude by (1) determining the 1,000-year earthquake, (2) adding 1.0 magnitude increment to the maximum historical event, and (3) using fault zone area. The average of these three estimates for the ETSZ is reported by Bollinger as  $m_b$  6.45, which converts to  $M$ 6.3 using the average of three relations tabulated in the response to RAI 2.5.2-5. The fault zone dimensions included in this average were restricted to causative faults assumed to be oriented north-south and east-west within the ETSZ, parallel to measured focal mechanism nodal planes. In addition, Bollinger (1992) assumed a low probability that the dimensions of seismogenic structures within the zone may extend along the entire 300-km-long northeast trending axis of the zone, and therefore, the ETSZ could be capable of producing a New Madrid size earthquake. He defined a second ETSZ source zone of the same dimensions as the primary source and assigned an  $M_{max}$  of  $m_b$  7.35 ( $M$ 7.8). Bollinger

assigned a probability of existence of only 5% to the large magnitude ETSZ source. Therefore, the Bollinger (1992) source model for the SRS gave a significantly higher weight to a moderate magnitude  $M_{max}$  for the ETSZ. The  $M_{max}$  weighted mean for the ETSZ in his model is **M6.4**.

The USGS source model (Frankel et al. 2002) defines the ETSZ  $M_{max}$  distribution as a single magnitude of **M7.5** with a weight of 100%. This  $M_{max}$  includes no uncertainty in the distribution and implies that the ETSZ source zone will produce earthquakes greater than that assigned to the Charleston seismic source, which was given an  $M_{max}$  distribution of **M6.8** to **M7.5** (Frankel et al. 2002).

In comparison, the  $M_{max}$  distribution for EPRI ESTs range from **M4.8** to **M7.5**. The EPRI ESTs considered a broad range of  $M_{max}$  in their incorporation of multiple expert opinions and approaches for estimating  $M_{max}$ , as part of their effort, which would be considered a SSHAC Level 4 study. The EPRI magnitude range incorporates the USGS **M7.5**, albeit at a much lower weight. The 5% weighted **M7.8** by Bollinger (1992) slightly exceeds the EPRI range, but the **M6.3** value was given nearly the entire weight (95%) in his characterization of the ETSZ. This smaller magnitude is much closer to the mean magnitude (~**M6.2**) of the EPRI study.

The Trial Implementation Project (TIP) (Savy et al. 2002) also provided a broad  $M_{max}$  distribution for the ETSZ. This study was designed to provide guidance in performing PSHA for nuclear plant sites, and specifically “ways to approach the issue of uncertainty in the characterization of seismic sources and in the development of ground motion models” (Savy et al. 2002). In this study, the ETSZ was characterized using multiple source zones each having a cumulative  $M_{max}$  distribution that incorporated the opinions of five different experts. The magnitude distributions for all ETSZ source zone representations ranged from as low as **M4.5** to as high as **M7.5**, with the mode of about **M6.5** for almost each distribution (Savy et al. 2002, pages F-12 to F-19 of Appendix F). The broad distribution of the TIP study magnitude distribution for the ETSZ source zones is very similar to the EPRI distribution of **M4.8** to **M7.5**. Both of these distributions have regarded **M7.5** as the uppermost limit on  $M_{max}$  for the ETSZ.

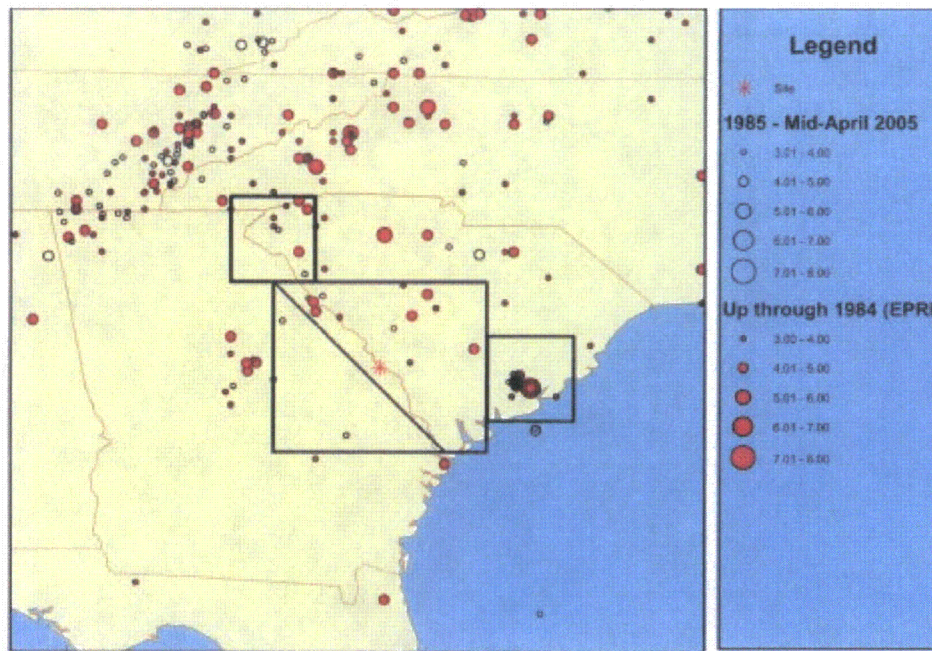
The ETSZ is characterized by abundant seismicity, but has yet to produce a recorded event greater than **M5**, which is about the minimum magnitude used to characterize seismic sources in modern PSHA studies. In our opinion, we believe that there is sufficient uncertainty in the  $M_{max}$  potential of the ETSZ that a broad range of magnitudes is appropriate and that the EPRI model sufficiently captures the range of more recent  $M_{max}$  distributions for this source. While the ETSZ may be capable of producing a **M7.5**, we do not believe that a weight of 0.5 to 1.0 for this magnitude represents the range of expert opinion reflected in the post-EPRI studies by Bollinger (1992) and Savy et al. (2002). The exception, of course, is the USGS model that assigns a single magnitude of **M7.5**.

The next revision to the ESP application will address as appropriate the information provided in this response.

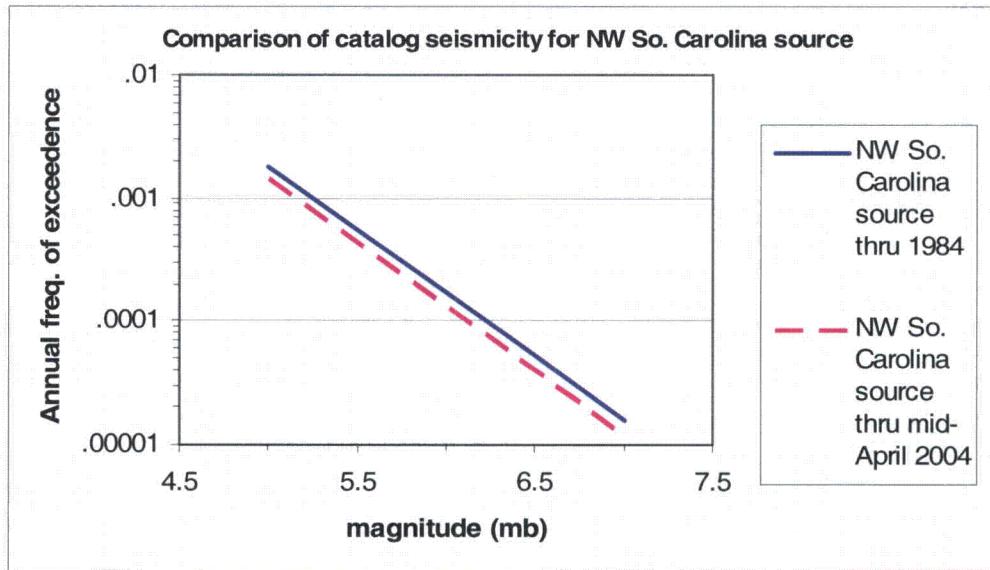
**2.5.2-18** SSAR Section 2.5.2.4.2 describes the effects of the new regional earthquake catalog. Figure 2.5.2-16 shows the two areas used to examine the effect of the new seismicity information. Please provide a justification for the geometries of the two areas.

Response:

Several areas were used to examine the effect of the new regional earthquake catalog. RAI Figure 2.5.2-18A shows those regions. All four regions showed the same result, that additional seismicity from 1985 to mid-2004 does not increase estimated activity rate in the area around the Vogtle site. As an example, RAI Figure 2.5.2-18B shows the effect of additional seismicity in the square, northwest-South Carolina source shown in RAI Figure 2.5.2-18A. The estimated activity rate decreases, similar to what is shown in SSAR Figure 2.5.2-18. We conclude that any region in South Carolina that would affect the seismic hazard of Vogtle would have estimated activity rates stay constant or decrease, if the new regional earthquake catalog were added to the analysis.



RAI Figure 2.5.2-18A: Seismicity in southeastern US, showing earthquakes in the EPRI catalog (red dots) through 1984 and additional seismicity, 1985—mid April 2004 from the updated regional earthquake catalog.



RAI Figure 2.5.2-18B: Comparison of estimate activity rates for the square source in northwest South Carolina shown in RAI Figure 2.5.2-18A, for the original EPRI catalog and including the updated regional catalog.

**2.5.2-19** SSAR Section 2.5.2.5.1 describes the development of the site amplification functions and the soil uniform hazard response spectra (UHRS) for the 10-4 and 10-5 hazard levels. Please provide a detailed step-by step discussion of the methodology used to develop the site amplification functions (i.e. Steps 1 to 6 in SSAR Section 2.5.2.5.1.1) and the 10-4 and 10-5 soil UHRS. If possible, please illustrate each step with relevant data.

In addition, please discuss the following:

- In Step 5 of SSAR Section 2.5.2.5.1.1, what does the “envelope motion” refer to?
- In Step 6, please explain why either the high- or low-frequency mean amplification factor was used instead of their envelope?
- Step 6 states that “at some intermediate frequencies between 2 and 8 Hz, the high frequency (HF) and low frequency (LF) soil amplification factors (AF) are weighted in order to achieve a smooth transition between HF and LF spectra”. Please provide more information regarding this weighting procedure.

Response:

The six steps described in Section 2.5.2.5.1 are repeated and expanded here, to provide a more detailed description of the method used to calculate soil UHS.

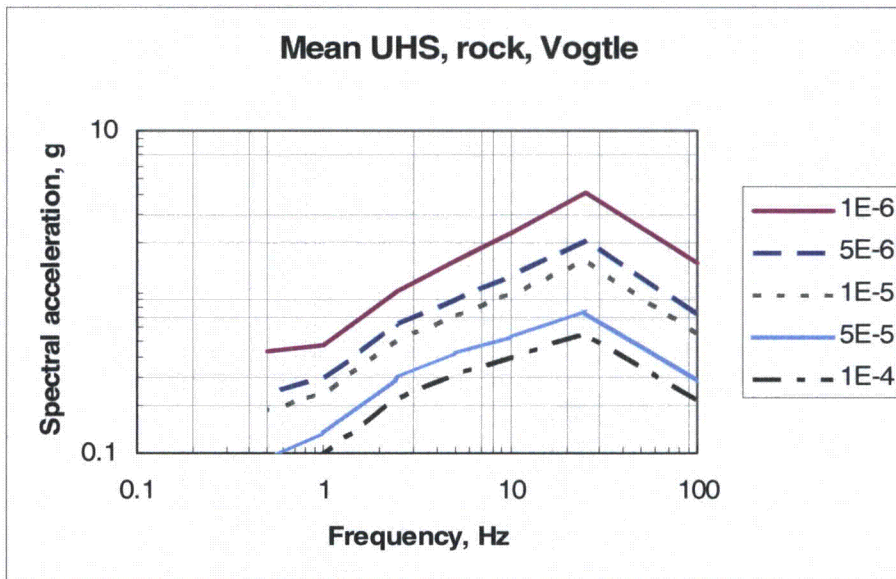
#### STEP 1: ROCK HAZARD

SECTION 2.5.2.5.1, STEP 1.: “The seismic hazard is calculated for hard rock conditions for the seven structural frequencies, over a range of ground motion amplitudes, resulting in a range of annual frequencies of exceedance.”

STEP 1: PSHA is performed for hard rock conditions for 7 structural frequencies to calculate the  $10^{-4}$ ,  $5 \times 10^{-5}$ ,  $10^{-5}$ ,  $5 \times 10^{-6}$ , and  $10^{-6}$  rock uniform hazard spectral [UHS] ordinates at the 7 frequencies. Values are reported numerically in SSAR Table 2.5.2-16 and graphically in SSAR Figure 2.5.2-21, repeated here:

RAI Table 2.5.2-16 Hard Rock Mean UHS Results (in g) for VEGP ESP

Mean annual frequency of exceedance	Spectral frequency						
	PGA	25 Hz	10 Hz	5 Hz	2.5 Hz	1 Hz	0.5 Hz
$10^{-4}$	0.214	0.551	0.399	0.317	0.223	0.101	0.0653
$5 \times 10^{-5}$	0.288	0.762	0.532	0.412	0.294	0.134	0.0924
$10^{-5}$	0.559	1.54	0.983	0.728	0.512	0.235	0.185
$5 \times 10^{-6}$	0.747	2.06	1.28	0.914	0.635	0.294	0.241
$10^{-6}$	1.48	4.09	2.33	1.54	1.02	0.465	0.423



SSAR Figure 2.5.2-21 Mean Uniform Hazard Spectra, Hard Rock Conditions, for VEGP ESP

**STEP 2: DEAGGREGATION**

SECTION 2.5.2.5.1, STEP 2: “For ground motion amplitudes corresponding to annual frequencies of  $10^{-4}$ ,  $10^{-5}$ , and  $10^{-6}$ , the seismic hazard is deaggregated for high frequencies (HF) and low frequencies (LF), as described in Section 2.5.2.4.6, to determine the dominant magnitudes and distances for those amplitudes and frequencies.”

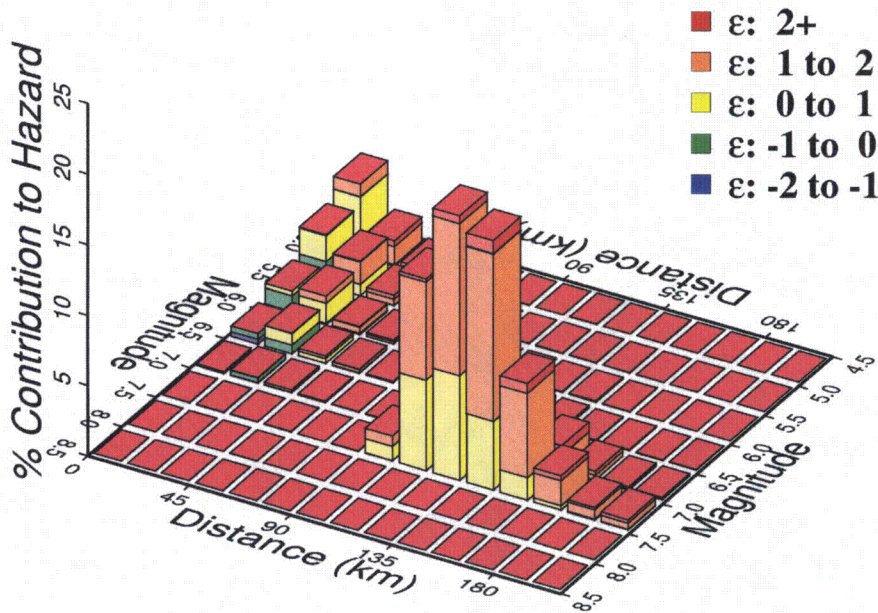
STEP 2. Using the guidance of Appendix E of Reg. Guide 1.165 [RG1.165], determine the mean magnitude  $M_{bar}$  and mean distance  $D_{bar}$  of earthquakes contributing to the hazard for ground motions with mean annual frequencies of exceedance (MAFE) of  $10^{-4}$ ,  $10^{-5}$ , and  $10^{-6}$  for 1 & 2.5 Hz [LF] (combined deaggregation) and for 5 & 10 Hz [HF] (combined deaggregation). These values of  $M_{bar}$  and  $D_{bar}$  are similar enough that one set of  $M_{bar}$  and  $D_{bar}$  values can be used for LF and one set can be used for HF. Results for the 3 MAFEs are shown in SSAR Table 2.5.2-17, repeated below, along with the recommended values. The recommended values were chosen to be central values that represent results for the 3 MAFEs, using 2 significant figures. SSAR Figure 2.5.2-22, also repeated below, shows that

these value of Mbar and Dbar capture the small, nearby earthquakes and large, distant earthquakes that contribute to the hazard.

SSAR Table 2.5.2-17, Computed and Recommended Mbar and Dbar Values Used for Development of High and Low Frequency Target Spectra

<i>High Frequency (5-10 Hz)</i>				
	$10^{-4}$	$10^{-5}$	$10^{-6}$	Recommended Values
<b>Mbar (Mw)</b>	5.6	5.6	5.7	5.6
<b>Dbar (km)</b>	17.6	11.4	9.0	12
<i>Low Frequency (1-2.5 Hz)</i>				
	$10^{-4}$	$10^{-5}$	$10^{-6}$	Recommended Values
<b>Mbar (Mw)</b>	7.2	7.2	7.2	7.2
<b>Dbar (km)</b>	136.5	134.3	133.0	130

**High Frequency, 1.0e-4**

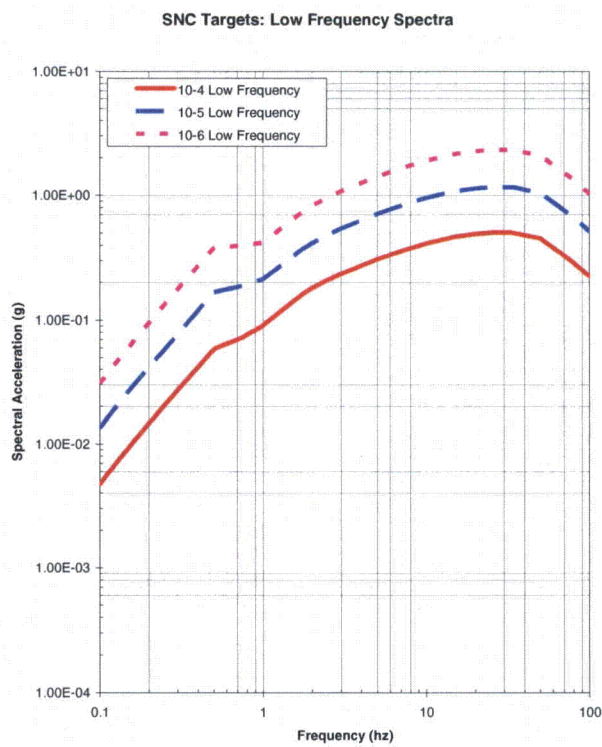
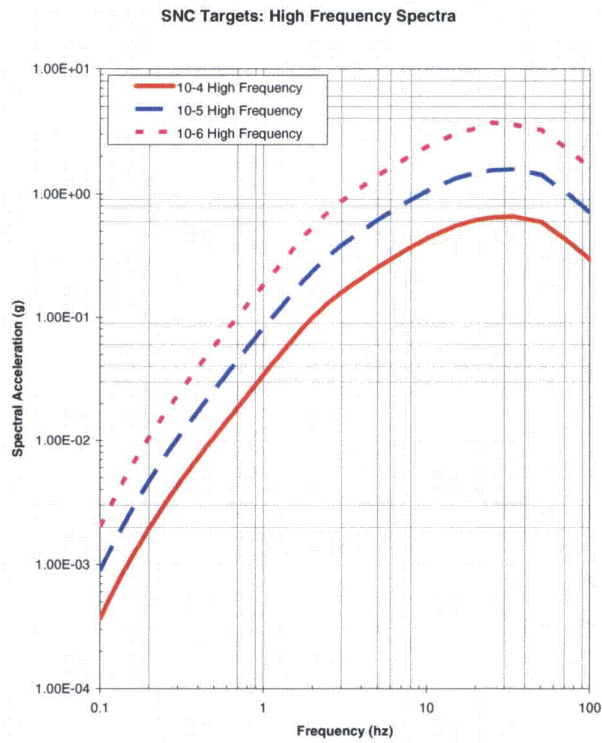


SSAR Figure 2.5.2-22 Magnitude-Distance Deaggregation for High Frequencies,  $10^{-4}$  Mean Annual Frequency of Exceedance

STEP 3: ROCK SPECTRA

SECTION 2.5.2.5.1, STEP 3.: “HF hard rock spectra are developed to represent earthquakes dominating the 5-10 Hz ground motions, and LF hard rock spectra are developed to represent earthquakes dominating the 1-2.5 Hz ground motions. These hard rock spectra represent the mean magnitude and distance of earthquakes that dominate the seismic hazard for those structural frequencies.”

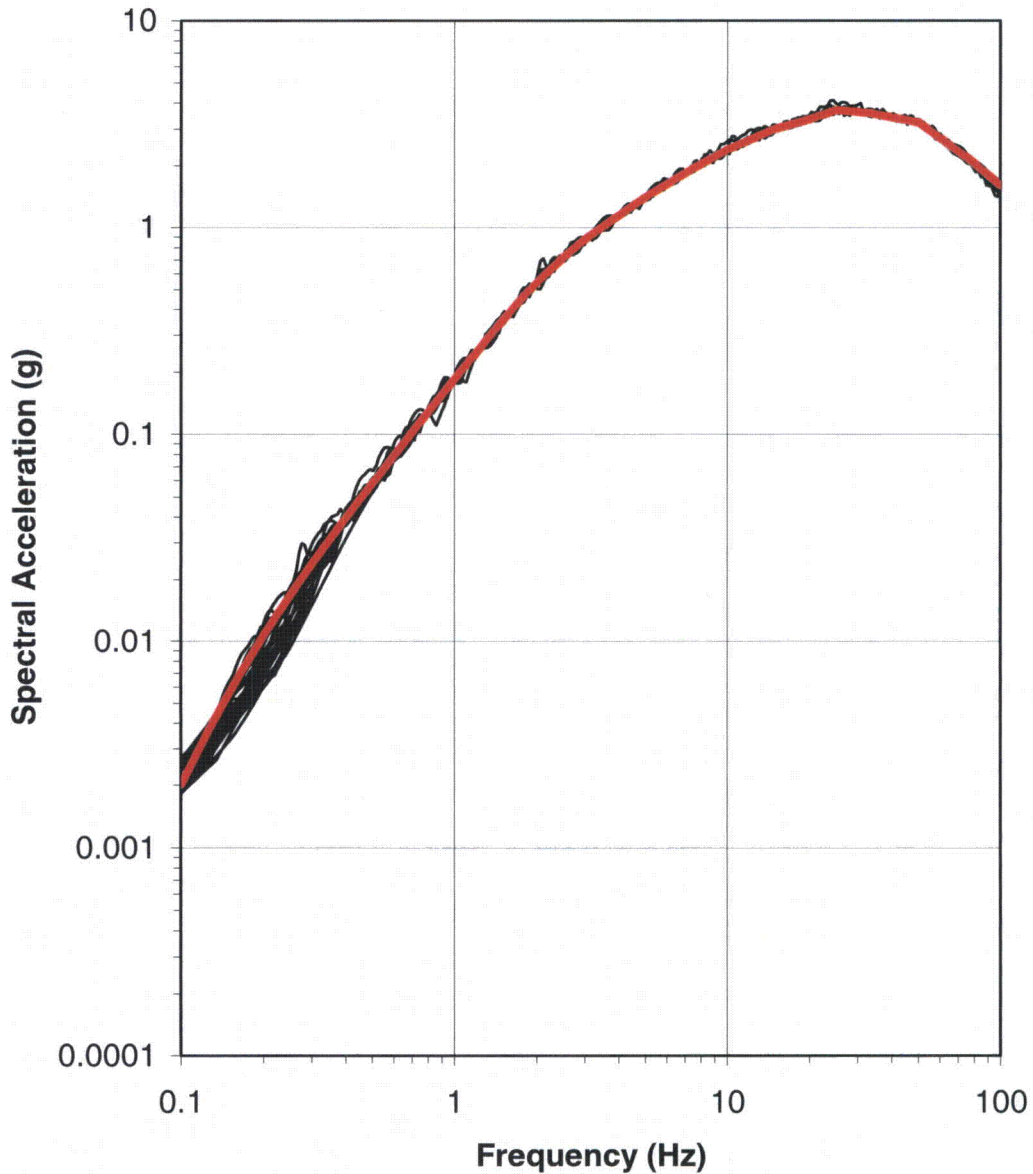
STEP 3A: Use the Mbar and Dbar values from Step 2 to generate HF and LF hard rock spectral shapes using the recommended shapes in NUREG/CR-6728. Following Reg. Guide 1.165, scale the HF spectral shapes to match the 7.5 Hz spectral acceleration equal to the linear average of the spectral accelerations at 5 and 10 Hz for each of the three MAFEs. Similarly, scale the LF spectral shapes to match the 1.75 Hz spectral acceleration equal to the linear average of the spectral accelerations at 1 and 2.5 Hz for each of the three annual frequency levels. This step results in smooth spectra for each of the three MAFEs. The spectra are illustrated in SSAR Figure 2.5.2-35, repeated below.



SSAR Figure 2.5.2-35 High and Low-Frequency Target Spectra for the Three Annual Probability Levels of  $10^{-4}$ ,  $10^{-5}$ , and  $10^{-6}$

STEP 3B. The spectra from Step 3A are used as target spectra to spectrally match 30 time histories for each frequency band [HF and LF] and each MAFE [ $10^{-4}$ ,  $10^{-5}$ , and  $10^{-6}$ ], resulting in 180 time histories. This step is illustrated for HF and a MAFE of  $10^{-6}$  in SSAR Figure 2.5.2-36a, repeated below.

Spectral-Matched Time History Spectra: RP6HF



SSAR Figure 2.5.2-36a, High Frequency ( $10^{-6}$ ) Match for the 30 Time Histories

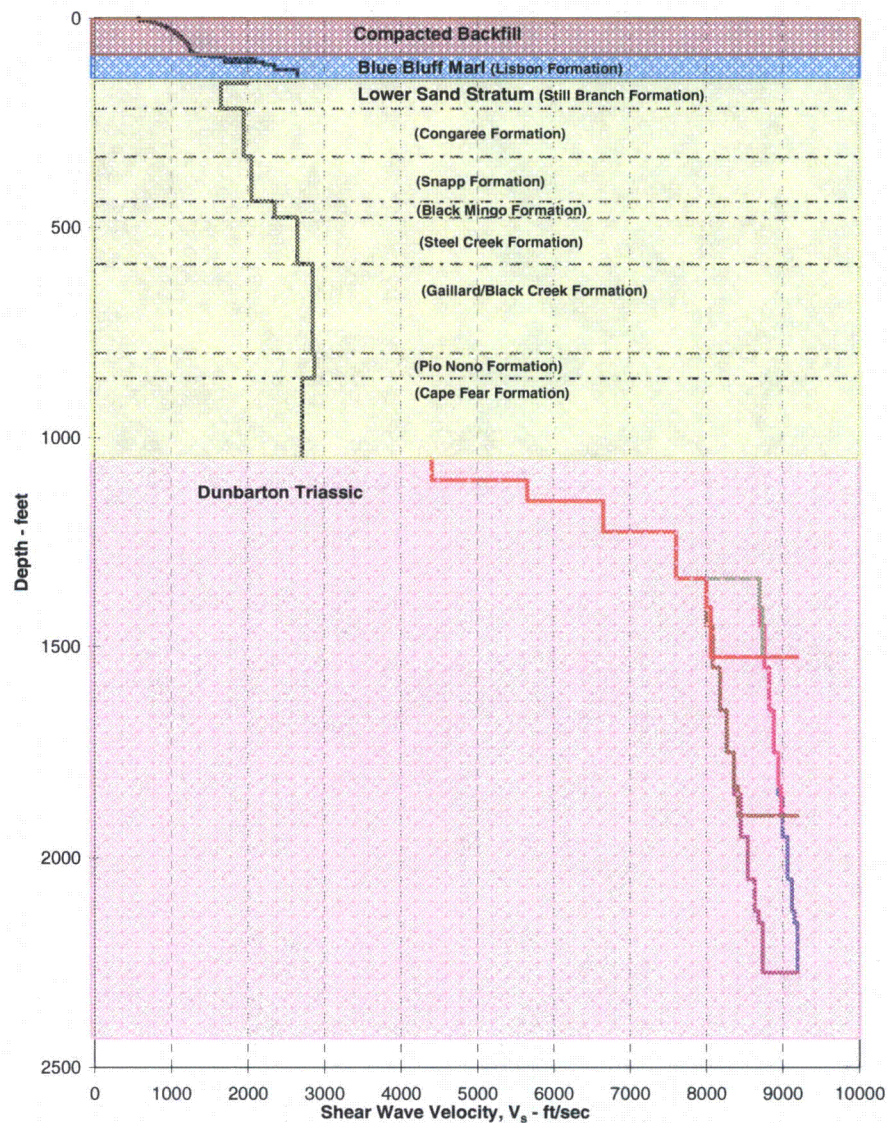
Note: Heavy red line is the target spectrum and thin black lines are the individual matches.

STEP 4: CALCULATE SOIL AMPLIFICATION

SECTION 2.5.2.5.1, STEP 4. "The rock and soil column is modeled, and soil amplitudes are calculated at the control point elevation for input hard rock motions corresponding to frequencies of exceedance of

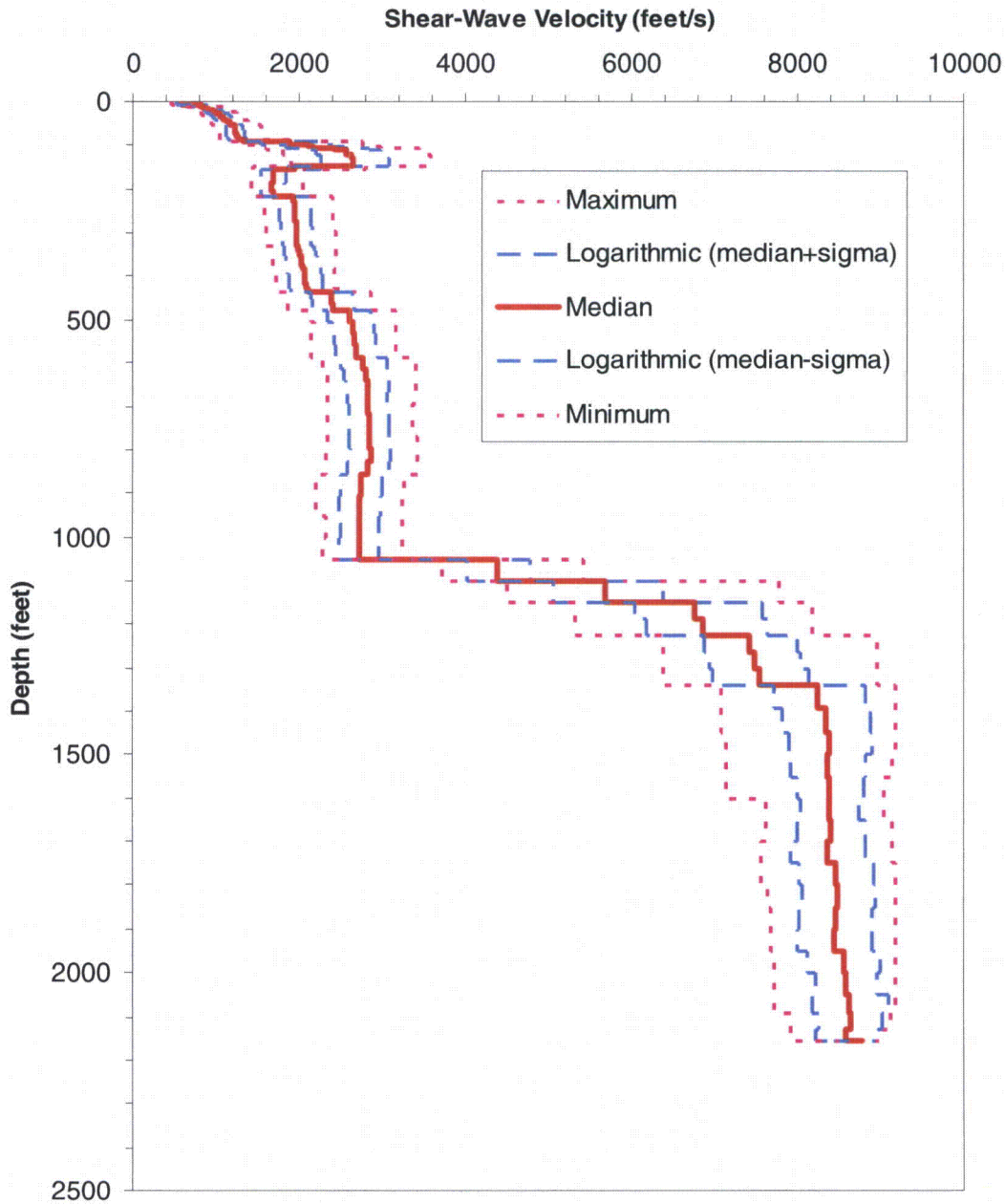
10-4, 10-5, and 10-6. These calculations are made separately for ground motions dominating the HF hard rock motion and the LF hard rock motion, and the input motions have a spectrum determined by the HF or LF hard rock spectral shape, as appropriate. Multiple hard rock motions are used, and multiple soil column properties are used, so that the mean soil amplitudes can be determined accurately.”

STEP 4A: Mean soil/rock column characteristics are determined using both EPRI and SRS material curves. These soil/rock characteristics are shear-wave velocity, stiffness, and damping (the latter two are specified for each layer as a function of soil strain). The soil/rock column is modeled to a depth at which the rock shear-wave velocity equals 9200 fps. SSAR Figure 2.5.4-7 below illustrates one of the mean shear-wave velocity profiles vs. depth.



SSAR Figure 2.5.4-7 – Shear Wave Velocity for SHAKE Analysis

**STEP 4B:** Soil and rock column characteristics (shear-wave velocities vs. depth, stiffness, and damping vs. soil strain for each layer) are randomized accounting for estimated uncertainties in each characteristic and for correlation in characteristics among adjacent layers. Using simulation, 60 soil/rock column characteristics are generated for the EPRI mean material curves, and 60 characteristics are generated for the SRS mean material curves. SSAR Figure 2.5.2-34, repeated below, illustrates the median, median  $\pm$  sigma, and maximum/minimum shear-wave velocities vs. depth for one set of the simulated shear-wave velocities.



SSAR Figure 2.5.2-34 Summary Statistics Calculated from the 60 Shear-Wave Velocity Profiles

Note: Statistics do not include the velocities on the crystalline bedrock.

STEP 4C: The dynamic site response to shaking is calculated using software SHAKE for each of the spectrally matched time histories from Step 3B and each set of soil characteristics from step 4B. In addition to the time histories derived for the 3 MAFEs indicated in Step 3B, an additional set of low-motion time histories was defined to represent linear soil/rock behavior at 5% of the  $10^{-4}$  ground motion. SHAKE analyses were conducted for 300 structural frequencies between 0.1 Hz and 100 Hz, at three horizons with depths of 0, 40, and 86 feet. This step consists of 960 SHAKE analyses, as follows:

Ground motion levels [low, $10^{-4}$ , $10^{-5}$ , and $10^{-6}$ ]	4
Frequency bands [HF and LF target spectra]	× 2
Material curve models [EPRI and SRS]	× 2
60 randomized soil/rock columns	× 60
Total SHAKE analyses:	960

For the SHAKE analyses, each of the 30 time histories from Step 3B is randomly paired with 2 of the randomized soil/rock columns, to achieve a random group of 60 input motions and soil/rock characteristics. Each SHAKE analysis produces amplification results at the 3 depths.

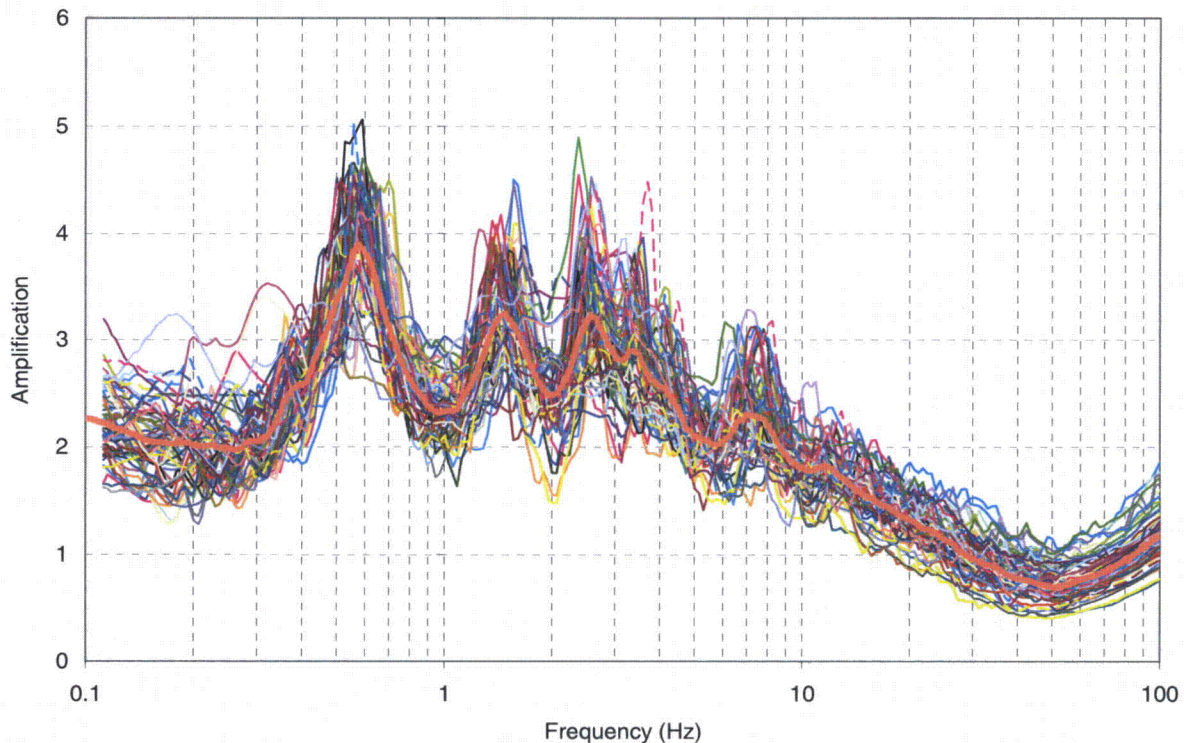
STEP 5: SOIL AMPLIFICATION FACTORS

SSAR 2.5.2.5.1, STEP 5: “The soil amplification factors (AFs) are developed at 300 frequencies using analyses described in this section based on the HF and LF hard rock spectral shapes. The AFs represent the mean spectral acceleration (SA) at the control point, divided by input SA at hard rock, at each frequency. At each frequency, the envelope motion is determined. This is the motion (HF or LF) that gives the higher mean soil motion, for that structural frequency and MAFE. At frequencies above 8 Hz, this is always the HF motion. At frequencies below 2 Hz, this is always the LF motion. At intermediate frequencies, the envelope motion depends on the frequency and the MAFE.”

STEP 5A: The mean and standard deviation of amplification factors [AFs] (soil SA divided by rock SA at each of the 300 structural frequencies) is calculated using the 60 randomized sets of soil/rock characteristics. (Means and standard deviations are calculated logarithmically.) This results in 48 sets of mean AFs (one set being for the 300 structural frequencies), as follows:

Ground motion levels [low, $10^{-4}$ , $10^{-5}$ , and $10^{-6}$ ]	4
Frequency bands [HF and LF target spectra]	× 2
Material curve models [EPRI and SRS]	× 2
Depth horizons [0, 40, and 86 feet]	× 3
Total sets of mean AFs:	48

SSAR Figure 2.5.2-37, repeated below, illustrates the 60 individual AFs and the mean AF across the frequency range of 0.1 Hz to 100 Hz, for the 10-4 MAFE, HF input, EPRI mean material curves, and 86' depth.



SSAR Figure 2.5.2-37 Typical Results of Spectral Amplification at 86-ft Depth (Top of Blue Bluff Marl) Using EPRI Degradation Curves for High Frequency Time Histories of 10-4 MAFE Input Motion Level

STEP 5B: The mean AFs for the EPRI and SRS material curves are equally weighted, to give 8 mean AFs across the frequency range 0.1 Hz to 100 Hz, for each depth. These 8 mean AFs correspond to the 4 ground motion levels and to the HF and LF input motions.

STEP 5C: The controlling HF or LF input motion is determined over the frequency range 0.1 Hz to 100 Hz for each MAFE, by examining the envelope of soil response to the HF and LF rock motion. Note from Figure 2.5.2-35 (in the SSAR and above) that, at high frequencies, the HF rock input motion exceeds the LF rock input motion. At low frequencies, the reverse is true. This means that the HF input motion will control the high frequencies (above 8 Hz) and the LF input motion will control the low frequencies (below 2 Hz). In between, the controlling motion depends on the MAFE and the frequency. This step results in one set of mean AFs (across the frequency range 0.1 Hz to 100 Hz) for each MAFE and for each depth horizon.

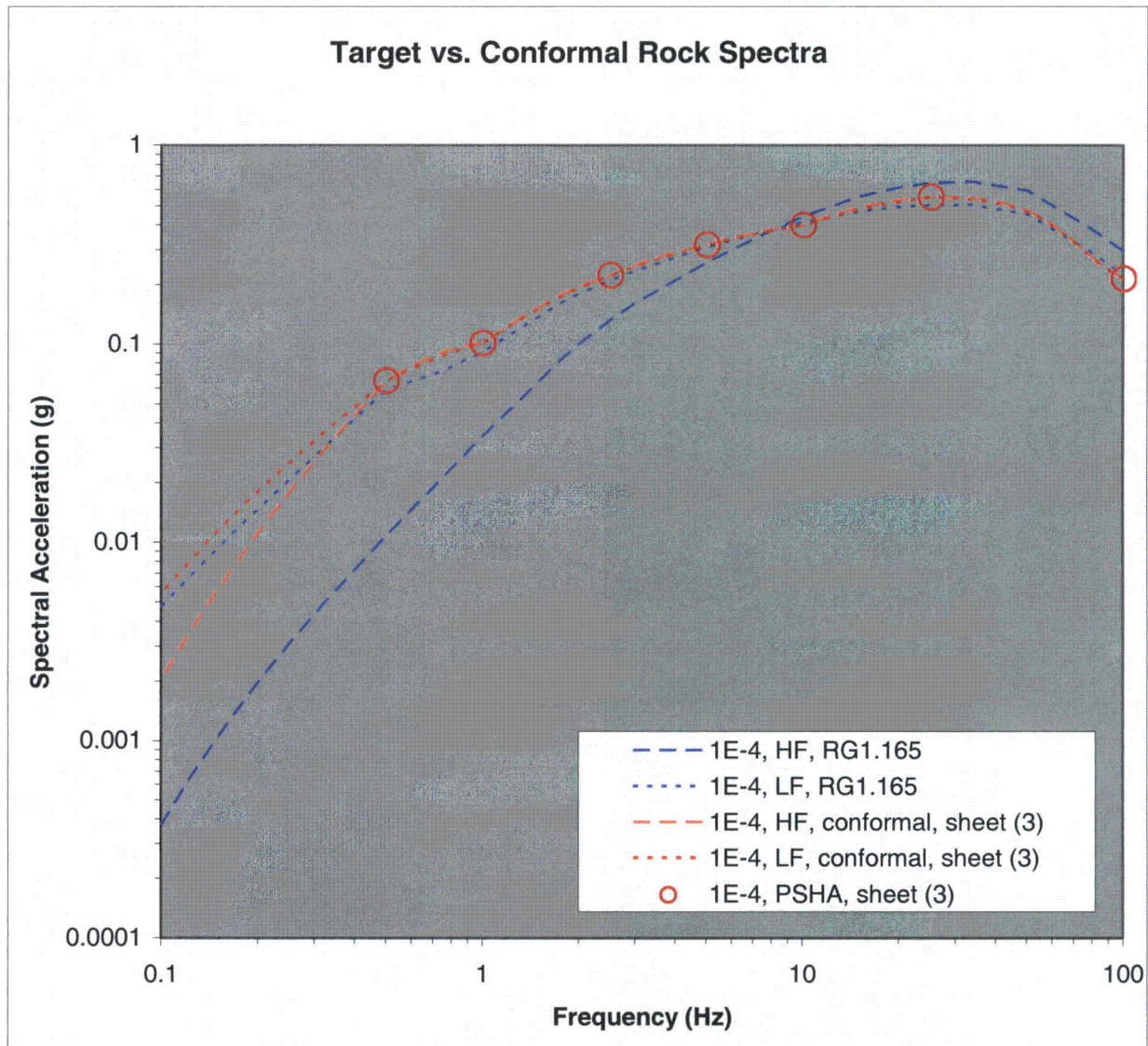
#### STEP 6: CALCULATE SOIL UHS

SSAR Step 6: "The uniform hazard response spectra at MAFEs of 10-4 and 10-5 at the control point location are calculated as follows. Starting from the 10-4 and 10-5 SA hard rock values (from the hazard calculations described in 2.5.2.4) at the seven structural frequencies, interpolation is performed between those SA values to obtain 10-4 and 10-5 SA values at the 300 structural frequencies using the HF and LF spectral shapes for hard rock. The choice of HF or LF is based on the envelope motion determined in the previous step. The UHS for 10-4 at the control point location is calculated by multiplying the hard rock 10-4 SA values at the 300 frequencies by the mean AFs for 10-4 from step 5, again using the HF or LF mean AF corresponding to the envelope motion. (At some intermediate frequencies between 2 and 8 Hz,

the HF and LF AFs are weighted in order to achieve a smooth transition between HF and LF spectra.) The UHS for 10-5 is calculated in a similar way, using the 10-5 rock SA values and the 10-5 AFs.”

STEP 6A: Similar to Step 3A, use rock spectral shapes recommended in NUREG/CR-6728 to develop rock spectra for the HF and LF controlling earthquakes. In this step, however, the rock spectra are adjusted to equal the 7 PSHA structural frequencies at the 3 MAFEs of interest (10-4, 10-5, and 10-6). The spectral shapes are used to interpolate between these frequencies, and to extrapolate below 0.5 Hz. Because both the HF and LF spectra are constrained to equal the 7 PSHA structural frequencies at the 3 MAFEs of interest, the resulting HF and LF spectral shapes are similar, particularly at high frequencies, and a single continuous rock spectrum is derived from 0.1 Hz to 100 Hz that equals the 7 PSHA structural frequencies at the 3 MAFEs of interest. RAI Figure 2.5.2-19 illustrates the “conformal” HF and LF spectra (the red curves) compared to the RG1.165 spectra from Step 3A (the blue curves).

Constraining the rock spectra in this step to equal the amplitudes at the 7 structural frequencies at which the PSHA was calculated ensures that the proper rock motion at each structural frequency will be used to calculate the soil amplitude, for that MAFE.



RAI Figure 2.5.2-19 Rock spectra (red curves) conformed to equal PSHA results (circles), compared to rock spectra scaled at 1.75 Hz and 7.5 Hz according to RG1.165.

STEP 6B: Multiply the rock spectra for each MAFE from Step 6A, times the mean AFs from Step 5C, at each frequency in the range 0.1 Hz to 100 Hz, to calculate soil UHS for each MAFE. At frequencies above 8 Hz, this spectrum is controlled by the HF AFs. At frequencies below 2 Hz, this spectrum is controlled by the LF AFs. At intermediate frequencies (5 to 8 Hz for 10-4, 4 to 6 Hz for 10-5, and 2 to 5 Hz for 10-6) a weighted average of HF and LF spectra is used to achieve a smooth transition between the HF and LF parts of the spectrum.

**SUMMARY**

The above 6 steps summarize the calculation of soil UHS for each depth. These soil spectra are used to develop the depth-specific DRS.

**2.5.2-20 SSAR Section 2.5.2.5.1.3 describes the development of low- and high- frequency target spectra using the average of the single and double corner source models from NUREG/CR-6728. Please explain why the 2004 EPRI (EPRI 1009684 2004) ground motion models were not used instead.**

Response:

The 2004 EPRI ground motion report (EPRI 1009684) gives equations to estimate spectral acceleration at 7 structural frequencies (100, 25, 10, 5, 2.5, 1, and 0.5 Hz). To properly represent rock motion for input to a site response analysis, it is necessary to interpolate between these 7 structural frequencies to obtain a realistic spectral shape, rather than using linear interpolation. For this task, NUREG/CR-6728 was used, because one of its goals was specifically to develop realistic spectral shapes for the eastern US to use in earthquake ground motion analyses.

**2.5.2-21 SSAR Table 2.5.2-17 and Section 2.5.2.5.1.3 provides the computed and recommended Mbar and Dbar values used for the development of the high- and low-frequency target response spectra. Please explain how the “recommended” Dbar and Mbar values were calculated.**

Response:

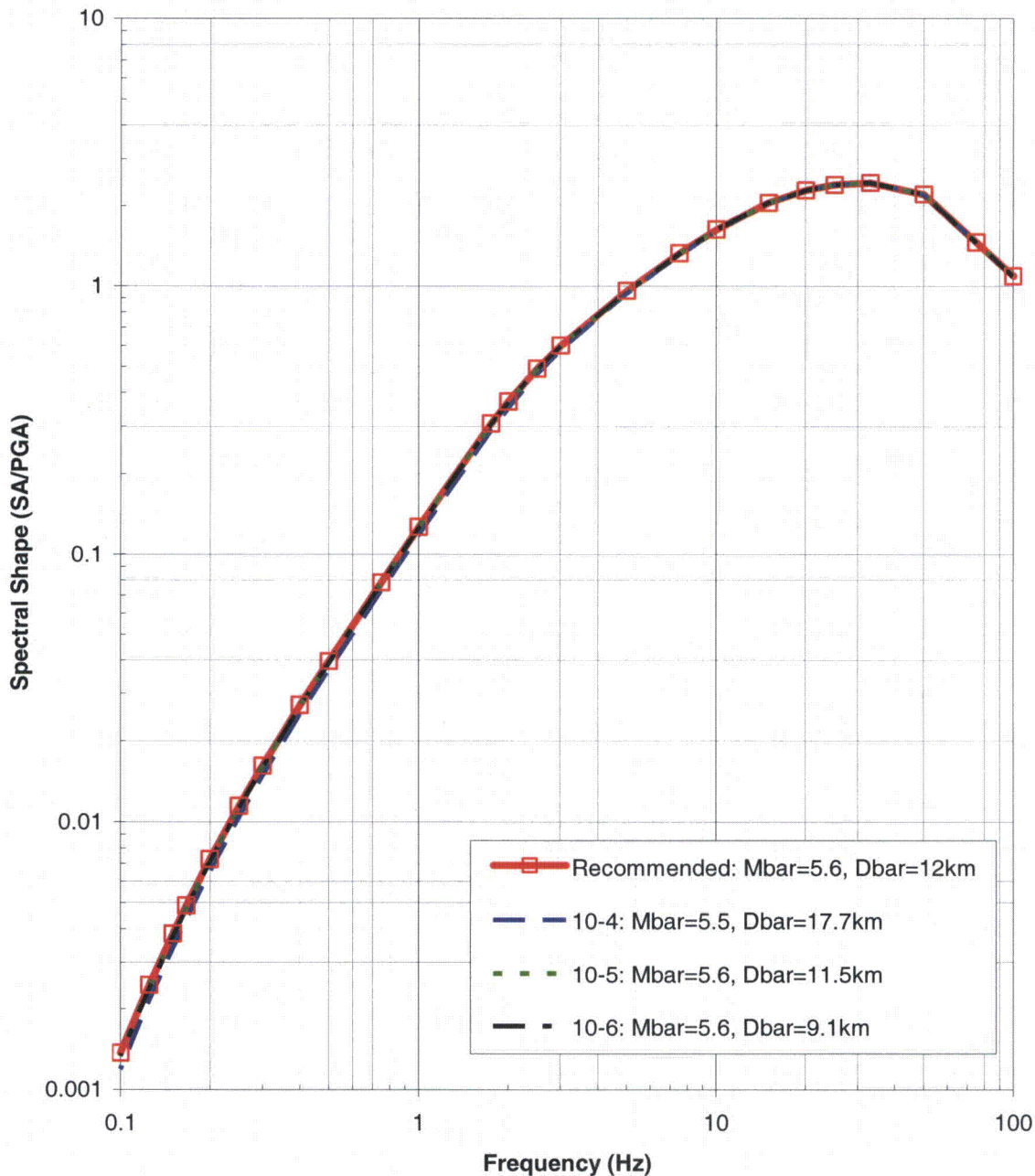
Mean magnitude (Mbar) and distance (Dbar) values were computed for three annual probability levels:  $1 \times 10^{-4}$ ,  $1 \times 10^{-5}$ , and  $1 \times 10^{-6}$  based on the seismic hazard curves for both the high- and low-frequency cases. Table 2.5.2-17 of the SSAR lists these values along with the recommended magnitude and distance values used in the analysis. These recommended values were selected such that they approximately represent the range in Mbar and Dbar values computed for the three annual probability levels for both the high- and low-frequency cases based on the bi-modal distribution of the deaggregation. These recommended values were not computed based on a statistical average or otherwise from the explicit values for each of the three annual probability levels. For the low frequency case, the recommended distance value was assigned of distance of 130 km based on the source to site distance for the Charleston source. For the high frequency case, the recommended distance is approximately equal to the log-average of the three computed values rounded to the nearest km. The recommended magnitude values for both the high- and low-frequency cases is equal to the linear average of the three magnitude values rounded to the nearest tenth of a magnitude unit.

These recommended Mbar and Dbar values were used to simplify the analysis, rather than the computed values at the three annual probability levels, for the development of the corresponding target spectra and to a lesser extent in the time history selection procedure for the site response analysis. RAI Figure 2.5.2-21a shows the difference in spectral shapes for the high-frequency case using the recommended magnitude and distance values and the computed magnitude and distance values for the three annual probability levels. The same comparison is presented in RAI Figure 2.5.21b for the low-frequency case. Based on these comparison plots, the use of the recommended magnitude and distance values in place of the computed magnitude and distance values for each of the three annual probability levels would not significantly change the results of the site response analysis.

The recommended magnitude and distance values were also used as guides in selecting the seed input time histories for the spectral matching analysis associated with the site response analysis. Based on the selection of time histories which fall within a given magnitude and distance range and the similarity between the recommended and computed magnitude and distance values, the use of the recommended values would not change the selected time histories used in the site response analysis.

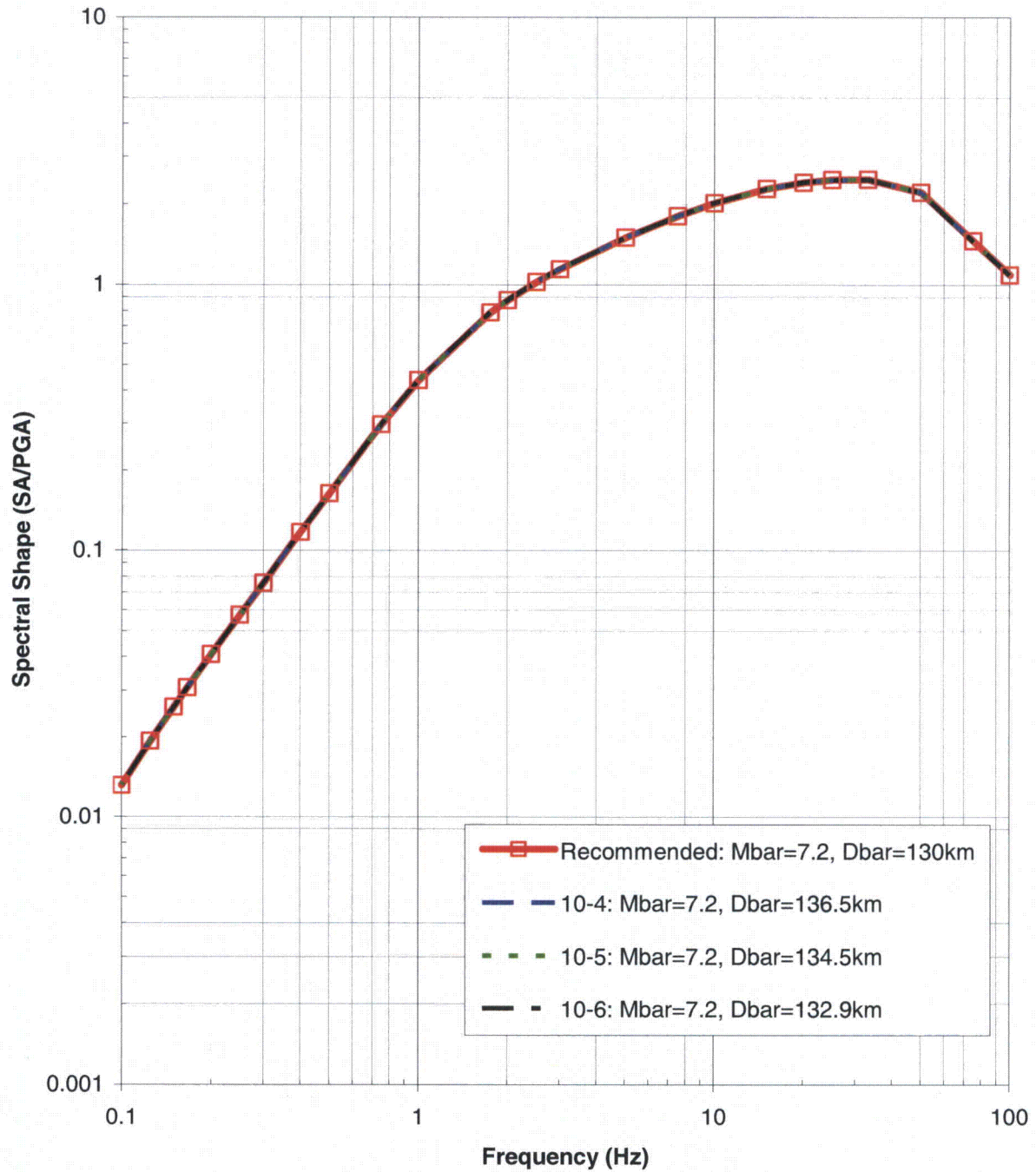
The next revision to the ESP application will address as appropriate the information provided in this response.

### SNC (High Frequency): NUREG CR-6728 Spectral Shapes



RAI Figure 2.5.2-21a Comparison between high-frequency spectral shapes using the recommended magnitude and distance values and the computed magnitude and distance values for the three annual probability levels of  $1 \times 10^{-4}$ ,  $1 \times 10^{-5}$ , and  $1 \times 10^{-6}$ .

### SNC (Low Frequency): NUREG CR-6728 Spectral Shapes



RAI Figure 2.5.2-21b. Comparison between low-frequency spectral shapes using the recommended magnitude and distance values and the computed magnitude and distance values for the three annual probability levels of  $1 \times 10^{-4}$ ,  $1 \times 10^{-5}$ , and  $1 \times 10^{-6}$ .

**2.5.2-22 SSAR Section 2.5.2.5.1.4 describes the spectral matching of the selected seed time histories to the target response spectra and states that the “spectral matching criteria given in NUREG/CR-6728 (McGuire et al. 2001) were used to check the average spectrum from the 30 time histories for a given frequency range (high- or low-frequency) and annual probability level. This is the recommended procedure in NUREG/CR-6728 (McGuire et al. 2001) when multiple time histories are being generated and used.” In addition, Section 2.5.2.5.1.5 states that “Each of the 60 randomized soil profiles were paired with 30 seed time histories (each time history was applied to two of the randomized soil profiles)”.**

**Please provide a justification for not using the criteria provided in NUREG/CR-6728 to check each individual time history against the target spectrum.**

Response:

For the site response analysis a total of 30 acceleration horizontal time histories were modified to be spectrum compatible to given target spectrum. Target spectra were developed for both the high- and low-frequency cases at each of the three annual probability levels:  $1 \times 10^{-4}$ ,  $1 \times 10^{-5}$ , and  $1 \times 10^{-6}$ . This resulted in a total of 180 spectrum compatible acceleration time histories for the site response analysis. For a given suite of 30 time histories, the spectral matching criteria given in NUREG CR-6728 were followed. Specifically, item (e) of the general criteria recommended for evaluating the adequacy of the artificially developed ground motions states,

“(e) The computed 5% damped response spectrum of the artificial ground motion (if one motion is used for analysis) or the mean of the 5% damped response spectra (if a suite of motion is used for the analysis) should not exceed the target spectrum at any frequency by more than 30% (a factor of 1.3) in the frequency range between 0.2 Hz and 25 Hz.”

The average site response amplification factors were developed for each given suite of 30 input spectrum compatible time histories (i.e., given high- or low-frequency case for a given annual probability level) and the 60 randomized soil profiles. Based on this use of multiple time histories matched to the same target spectrum for the site response analysis and the criteria given in NUREG CR-6728 and listed above, the compliance between the average response spectrum from a given set of 30 input spectrum compatible time histories and the respective target spectrum was checked rather than the individual 30 spectrum compatible time histories to the target spectrum.

The next revision to the ESP application will address as appropriate the information provided in this response.

**2.5.2-23 SSAR Section 2.5.2.5.1.5 describes the results of the site response calculations for the ESP site. Please discuss the results of site response calculations in terms of the following:**

- a. The effects of the six alternative site response profiles in terms of the different depths to the top of the Paleozoic crystalline rocks.**
- b. The possible effects of the Pen Branch fault zone (i.e. as a low velocity zone or weak zone).**
- c. The effects of the low velocity zones within the Blue Bluff Marl and Lower Sand Stratum.**

**In addition, please justify the adequacy of using an equivalent-linear approach rather than a nonlinear approach to model site response at the ESP site.**

Response:

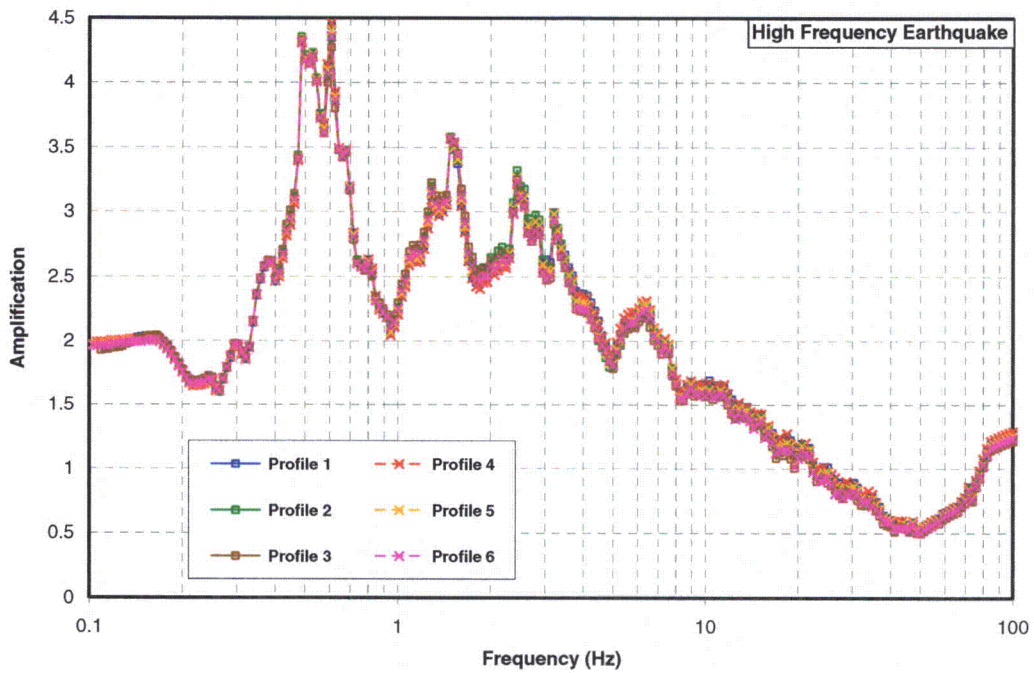
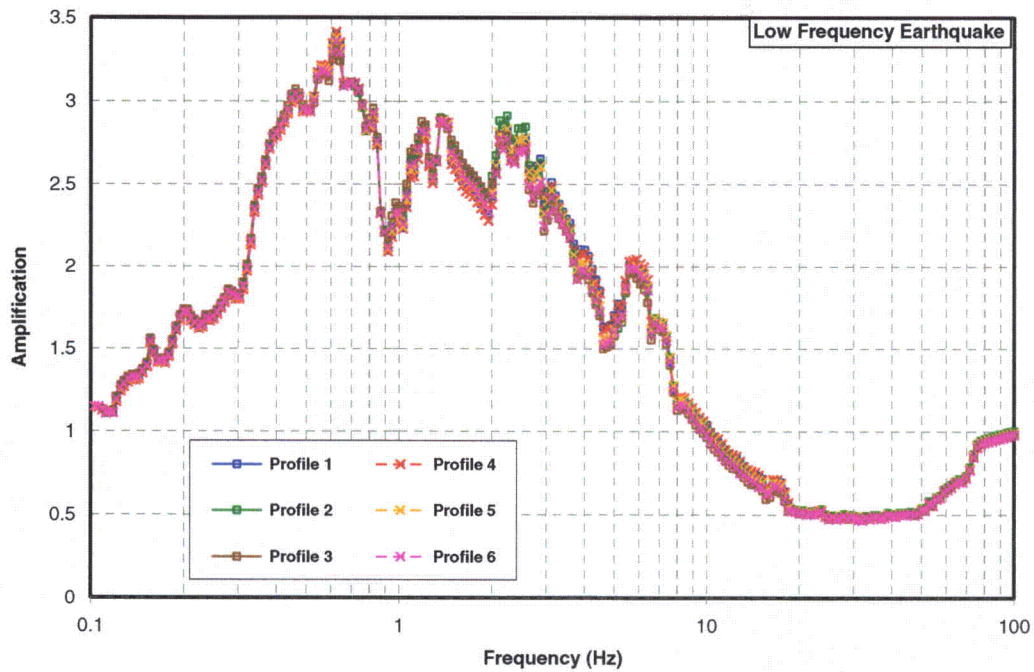
The site response analyses of the ESP site used six base profiles to represent the properties of the rock strata located below depth of 1049 ft. RAI Table 2.5.2-23A below presents the rock shear velocity profiles:

RAI Table 2.5.2-23A. ESP Site Base Profiles - Rock Shear Velocities

Top of Layer Depth (ft)	Vs (fps)		Top of Layer Depth (ft)	Vs (fps)		Top of Layer Depth (ft)	Vs (fps)	
	Prof. 1	Prof. 4		Prof. 2	Prof. 5		Prof. 3	Prof. 6
1049	4400	4400	1049	4400	4400	1049	4400	4400
1100	5650	5650	1100	5650	5650	1100	5650	5650
1150	6650	6650	1150	6650	6650	1150	6650	6650
1225	7600	7600	1225	7600	7600	1225	7600	7600
1338	8000	8700	1338	8000	8700	1338	8000	8700
1405	8059	8739	1450	8090	8760	1450	8090	8760
<b>1525</b>	9200	9200	1550	8180	8820	1550	8180	8820
			1650	8270	8880	1650	8270	8880
			1750	8360	8940	1750	8360	8940
			1830	8414	8976	1850	8450	9000
			<b>1900</b>	9200	9200	1950	8540	9060
						2050	8630	9120
						2128	8679.5	9153
						2155	8733.5	9189
						<b>2275</b>	9200	9200

This table is similar to SSAR Table 2.5.4-11 Part B. The profiles are grouped in three pairs with each pair of profiles having the crystalline rock at different depth (1525 ft for profiles 1 and 4, 1900 ft for profiles 2 and 5 and 2275 ft for profiles 3 and 6).

Two acceleration time histories were developed compatible with the high frequency (HF) (5-10 Hz) and low frequency (LF) (1-2.5Hz) target spectra at  $1 \times 10^{-5}$  probability level. SHAKE analyses were performed where the acceleration time histories were applied as outcrop object motion at the top of the crystalline bedrock. RAI Figure 2.5.2-23A compares the results of the SHAKE analyses of the six base profiles for the 5% damping acceleration response spectra (ARS) amplifications at the top of the Blue Marl at 86 ft depth. The small difference in the ARS amplifications indicate that the effect of the depth of the crystalline rock on the site response at 86 ft depth horizon where the SSE design motion is defined is relatively small, particularly in comparison to the variability of total [soil and rock] site response when soil/rock column model randomization and multiple time histories are considered (see SSAR Figure 2.5.2-37).



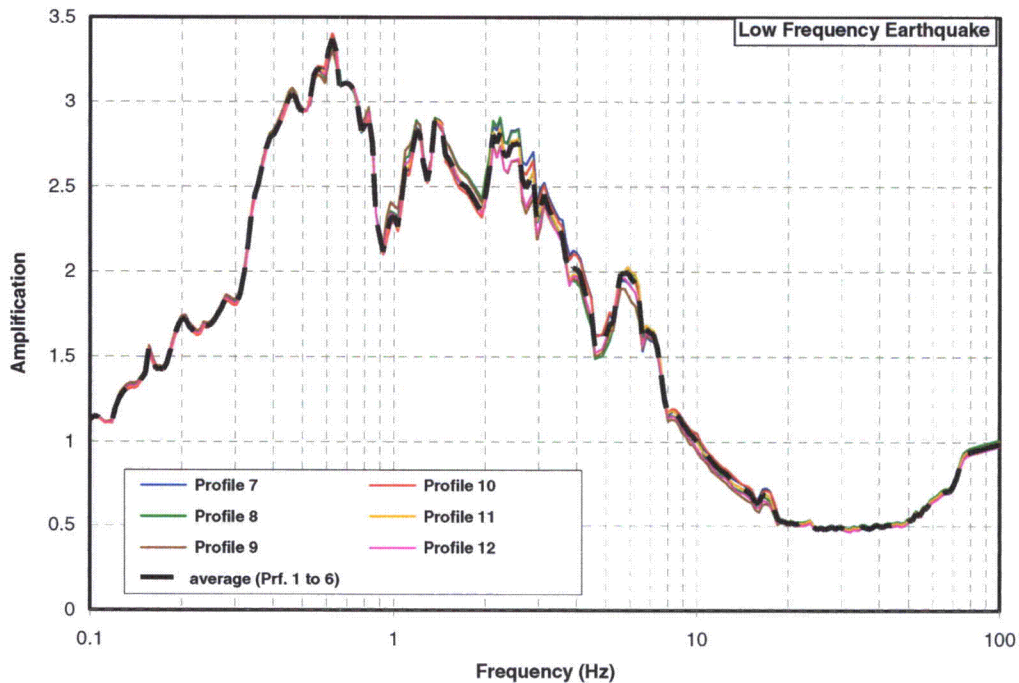
RAI Figure 2.5.2-23A. ESP Base Profiles – 5% Damping ARS Amplifications at 86 ft Depth

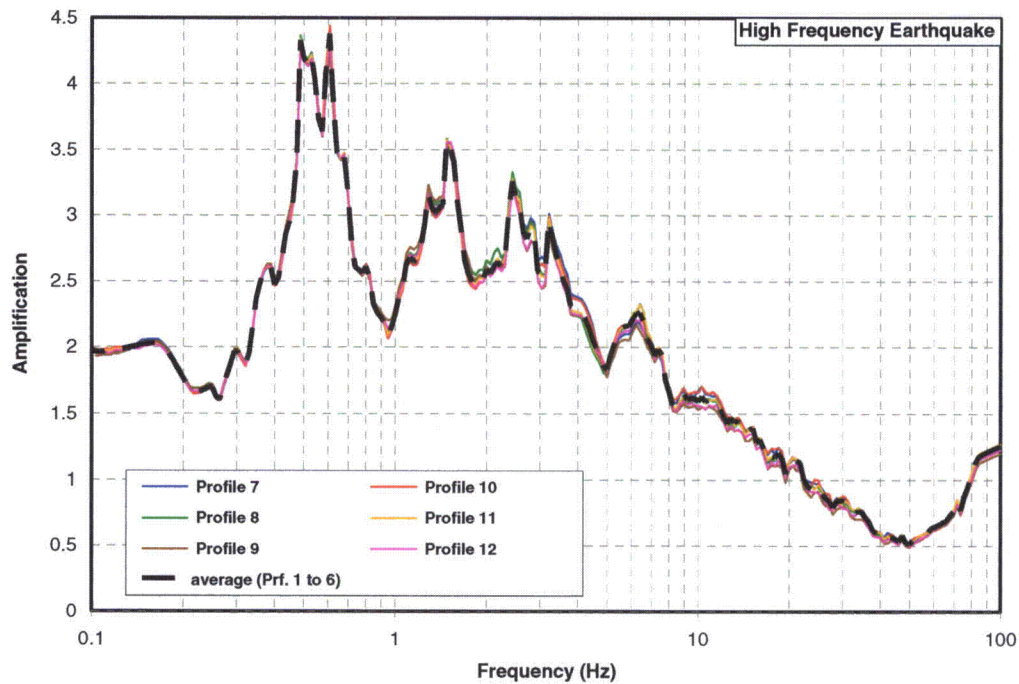
The rock shear velocities of the six base profiles in RAI Table 2.5.2-23 were modified to include the low velocity zone as listed in RAI Table 2.5.2-23B. Shake analyses were performed using the LF and HF acceleration time histories in order to calculate ARS amplifications at 86 ft depth where the SSE motion is defined.

RAI Table 2.5.2-23B. Rock Shear Velocities of the ESP Site Profiles with Low Velocity Zone -

Top of Layer Depth (ft)	Vs (fps)		Top of Layer Depth (ft)	Vs (fps)		Top of Layer Depth (ft)	Vs (fps)	
	Prof. 7	Prof. 10		Prof. 8	Prof. 11		Prof. 9	Prof. 12
1049	4400	4400	1049	4400	4400	1049	4400	4400
1100	5650	5650	1100	5650	5650	1100	5650	5650
1150	6650	6650	1150	6650	6650	1150	6650	6650
1225	7600	7600	1225	7600	7600	1225	7600	7600
1338	8000	8700	1338	8000	8700	1338	8000	8700
1405	7005	7703	1450	8090	8760	1450	8090	8760
1525	9200	9200	1550	8180	8820	1550	8180	8820
			1650	8270	8880	1650	8270	8880
			1740	8342	8928	1750	8360	8940
			1780	7342	7928	1850	8450	9000
			1900	9200	9200	1950	8540	9060
						2050	8630	9120
						2128	8679.5	9153
						2155	7679.5	8153
						2275	9200	9200

RAI Figure 2.5.2-23B shows the 5% damping ARS amplifications results at 86 ft depth obtained from the analyses of low velocity profiles 7 to 12. These ARS amplifications are compared with the log-average of the ARS amplifications obtained from the analyses of the base ESP profiles shown in RAI Figure 2.5.2-23. The comparison indicates that effects of the Pen Branch fault zone (i.e. as a low velocity zone) on the response of the site at the two SSE horizons are small.





RAI Figure 2.5.2-23B Low Velocity Profiles – 5% Damping ARS Amplifications at 86 ft Depth

The base case shear wave velocity profile is shown on SSAR Figure 2.5.4-7 and is summarized on SSAR Table 2.5.4-11. The trend is for the shear wave velocity to gradually increase with depth within the Blue Bluff Marl. However, a 3-ft thick zone of lower shear wave velocity was encountered in the Blue Bluff Marl between depths of 102 and 105 ft. The shear wave velocity in the Lower Sand Stratum shows an initial trend of decreasing with depth immediately beneath the Blue Bluff Marl. The shear wave velocity reaches its lowest values in the depth range of 156 to 216 ft, and then resumes the trend of increasing with depth. The low velocity zones in the Blue Bluff Marl and in the Lower Sand Stratum were incorporated in the site response calculations, i.e., the site response calculation results inherently reflect the inclusion of these low velocity zones. The calculations were performed using the base case shear wave velocity profile that is based on field measurements, and randomized profiles.

RAI Table 2.5.2-23C summarizes the results for the maximum soil strains obtained from the SHAKE analyses of the randomized profiles of ESP site. The table shows that the maximum soil strain remained below 0.6%. The equivalent linear approach is adequate for this low level of soil strain.

RAI Table 2.5.2-23C, SHAKE Analyses of Randomized Profiles – Maximum Soil Strains

Earthquake Probability Level	EPRI Randomized Profiles		SRS Randomized Profiles	
	LF Earthq.	HF Earthq.	LF Earthq.	HF Earthq.
10 <sup>-4</sup>	0.078%	0.067%	0.082%	0.068%
10 <sup>-5</sup>	0.592%	0.300%	0.287%	0.353%

The next revision to the ESP application will address as appropriate the information provided in this response.

**2.5.2-24 SSAR Sections 2.5.2.7.1.1 to 2.5.2.7.1.3 describe the development of vertical-to-horizontal response spectral (V/H) ratios based on the results of NUREG/CR-6728 and Lee (2001).**

**a. Please justify your rationale for assigning the approximate weights of 1:3 to the respective “near” and “far” estimates of V/HCEUS, Soil.**

**b. Please discuss the similarities and differences between the site-specific soil profile used by Lee (2001) and the Vogtle ESP site response profile.**

**c. Please justify in greater detail your rationale for the relative weights assigned to the NUREG/CR-6728 and Lee (2001) results and the final smoothing.**

**In addition, SSAR Section 2.5.2.7.1.3 states that “both results give minimum V/H values, particularly in the lower frequencies, which appear lower than engineering judgment may suggest acceptable in the current state-of-knowledge”. Please explain the meaning of this statement in greater detail and its implication for the final ESP site V/H ratios.**

Response:

While Reg. Guide 1.60 presents a fixed functional relationship for V/H – basically, 1.0 for high frequencies and 2/3 for low frequencies – it is recognized in the seismic ground motion community of experts (see EPRI, 1993, or McGuire and others, 2001) that V/H varies with magnitude, distance, site conditions, and tectonic environment [e.g., western US vs. central and eastern US]. This is discussed in SSAR Section 2.5.2.7.1. The SSAR attempts to consider these variables in establishing a V/H that considers some degree of Vogtle site-specificity.

In the development of the horizontal ground motions from the PSHA, the results of hazard deaggregations are presented that indicate the distribution of hazard contribution by magnitude and distance for different frequencies and hazard levels. From SSAR Figures 2.5.2-22 through 2.5.2-27 it can be seen that the “near” and “far” modes correspond to smaller magnitude and larger magnitude events, respectively. Consistent with the dominant seismic events considered for the site response analysis – see SSAR Section 2.5.2.5.1.3 – a “near” event of magnitude M5.6 at 12 km and a “far” event of M7.2 at 130 km are assumed to be reasonable mean dominant events contributing to an estimate of V/H. As V/H varies by magnitude and distance, it is desirable to estimate the relative contribution of these two representative events to the development of V/H by ascribing weights to the “near” and “far” events.

SSAR Figure 2.5.2-30 presents a different view of high-frequency deaggregation – contribution over magnitude has been summed, and the explicit dependence on magnitude is lost. However, from the other figures of magnitude-distance deaggregation, it is known that the distinct bimodal character of the “near” [i.e., <20km] and “far” [~130km] modes correspond to smaller magnitude and larger magnitude events, respectively. In this figure about ¾ of the area under the 10-4 hazard probability density curve corresponds to the “far” event mode, while about ¼ of the area corresponds to the “near” mode. Similarly, for the 10-5 hazard the area under the probability density curve is about equal for the “near” and “far” modes. As indicated in SSAR Table 2.5.2-22, the horizontal SSE, as derived following the ASCE 43-05 methodology, is equal to, or only slightly greater than, the 10-4 uniform hazard response spectrum at high frequencies. Therefore, the relative contribution of the “far” and “near” events may be estimated from the 10-4 deaggregation: ¾ to ¼ or 3:1.

As described above, emphasis in choosing the relative contributions to V/H of “near” and “far” earthquakes was focused on the high-frequency part of the spectrum. The same assessment at the low-

frequency end of the spectrum is not as sensitive to magnitude and distance nor, therefore, to the distinction between “near” and “far” events. And, as discussed in the SSAR and below, the V/H ratio chosen for low-frequency motions was ultimately based on engineering precedent and judgment.

The SRS site-specific soil profile is not published in Lee (2001) so that discussion of similarities and differences between it and the Vogtle ESP soil profile (see SSAR Figure 2.5.4-7) cannot be made. Nevertheless, given the proximity of SRS to the Vogtle ESP site, the site conditions at SRS were assumed likely to be more comparable to those at the Vogtle ESP site than the generic CEUS soil profile used in NUREG/CR-6728. This is the reason the Lee (2001) V/H ratios were considered. Despite expected gross similarities, as well as possible notable smaller-scale differences in soil profiles between SRS and the Vogtle ESP site, the approach used to develop V/H was to use an approximate envelop, rather than an average or weighted average, of the estimates resulting from consideration of Lee (2001) and NUREG/CR-6728 as a guide for the recommended V/H.

As discussed above, relative weights for “near” and “far” event contributions to V/H were considered within each of the two V/H estimates – i.e., NUREG/CR-6728 [SSAR Section 2.5.2.7.1.1] and Lee (2001) [SSAR Section 2.5.2.7.1.2] – however, weights were not applied to the results of the two estimates themselves to derive the final SSE V/H. Rather an approximate envelop of the two results was recommended as an alternative to the generic V/H ratios presented by Reg. Guide 1.60. This is discussed in SSAR Section 2.5.2.7.1.3 and as shown in SSAR Figure 2.5.2-43. From this figure it is clear that the V/H ratios of Lee (2001) have been approximated by two log-log line segments for frequencies between 1 and 100 Hz while for lower frequencies a constant ratio of 0.5 (a value greater than either the Lee or NUREG/CR-6728 in this frequency range) has been recommended. This final log-log line segment smoothing of the approximate envelope of the Lee or NUREG/CR-6728 values is in accord with the type of simple smoothing used in Reg. Guide 1.60, whose frequency-dependent V/H ratio values are also shown in SSAR Figure 2.5.2-43.

Following the response above for the use of the approximate envelope of the two V/H estimates, the recommended V/H in SSAR Figure 2.5.2-43 follows this guidance, except in a range of low frequencies – about 0.25 to 1.0 Hz – where the literal envelop would dip to V/H values less than 0.2.

As discussed above, the intent for the V/H developed for the Vogtle site was to derive more modern and site or region-specific modification of the Reg. Guide 1.60 V/H, maintaining the smooth or simple character of that function. A V/H function with values that drop to less than 0.2 in a narrow range of low frequencies (as do both the Lee (2001) and NUREG/CR-6728 models) would have been a significant departure in shape and amplitude from the Reg. Guide 1.60 V/H which varies very gradually from 0.70 to 0.67 over the same frequency range. Following the literal envelop would have given a vertical SSE that largely eliminated the resonance peak seen in the horizontal SSE at ~0.55 Hz. Given the current lack of a robust methodology for explicitly determining CEUS V/H for soil sites, it was judged to be better to maintain the resonance peak and simple V/H function analogous to that presented in Reg. Guide 1.60.

**2.5.3-1 SSAR Sections 2.5.3.1.2 and 2.5.3.1.7 refer to features mapped by McDowell and Houser (1933) and Bartholomew et al. (2002), including “clastic dikes”, that these authors interpreted as possibly related to tectonism during late Eocene to late Miocene. These features are attributed to a non-tectonic origin in SSAR Sections 2.5.3.1.2, 2.5.3.1.7, and 2.5.3.8.2.2 without any discussion of the field evidence for this conclusion.**

**Please discuss criteria used to determine that these features are non-tectonic in origin and related to pedogenic soil-forming processes, including a comparison with characteristics of clastic dikes mapped in trenches in the site area which are also described as non-tectonic features in the SSAR.**

Response:

McDowell and Houser (1983) compiled the locations of small-scale deformation and sedimentary structures in the vicinity of VEGP site and the SRS. They infer that “all of these features ... were produced by gravity-induced deformation as a result of loading, compaction, slump, sliding, or in some cases possibly by tectonic deformation.” Only six localities of “clastic dikes” were listed by McDowell and Houser (1983), who further indicate “the origin of clastic dikes (table 3) is not clear.”

Based on our own reconnaissance of exposures in the Site Area, we have documented abundant “clastic dikes” that have characteristics consistent with a pedogenic or weathering origin, but no features that can reasonably be interpreted to have formed as a result of injected sand. Our field reconnaissance of “clastic dikes” exhibited the following primary characteristics, which were summarized by the Bechtel (1984) study of these features within a large trench exposure on the VEGP site:

1. The dikes are widely distributed through the region in deeply weathered clayey and silty sands of the Eocene Hawthorne and Barnwell Formations.
2. The dikes occur in nearly all exposures of the weathered profile but are rare in exposures of stratigraphically lower, less weathered sediment.
3. The dikes contain a central zone of bleached host rock bounded by a cemented zone of iron oxide. Some dikes contain a clay core.
4. Grain size analyses on samples indicate that the dike interval contains the same grain distribution as the host sediment with slightly more silt and clay (excluding clay core).
5. The dikes and associated mottling decrease downward in density and size. In most cases, the dikes taper downward and pinch-out over a 5- to 15-ft distance.

In contrast to the non-tectonic “clastic dikes”, Bartholomew et al. (2002) describe clastic dikes that cut across poorly bedded clay-rich strata and are filled with massive, medium to coarse sand. They emphasize that these features represent true clastic dikes and not features that have commonly been referred to as “clastic dikes”, a term that has inappropriately been applied for decades to features that are probably related to weathering along joints or fractures. However, the clastic dikes identified by Bartholomew et al. (2002) are syndepositional due to the presence of marine animal burrows that cross cut the dikes.

The formation of these dikes occurred during the late Eocene while the sediments were in a subaqueous marine environment (Bartholomew et al. 2002). Whether these clastic dikes of Bartholomew et al. (2002) formed as a result of seismic shaking or some other process related to soft sediment deformation (e.g., compaction and de-watering), the age of these features is significantly older than Quaternary, and therefore do not reflect geologically recent seismic activity. As previously stated in the SSAR, even if these features are of tectonic origin, they constitute evidence for earthquakes that occurred during or prior to the late Miocene.

The next revision to the ESP application will address as appropriate the information provided in this response.

**2.5.3-2 SSAR Sections 2.5.3.8.2.1 and 2.5.3.8.2.2 discuss features interpreted to be non-tectonic in origin that include warped bedding, fractures, small-scale faults, injected sand dikes, and clastic dikes. Warped bedding, fractures, small-scale faults, and injected sand dikes are interpreted to indicate local dissolution of the underlying Utley Limestone and resultant plastic and brittle collapse of overlying Tertiary sediments which occurred more than 10,000 years ago. No formation mechanism is described for the injected sand dikes. The clastic dikes are interpreted to result from weathering and pedogenic soil-forming processes that were enhanced along older fractures initially produced by dissolution of the underlying Utley Limestone.**

**a. Please describe where these non-tectonic features are located relative to the proposed trace of the Pen Branch Fault at the VEGP site.**

**b. Please discuss field data, observations, and reasoning which resulted in the conclusion about a dissolution origin for the warped bedding, fractures, small-scale faults, and injected sand dikes, including a specific explanation of the formation mechanism for the injected dikes.**

**c. Please discuss field data, observations, and reasoning which resulted in the conclusion that the injected sand and clastic dikes do not represent a response to Quaternary or Holocene earthquakes.**

Response:

A variety of abundant non-tectonic deformation features were the focus of detailed studies in a large trench at the VEGP site (Bechtel 1984). As shown on SSAR Figure 2.5.1-34, the trench is located within the upper portion of the monocline in the Blue Bluff marl and near the trace of the Pen Branch fault. The trace of the fault shown on SSAR Figure 2.5.1-34 and others in the SSAR is not a surface projection of the fault, but rather the location of the fault where it intersects the contact between basement rock and overlying Coastal Plain deposits. In addition to the features documented in the trench, "clastic dikes" have been observed in other excavations at the site and are likewise concluded to be of non-tectonic origin.

The dissolution origin for the warped bedding, fractures, small-scale faults, "clastic dikes" and sand-injected dikes is interpreted largely from the observations and detailed documentation of these features in a large trench exposure that was over 900 ft long, 30 to 45 ft deep, and 25 to 40 ft across (Bechtel 1984). The high concentration of these features within the trench and the spatial and kinematic relationships between different types of deformation features provide some of the best information regarding their origin (see RAI Figure 2.5.3-2A). Field mapping efforts performed as part of the VEGP ESP application also identified "clastic dikes" within the VEGP site and surrounding site area, and similarly concluded these features are of a non-tectonic origin based on field observations.

As described in Bechtel (1984), "The lateral and vertical dimensions of the trench permitted accurate determination of the relationships of all the structures to one another and to the host sediment, while detailed mapping of both walls provided data for three-dimensional reconstruction and analysis of the structures. In addition, previous VEGP geologic investigations have accurately defined the subsurface stratigraphy at the site." For this RAI response, much of the description of the features and field relationships observed in the trench exposure are taken from the Bechtel (1984) report.

Evidence for dissolution (extensive leaching and solution cavities) of the Utley limestone at the site is well-documented (USNRC 1985). The Utley limestone lies below the Eocene sands, in which the small deformational features occur, and directly above the Blue Bluff marl. Due to the evidence of dissolution,

the Utley limestone and overlying deposits were excavated and removed for Units 1 and 2 and will also be removed for the construction of Units 3 and 4.

The 3-dimensional nature of the warped bedding, combined with the spatial and kinematic relationships of the small-scale faults and fractures along the margins of the more strongly warped depressions, clearly demonstrates a dissolution or sediment collapse origin. The highly irregular, discontinuous nature of folding is consistent with a non-tectonic dissolution origin and inconsistent with a tectonic origin, since there are no laterally persistent fold axes (see RAI Figure 2.5.3-2B following this response). If this minor fold deformation was associated with the underlying Pen Branch fault, fold axes should be laterally persistent and parallel to the fault. The discontinuous nature of domes and depressions in an “egg carton” or “dimpled” pattern reflects the more random, non-tectonic process of dissolution. The concentration of fractures and small normal faults at the margins of the structural lows (Sta 450 in RAI Figure 2.5.3-2A following this response) illustrates that the minor folding is a result of dissolution collapse in underlying strata, as opposed to localized, differential uplift of the domes.

Most of the small-scale faults have normal displacement toward or into the depressions and a few exhibit minor reverse slip near the crests of some arches (Bechtel 1984). These features are of limited dimensions and cannot be traced laterally across the width of the trench. The orientations of fractures and small faults are locally consistent with the limbs of the individual arches and depressions, but vary strongly from fold to fold. In some cases, such as Sta 450 in RAI Figure 2.5.3-2B, the small faults actually arc over the centers of some of the depressions. These field relationships all support an origin related to very localized settlement of the depressions resulting from dissolution and collapse of underlying strata.

A true clastic dike is formed by injection of sand into a fracture from a source stratigraphically above or below. The term “clastic dike” has been widely mis-used in the literature to describe features that, based on observations from the Bechtel (1984) trench and other studies, including the ESP project, formed primarily as a result of weathering and soil-forming processes. Some of the principal reasons that “clastic dikes” do not represent features produced from earthquake ground shaking are summarized by Bechtel (1984) as:

1. The dikes are widely distributed through the region in deeply weathered clayey and silty sands of the Eocene Hawthorne and Barnwell Formations.
2. The dikes occur in nearly all exposures of the weathered profile but are rare in exposures of stratigraphically lower, less weathered sediment.
3. The dikes contain a central zone of bleached host rock bounded by a cemented zone of iron oxide. Some dikes contain a clay core.
4. Grain size analyses on samples indicate that the dike interval contains the same grain distribution as the host sediment with slightly more silt and clay (excluding clay core).

The dikes and associated mottling decrease downward in density and size. In most cases, the dikes taper downward and pinch-out over a 5- to 15-foot distance. RAI Figure 2.5.3-2C following this response shows an example of downward termination of a “clastic dike” in a large quarry exposure near the meteorological tower in the southern portion of the VEGP site. RAI Figure 2.5.3-2C also shows the decrease in small dikes and mottling downward from the more strongly developed soil at the ground surface.

The injected sand dikes occur at three localities in the trench and were not observed at any other location either on or off the VEGP site during the ESP mapping effort. The sand dikes, as identified by Bechtel

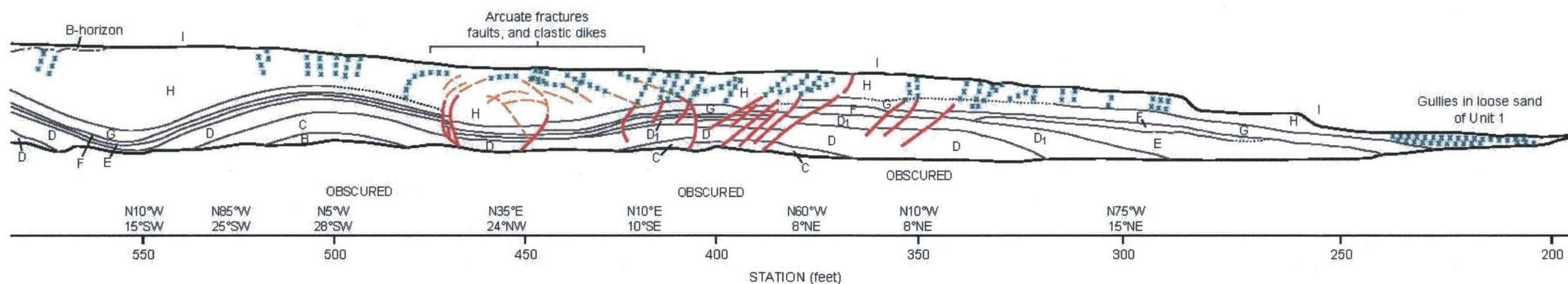
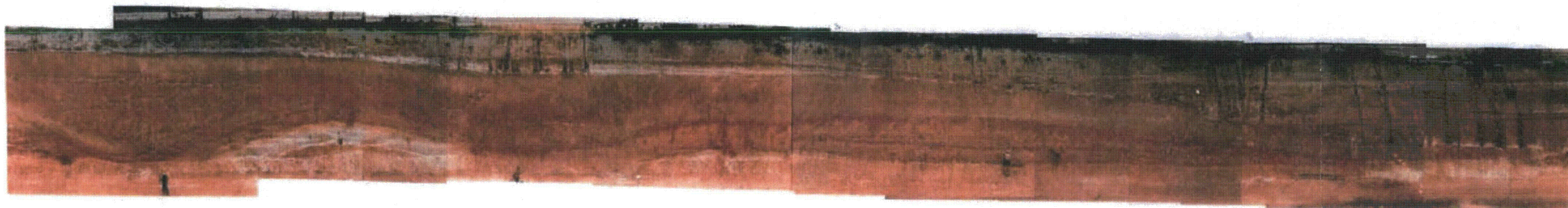
(1984), consist of lavender, loosely consolidated, well sorted, very fine, clean quartz sand and are confined to a single unit (Unit D) within the trench. These dikes were likely formed by fluid or plastic injection of a source sand from underlying sand beds of Unit C. The close spatial association of the sand dikes with limbs of the depressions suggests that the liquid injection resulted from development of the depression.

The injected sand dikes and “clastic dikes” are estimated to be of significant age. The sand dikes are interpreted to have formed from an early phase of sediment collapse following the Eocene deposition of the strata and prior to the development fracturing, jointing, and minor faulting associated with a subsequent sediment collapse that resulted in the formation of small faults that offset the sand dikes. The sand dikes predate a Miocene erosional event. The “clastic dikes” are interpreted to be younger than the sand dikes. “Clastic dikes” probably developed during a major weathering event that produced the relict paleosol on Unit H and are thus older than (1) middle to late Pleistocene erosion event of Unit H paleosol and (2) deposition of the late Pleistocene and Holocene eolian sand of Unit I (Bechtel 1984). The SER (USNRC 1985) concluded that the “clastic dikes” are likely great in age and that “there is no evidence that these features represent a safety issue for the plant, whatever their origin.”

#### References

(USNRC 1985) US Nuclear Regulatory Commission, Safety Evaluation Report related to the operation of Vogtle Electric Generating Plant, Units 1 and 2, Docket Nos. 50-424 and 50-425, June 1985.

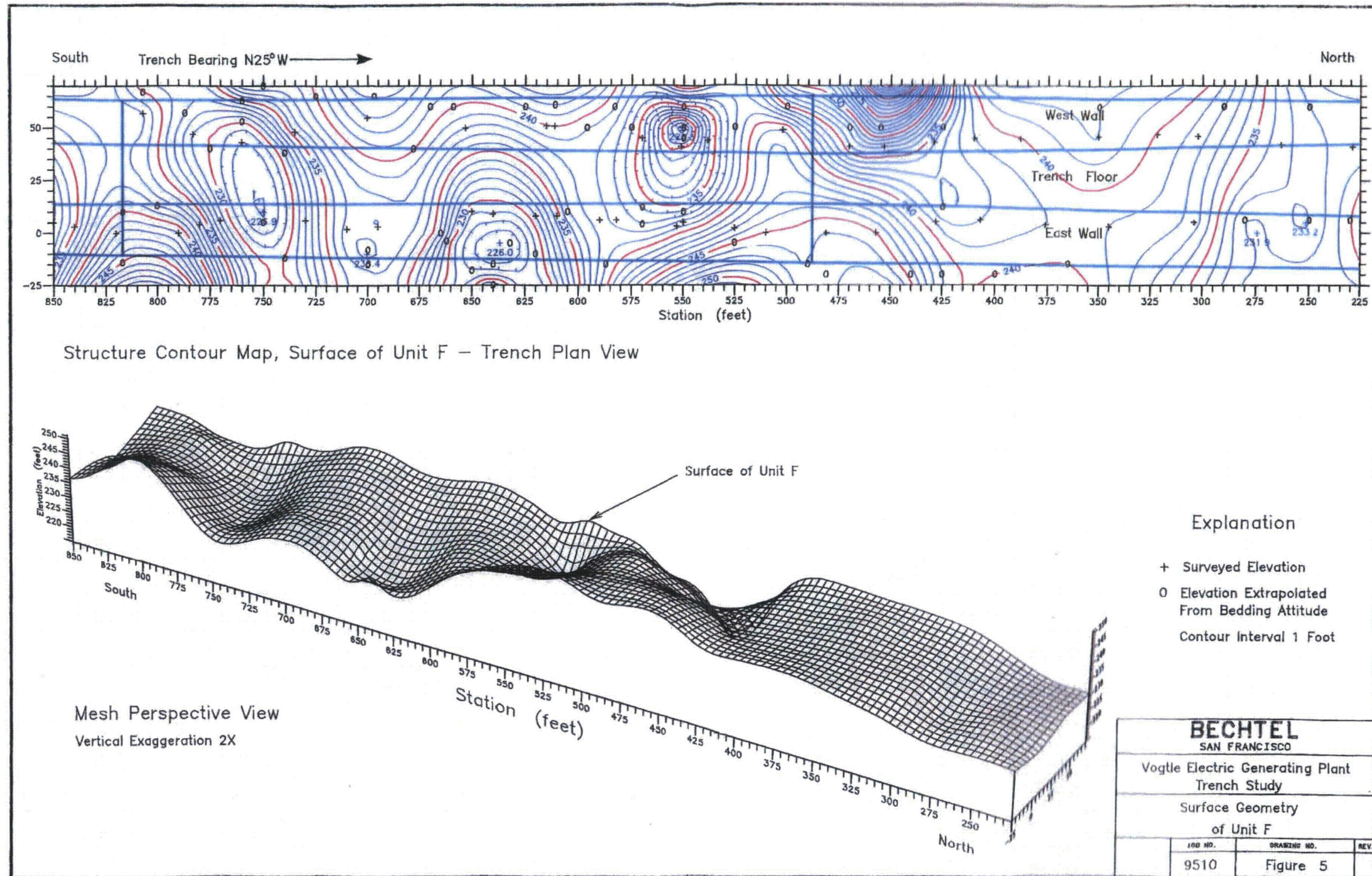
The next revision to the ESP application will address as appropriate the information provided in this response.



Modified after Figure 3, Bechtel (1984)

Explanation			
	Lithologic contact, dotted where poorly exposed		Eolian sand
	Offset (minor fault)		Hawthorn (?) Formation
	Major fracture or joint		Barwell (?) Group
	"Clastic" dike		
	Base of soil B-horizon		

RAI Figure 2.5.3-2A Photo Mosaic and Geologic Interpretation of a Portion Trench, West Wall



RAI Figure 2.5.3-2B. Surface Geometry of Unit F Illustrating Localized Nature of Deformation



**RAI Figure 2.5.3-2C. Photograph Illustrating Downward Termination of a "Clastic Dike."**

**2.5.4-1 SSAR Section 2.5.4.2.2 states that information has been taken from the 14 borings and 10 cone penetrometer tests performed during the ESP subsurface investigation. However, Section 2.2.1 of Appendix 2.5A, “Geotechnical and Laboratory Testing Data Report,” to SSAR Section 2.5 states that 12 borings, designated B-1001 through B-1011 and B-1013, were drilled at the site. Please clarify this inconsistency and also describe how the other 2 borings were taken.**

Response:

The number of borings drilled during the ESP subsurface investigation is fourteen (14), as briefly stated in Section 2.5.4.2.2 and further described in Section 2.5.4.3.2. These borings can be alternatively described as follows:

- Eleven (11) borings (B-1001, B-1002, B-1004 through B-1011 and B-1013) were drilled and sampled at regular depth intervals. The termination depths of these borings ranged from 98.9 ft (B-1009) to 304 ft (B-1004).
- One (1) boring (B-1003) was continuously cored through soil and rock to a depth of 1,338 ft.
- Boring B-1002A was drilled without sampling to a depth of 105 ft, and C-1005A was drilled without sampling to a depth of 60 ft. These two borings were drilled to allow the performance of suspension P-S velocity logging to measure shear wave velocities above the Utley Limestone where drilling fluid loss was observed.

A summary of the 14 ESP borings is shown on SSAR Table 2.5.4-7, and their locations are shown in SSAR Figure 2.5.4-1.

Section 2.2.1 on Page 2.5A-5 of Appendix 2.5A provides essentially the same information described above and in Sections 2.5.4.2.2 and 2.5.4.3.2 of the SSAR. The first paragraph of Section 2.2.1 of Appendix 2.5A talks about the 12 borings with sampling/coring (same as the first two bullets of this response). The third paragraph of Section 2.2.1 of Appendix 2.5A talks about the 2 borings without sampling/coring (same as the last bullet of this response).

In summary, there’s no inconsistency between Sections 2.5.4.2.2 and 2.5.4.3.2 of the SSAR and Section 2.2.1 of Appendix 2.5A.

**2.5.4-2 SSAR Section 2.5.4.2.1 states that the Upper Sand Stratum (Group 1 soils) will be completely removed and replaced with compacted structural fill prior to the construction of VEGP Units 3 and 4. SSAR Section 2.5.4.5.3 describes the sources and quality control of the structural fill.**

**a. Please explain whether the excavation and backfill will cover only the foot-print of the power block or extend to certain distance from the foundation footprint.**

**b. If the site excavations will not extend to significant distances to the side of the plant, shouldn’t the seismic hazard calculations be carried to the free-ground surface including the Barnwell Group in the base-case site soil columns? What is the basis for this column analysis which presumes that the fill extends uniformly in all horizontal directions, while the actual excavation and backfill will extend only in the immediate vicinity of the plant? (Page 2.5.2-39)**

**c. SSAR Section 2.5.4.5.3 states that backfill will be placed with as much as 25-percent fines. This is significantly higher fines content than used for building foundations. How will compaction controls be implemented for such materials?**

Response:

- a) Two backfilled excavations will be associated with the safety-related footprints of Units 3 and 4, one for each unit, and will extend beyond their respective power block footprints. The minimum lateral extent of each excavation has been established by determining the stress zone as defined by a 1(H):1(V) slope extending from the bottom of the turbine, containment, and auxiliary building foundations at approximate bottom of foundation elevations of El. 216 ft msl for the turbine building and El 180 ft msl for the containment and auxiliary buildings to the top of the Lisbon Formation (Blue Bluff Marl) at 130 ft msl. The stress zone at the top of the Lisbon Formation will extend approximately 86 ft (El 216-El 130) horizontally beyond the footprint of the power block structures. The turbine building foundation governed this horizontal extension (since it is the higher foundation), and the 86 ft extension was conservatively used for all four sides of the excavation. The entire excavation, including the power block footprint, stress zone, and areas beyond the stress zone will be backfilled with compacted structural fill.
- b) The site excavations will extend to significant horizontal distances from the structures. With the base of the excavation extending approximately 86 feet outside the building footprints as described above, and with excavation side slopes at 2(H):1(V), the structural fill will extend more than 180 ft beyond the containment and auxiliary buildings at their foundation level, and will extend more than 250 ft beyond the edge of the turbine building at its foundation level.
- c) Sand and silty sand (SM) with no more than 25 percent fines obtained from on-site sources were used as structural backfill for Units 1 and 2, as described in VEGP Unit 1 & 2 FSAR Section 2.5.4.5.2.1. The same structural backfill criterion will be used for Units 3 & 4.

Compaction controls for placement of the backfill will be implemented through an independent soil testing firm. As identified in SSAR Section 2.5.4.5.3, this testing firm will maintain an on-site soils testing laboratory to control the quality of the fill material and the degree of compaction. Compaction will be monitored through field density testing performed at a minimum frequency of one test per 10,000 square ft per lift of placed fill. More detailed testing compaction control criteria will be developed during the COL.

**2.5.4-3 According to Table 2 of Appendix A, "Boring Data," to Appendix 2.5A of the SSAR, only 4 borings (B-1002, B1003, B1004 and B-1005) went through the Blue Bluff Marl material (Group 2 Zone) and reached the Lower sand Stratum (Group 3 Zone - coarse-to fine sand with interbedded thin seams of silt and/or clay). Since the top layer of soil (Group 1 soil) will be removed and backfilled with compacted structural fill prior to the construction of VEGP, Units 3 and 4, only the information collected from these 4 borings can be used for the investigation of Group 2 and Group 3 soil that are supposed to be the primary load-bearing component of safety-related facilities. Please provide justification for the following:**

**With the data from 4 borings and no significant samples taken in Group 3 zone, what is the basis for the development of geotechnical parameters of Groups 2 and 3 layers?**

**SSAR Section 2.5.2.5.1.2 indicates that base case soil velocity profiles together with their uncertainty were developed from the available data. If only 12 borings were taken at the site, and most of these borings did not extend to depths below 91 m (300 ft), how were these parameters developed?**

**Are there any indications of soft zones, such as those encountered at the Savannah site, in the upper soils of the profile above the Blue Bluff Marl which may be collapsible under a seismic event? Even though soils under the foundation footprint are to be removed, how far to the side of the plant does collapsibility become unimportant?**

**Soft soils were indicated in the lower soils below the Blue Bluff Marl. Standard Penetration Test (SPT) blow counts for the lower sands in B-1002 are indicated to be as low as 10 bpf (Page "4 of 6" of Soil Test Boring Record of Appendix A to Mactec's report). Please explain what is the implication of such low values even though the average blow count through this material is indicated to be about 60 bpf?**

Response:

a) Three (3) ESP borings (B-1002, B-1003 and B-1004) completely penetrated the Blue Bluff Marl (Lisbon Formation), and another nine (9) ESP borings extended partly into the marl. Borings B-1002 and B-1004 extended through the Still Branch Formation and penetrated into the Congaree Formation. Boring B-1003 extended all the way through the Lower Sand Stratum to bedrock at 1338-ft depth. Boring B-1005 did not completely penetrate the Blue Bluff Marl. From the borings in Blue Bluff Marl, 58 SPT N-values were obtained from Group 2 and 3 layers along with the corresponding SPT samples. Twelve tube samples were also obtained. Borehole geophysical tests including suspension P-S velocity logging were performed in the three borings that completely penetrated the marl.

The following laboratory test results were obtained from the SPT and tube samples:

33 natural moisture contents

19 Atterberg limits

19 grain-size curves

28 unit weights

15 undrained shear strengths (from unconsolidated-undrained triaxial tests)

The geotechnical parameters were derived primarily from the ESP field and laboratory test results. Parameters from VEGP Units 1 & 2, were also taken into consideration. We note that geotechnical properties of layers below the Congaree Formation will be of no engineering consequence for the design of plant foundations, as these layers are too deep.

Four borings will extend to a depth of 250 and two borings will extend to a depth of 400 ft during the COL subsurface investigation. These borings will provide additional data related to Group 2 and 3 layers.

b) The base case shear wave velocity profile in the Lisbon Formation, Still Branch Formation and in the upper portion of the Congaree Formation was derived from the results of the three suspension P-S velocity logging tests performed in these strata. One of the suspension P-S velocity logging tests extended into bedrock below the Lower Sands, and the results were used to derive the base case shear wave velocity profile below the top of the Congaree Formation.

As noted in SSAR Section 2.5.2.5.1.2.2, the randomization model that captures the uncertainty involved in the base case shear wave velocity profile for the in-situ soils used the logarithmic standard deviation of shear wave velocity as a function of depth set to values obtained from soil randomization performed at the SRS site.

c) "Soft zones" with SPT N-values  $\leq 5$  bpf were encountered in the upper soils of the profile at ESP boreholes B-1001, B-1004, B-1005 and B-1006. For such soils below the water table, it is probable that they would liquefy under certain seismic events, resulting in several and perhaps even many inches of settlement of the surface above the liquefied material.

The planned location of the nuclear island relative to the upper sands acknowledges the potential lack of stability of these sands. Our response to RAI 2.5.4-2(a) provides further details about the extent of the soil replacement in the power block area.

d) SPT-38 at 189 ft in boring B-1002 disclosed  $N = 9$  bpf, and is the only N-Value taken in the Lower Sand Stratum during the ESP subsurface investigation that indicates a loose relative density. This result was obtained in the Still Branch formation that is over 40 million years old, and that has a present overburden pressure approaching 7 tons/ft<sup>2</sup>. Sands of this age and depth cannot be in a loose condition under normal circumstances. Infilling of a cavity could result in a low blowcount, but there is no evidence of cavities in this formation.

The measured shear wave velocity in B-1002 was 1,320 ft/sec at 188.7 ft depth, and 1,200 ft/sec at 190.3 ft depth. These values indicate dense to very dense sands with typical N-values in the 45 to 50 bpf range, similar to the N-values measured in the soils above and below 189 ft. The caliper log for B-1002 showed a very constant diameter of about 3.75 in. at, above and below 189 ft. In short, the geophysical measurements taken at 189 ft depth in B-1002 show no physical or strength abnormalities.

The most plausible explanation for the low blowcount is that the SPT was taken through disturbed material at the bottom of the drill hole. This could be from the cuttings not being properly flushed out of the hole before sampling. Alternatively, a temporary imbalance of water pressure inside and outside the borehole could have caused some flow of the sand at the bottom of the boring. The sieve analysis performed on the SPT sample at 189 ft depth indicates a fine sand with less than 7% fines, indicating a material susceptible to flow.

In summary, the isolated very low N-value in the Still Branch formation was most probably due to poor sampling rather than loose in-situ material.

**2.5.4-4 SSAR Section 2.5.2.5.1.2 states that the backfill shear wave velocities were determined from measurements made on the existing backfill at the site under Units 1 and 2 as summarized in Tables 2.5.4-10 and 2.5.4-11. As indicated in these tables, the shear velocities in the top layers of backfill are well below 305 mps (1,000 fps). How were shear wave velocity values generated at depths of 15 m (50 ft) or more below the top of the backfill? Were effects of confinement considered?**

Response:

SSAR Section 2.5.2.5.1.2.1.1 states that, "Shear-wave velocity was not measured for the compacted backfill during the ESP subsurface investigation (APPENDIX 2.5A). Interpolated values based on measurements made on fill for existing Units 1 and 2 (Bechtel 1984) are used instead." The RAI implies that shear wave velocity measurements were made on the in-situ backfill for Units 1 and 2. In fact, the "measurements made on fill for existing Units 1 and 2" were laboratory measurements using resonant column tests. No in-situ shear wave velocity measurements were made for the compacted backfill before or during the ESP subsurface investigation. The shear wave velocity profile for the backfill was developed from the equations:

$$G_{\max} = 1000 \cdot K_2 \cdot (\sigma'_m)^{0.5}$$

$$V_s = (G_{\max}/\rho)^{1/2}$$

or

$$V_s = (G_{\max} \cdot g/\gamma)^{1/2}$$

- where: G = dynamic or low-strain shear modulus (psf)
- $\sigma'_m$  = mean principal effective stress (psf)
- $K_2$  = a parameter reflecting primarily the effect of void ratio or relative density and the strain amplitude of the motions. The value of  $K_2$  was determined to be 80 from resonant column test results.
- $V_s$  = shear wave velocity (fps)
- $\rho$  = density of the backfill sample
- $\gamma$  = unit weight of the backfill sample (pcf)
- g = acceleration of gravity = 32.2 ft/s<sup>2</sup>.

**2.5.4-5 SSAR Section 2.5.4.7.2.1 (Page 2.5.4-27) indicates that the EPRI 1993 soil degradation relationships were used to perform SHAKE analyses and derive the shear modulus reduction factors. It is the NRC staff's understanding that the appropriateness of using the EPRI 1993 curves for fine-grained soils is not obvious since they were generally developed for sands and but not fine grained silts or clays. (The degradation models at the Savannah River site were generated from laboratory testing of in-situ soils.) Please explain the significance of using such models for fine-grained soils on the computed results?**

Response:

The degradation curves included in EPRI 1993 cover the range of soils from gravels to high plasticity clays, and thus are appropriate for fine-grained soils. The curves for fine-grained soils are presented in Figures 7.A-16 (shear modulus reduction curves) and 7.A-17 (damping ratio curves) in terms of soil plasticity, and require the use of the plasticity index (PI). Our response to RAI 2.5.4-17 provides further details on how the degradation curves included in the SSAR were derived from the EPRI (1993) curves.

The soil degradation relationships for fine-grained soil (and also coarse-grained soils) used in the SSAR will be verified by laboratory testing of in-situ soil samples during the COL subsurface investigation.

**2.5.4-6 Regarding the ground water control, SSAR Sections 2.5.4.5 and 2.5.4.6 state that (1) the total depth of construction excavation to the Blue Bluff Marl bearing stratum will range from approximately 80 to 90 ft ( 4 to 27 m) below ground surface (SSAR Section 2.5.4.5.1), (2) the groundwater generally occurs at a depth of about 60 ft (18 m) below the existing ground surface (SSAR Section 2.5.4.6.1), and (3) due to the relatively impermeable nature of the Upper Sand Stratum, sump-pumping of ditches will be adequate to dewater the soil. Please explain what dewatering procedures and what criteria will be developed to "minimize effects on the surrounding area and the existing**

**power block”?” (The impact of the simple use of sumps and pumps on any existing area of the site will depend on the extent of time during which drawdown will occur.)**

Response:

The dewatering program as identified in SSAR Section 2.5.4.6 was developed based on the similar subsurface conditions to those encountered at Units 1 and 2 and based on the success of the dewatering program employed for Units 1 and 2. The planned dewatering program will utilize a series of ditches that drain to a sump or sumps. The sump(s) will be equipped with pumps to discharge the ground water inflow. The pumps will also have capacity to discharge storm water inflow. The ditches will be advanced below the progressing excavation. However, the dewatering program for Units 3 and 4 differs from Units 1 and 2 in that the excavation below the design groundwater elevation of 165 feet MSL will not remain open as long as it was for Units 1 and 2. At Units 1 and 2, various safety-related power block structures were founded on or in the Blue Bluff Marl, requiring the drawdown until backfilling around these structures exceeded EL. 165 ft MSL. All safety-related structures for Units 3 and 4 will be founded in the compacted backfill at or above an elevation of about 180 feet MSL. This founding level is about 15 feet above the design groundwater level. Once the Upper Sand stratum has been excavated and the Blue Bluff Marl level prepared, the excavation may be backfilled. The dewatering system will be maintained during the placement of compacted backfill. However, upon achieving the design founding level groundwater inflow should not impact construction and the drainage ditches and sump(s) will be maintained to control storm water inflow only. This will enable the excavation below the groundwater level to remain open for a much shorter length of time than was required for Units 1 and 2.

The duration that the excavation below the groundwater remains open will be determined by the constructor. Nevertheless, even if the excavation remains open for an extended period, the drawdown effects on the existing power block will be minimal. At the excavation site, the groundwater will be lowered about 45 feet; from El. 165 ft to El. 120 ft. Conservatively neglecting the cone of depression that the groundwater level will follow outside the excavation and projecting the 45-foot drop in groundwater level to the existing power block, the effective stresses beneath the power block will increase. However, this increase in effective stress ( $45 \text{ ft} \times 62.4 \text{ pcf} = 2,810 \text{ psf}$ ) at the projected bottom of the backfill will have little impact on settlement of the existing power block structures. The safety-related structures in the existing power block are either founded in compacted fill or in/on the Blue Bluff Marl. Data for the existing Units 1 and 2 granular backfill (Bechtel 1985-see list of references at the end of the response to this RAI) disclosed measured SPT N-values greater than 100 bpf. The design elastic modulus for this very dense backfill was 1,500 ksf. Likewise, the Blue Bluff Marl is characterized by design values of 80 bpf for the measured SPT N-value and 10,000 ksf for the elastic modulus. In addition, the preconsolidation pressure for the very hard Blue Bluff Marl is estimated at 80,000 psf. Given these stress-strain characteristics of the foundation materials, the potential drawdown effects (primarily settlement) associated with the excavation dewatering at Units 3 and 4 are expected to be minimal.

#### References

(Bechtel 1985) Bechtel Power Corporation, Geotechnical Verification Work-Report of Results, Vogtle Electric Generating Plant, August 1985.

**2.5.4-7 SSAR Section 2.5.4.2.2.2 states that 15 unconsolidated undrained (UU) tests were performed on Blue Bluff Marl samples and that the measured undrained shear strength ranged from 150 to 4,300 psf. Both of these values are significantly lower than the 10,000 psf design value. Please justify the wide range of values and why they differ substantially from the values measured previously for Units 1 and 2. In addition,**

**elaborate on how the Standard Penetration Test N-values measured during the ESP investigations support the use of the 10,000 psf design value.**

Response:

Laboratory measurements of undrained shear strength for the Blue Bluff Marl (Lisbon Formation) made as part of the ESP subsurface investigation yielded values ranging from 150 to 4,300 psf. A total of 15 UU tests were performed using 1 confining pressure corresponding to the overburden pressure. These values were deemed low because of qualitative and quantitative reasons outlined in the next paragraphs.

**Qualitative factors that suggest that the laboratory measured undrained shear strength for the Lisbon Formation is low:**

- CPTs could not be pushed below the Barnwell Group and into the Lisbon Formation because the soils were too hard.
- Shelby tubes could not be pushed into the Lisbon Formation without being damaged, suggesting a hard formation.
- Samples obtained by pitcher barrel were likely disturbed by the sampling, storage and transportation process.
- A design undrained shear strength value of 10,000 psf is adopted for the Lisbon Formation in the VEGP Unit 1 & 2 FSAR.
- Adoption of the 10,000-psf design value in the ESP is supported by other ESP site specific data, as described in the next paragraphs.

**Empirical Correlation with PI** – Peck et al. (1974) suggest the following correlation between plasticity index (PI) and the ratio of undrained shear strength ( $s_u$ ) over vertical effective stress ( $p$ ) of *normally consolidated* soft clays (Equation 4.8 on p. 93 of Peck et al. 1974):

$$s_u/p = 0.1 + 0.004PI$$

Using the value of 25% for PI we get

$$s_u/p = 0.1 + 0.004 \times 25 = 0.2$$

If we consider the ground water depth at 60 ft, we can take the vertical effective stress at the top of the Lisbon Formation (depth taken as 90 ft) as

$$p = 115 \times 60 + (115 - 62.4) \times 30 = 8,478 \text{ psf}$$

and

$$s_u = 0.2 \times 8,478 = 1,696 \text{ psf, say } 1.7 \text{ ksf}$$

A similar calculation at the bottom of the Lisbon Formation (depth taken as 150 ft) yields

$$p = 115 \times 60 + (115 - 62.4) \times 90 = 11,634 \text{ psf}$$

and

$$s_u = 0.2 \times 11,634 = 2,327 \text{ psf, say } 2.3 \text{ ksf}$$

In other words, 1.7 ksf to 2.3 ksf would be reasonable estimates of undrained shear strength at the top and bottom of the Lisbon Formation, **if** the Lisbon Formation were normally consolidated. Because the Lisbon Formation is highly overconsolidated, we can state that 1.7 to 2.3 ksf represent very low estimates of undrained strength for the Lisbon Formation, and can be used to invalidate the low laboratory measured values.

**Empirical Correlation with SPT N-value** - The undrained strength,  $s_u$ , was calculated from Terzaghi's correlation with the SPT N-value (Fig. 1.22, p. 38 of Winterkorn & Fang 1975 - see list of references at the end of the response to this RAI). This correlation is given by

$$s_u = N/8 \text{ (ksf)}$$

where: N = SPT N-value in blows per foot (bpf)

If we use the average N-value of  $N_{avg} = 83$  bpf we get

$$s_u = 83/8 \cong 10 \text{ ksf}$$

We note that the split barrel sampler did not penetrate the full 12 inches (1 foot) during most of the SPT sampling in the Lisbon Formation. In these cases the blow counts for the actual sampler penetration were linearly extrapolated to N-values corresponding to 12 inches of penetration. These linearly extrapolated N-values exceeded 100 bpf in most cases. A cutoff value of 100 bpf was used in the computation of  $N_{avg} = 83$  bpf, thus resulting in a conservative estimate of  $N_{avg}$ .

**Empirical Correlation with Shear Wave Velocity** - The correlation shown below between shear wave velocity,  $V_s$ , and cone tip resistance,  $q_t$  (figure on p. 103 of Mayne 2006 - see list of references at the end of the response to this RAI):

$$V_s = 1.75(q_t)^{0.627}$$

where:  $V_s$  = shear wave velocity (m/s)

$q_t$  = cone tip resistance (kPa)

Using the average value of 2,354 fps  $\cong$  717 m/s for  $V_s$  reported in Section 2.5.4.4.2.1 we get

$$q_t = (717/1.75)^{1/0.627} \cong 14,454 \text{ kPa} \cong 302 \text{ ksf}$$

Mayne (2006) suggests the following correlation between undrained shear strength,  $s_u$ , and cone tip resistance,  $q_t$  (figure on p. 62 of Mayne 2006):

$$s_u = (q_t - \sigma_{vo})/15$$

where:  $\sigma_{vo}$  = total vertical stress (ksf)

Using  $\gamma = 115$  pcf, then  $\sigma_{vo}$  at the bottom of the Lisbon Formation, i.e., 150 ft depth is

$$\sigma_{vo} = 150 \times 115 = 17,250 \text{ psf} = 17.25 \text{ ksf}$$

and we get

$$s_u = (302-17.25)/15 \cong 19 \text{ ksf}$$

The value of  $\sigma_{v0}$  is smaller at top of the Lisbon Formation, and will result in a slightly higher  $s_u$ -value.

Table 2 of Senapathy et al. (2001) (See list of references at the end of the response to this RAI.) summarizes values of  $G_{\max}/s_u$  from 15 clay sites. The values ranged from 535 to 1,539 with a median value of 828, and average value of 892.

We know that

$$G_{\max} = (V_s)^2 \cdot \gamma / g$$

Using  $V_s = 2,354$  fps (average for the Lisbon Formation), and  $\gamma = 115$  pcf, then the average  $G_{\max}$  for the Lisbon Formation is

$$G_{\max} = 2,354^2 \cdot 115 / 32.2 \cong 19,790,000 \text{ psf} = 19,790 \text{ ksf}$$

If we use the minimum and maximum values of  $G_{\max}/s_u$  reported by Senapathy et. al. (2001), we obtain:

$$s_u = 19,790 / 535 \cong 37 \text{ ksf, for } G_{\max}/s_u = 535$$

and

$$s_u = 19,790 / 1,539 \cong 12.9 \text{ ksf, for } G_{\max}/s_u = 1,539$$

In summary, the low undrained shear strength measured in the laboratory for the Lisbon Formation is likely due to disturbance introduced by the sampling, and sample storage and transportation process. Field evidence (impossibility of pushing Shelby tubes) and evidence from other available data (SPT N-values and geophysical test results) justify the use of  $s_u = 10,000$  psf for the Lisbon Formation. This value was also adopted in the VEGP Unit 1 & 2 FSAR.

References:

(Mayne 2006) Mayne, P.W., *Site Characterization by Seismic Piezocone*, Georgia Institute of Technology, Atlanta, GA, 2006.

(Senapathy et al. 2001) Senapathy, H., Clemente, J.L.M. and Davie, J.R., "Estimating dynamic shear modulus in cohesive soils", Proceedings International Conf. Soil Mechanics & Geotechnical Engrg., Istanbul, Turkey, 2001.

(Winterkorn and Fang 1975) Winterkorn, H.F. and Fang, H.Y., *Foundation Engineering Handbook*, Van Nostrand Reinhold Co., New York, NY, 1975.

**2.5.4-8 SSAR Section 2.5.4.2.2 states, "Previous laboratory test results indicate the Blue Bluff Marl to be highly preconsolidated ... the preconsolidation pressure of the Blue Bluff Marl stratum was estimated to be 80,000 psf. Settlements due to loadings from new structures would be small due to this preconsolidation pressure."**

**a) Provide a description of the "previous" laboratory testing methods and results.**

**b) Justify the assumption of an undrained shear strength of 16,000 psf as UU Test results range from 150 to 4,300 psf. Were consolidation tests performed to verify this assumption?**

**c) The preconsolidation pressure for the Blue Bluff Marl is given as 80,000 psf and is based on the plasticity index values (which ranged from 2 to 70 with an average value of 25) and a PI of 25, which results in a  $s_u/p$  (undrained shear strength / effective preconsolidation pressure) ratio of 0.2. Provide a complete description of the Skempton (1957) method used to determine the ratio of 0.2. Also, justify the use of 0.2 for the ratio in view of the wide range of PI values. In addition, justify the estimated preconsolidation pressure for the Blue Bluff Marl based on the wide range of PI values.**

**d) Justify your conclusion, “settlements due to loadings from new structures would be small due to this preconsolidation pressure,” in view of settlements for the current Units 1 and 2 and also with regard to the  $s_u/p$  ratio of 0.2, which indicates that the soil is under consolidated (0.25 is an indication of normally consolidated soil).**

Response:

a) The original data and interpretation are contained in Bechtel (1974b). The responses provided here are largely excerpts from this reference. Laboratory tests included one hundred and ninety one 1-point unconsolidated-undrained (UU) triaxial tests, and thirty eight consolidation tests.

The 1-point UU tests disclosed undrained shear strength values in the range of 260 psf to 500,000 psf. Thirty of the UU tests, i.e., 15.7% of all measurements, disclosed undrained shear strength values lower than 10,000 psf. Twenty five of the UU tests that disclosed undrained shear strength values lower than 10,000 psf also disclosed larger strains at failure, which was considered to be due to disturbance either during sampling or preparation of test specimens. This leaves five tests on good quality samples, i.e., 2.6% of all measurements disclosed undrained shear strength values lower than 10,000 psf. Thus, adoption of a 10,000-psf design value can be considered conservative based on the available data.

The consolidation tests were performed using vertical pressures that reached 64 ksf for all thirty eight specimens. Most of the test results (void ratio versus vertical effective stress curves) showed very flat curves that indicated that the preconsolidation pressure had not been achieved.

b) The 16,000 psf value is the average undrained shear strength value based on previous laboratory test results contained in Bechtel (1974b) for Units 1 and 2. The 16,000 psf average value was calculated from the 1-point unconsolidated-undrained (UU) triaxial tests that disclosed undrained shear strength of less than 50,000 psf. This average includes the results of one hundred and eighty five tests, because only six tests disclosed undrained shear strength of more than 50,000 psf. Results from tests performed on samples deemed disturbed (twenty five of them, as explained above) were included in this average.

c) The Skempton (1957) method used to determine the ratio  $s_u/p = 0.2$  is the same method described in our response to RAI 2.5.4-7, i.e.,

$$s_u/p = 0.1 + 0.004PI$$

Using the average value of 25% for PI we get

$$s_u/p = 0.1 + 0.004 \times 25 = 0.2$$

If we use  $s_u = 16,000$  psf and  $s_u/p = 0.2$ , we obtain

$$p = 16,000/0.2 = 80,000 \text{ psf}$$

We know that the vertical effective stress in the Lisbon Formation ranges from 8,478 psf at the top of the layer to 11,634 psf at the bottom of the layer (see our response to RAI 2.5.4-7). Thus, the calculated value of  $p = 80,000$  psf is 6.9 to 9.4 times larger than the vertical effective stress. We can conclude that the Lisbon Formation is highly overconsolidated with overconsolidation ratios (OCRs) in the range of 6.9 to 9.4.

Use of the average value  $PI=25\%$  is justified as a common geotechnical practice. It would be unreasonable to consider outlying measured values in these types of calculations. However, let's consider the extreme low measured value of  $PI=2\%$ , and follow the same procedure used for  $PI=25\%$ . We obtain the following:

$$s_v/p = 0.1 + 0.004 \times 2 = 0.108$$

If we use  $s_u = 16,000$  psf and  $s_v/p = 0.108$ , we obtain

$$p = 16,000 / 0.108 \cong 148,000 \text{ psf}$$

Using the vertical effective stress in the Lisbon Formation ranging from 8,478 psf at the top of the layer to 11,634 psf at the bottom of the layer (see our response to RAI 2.5.4-7), the calculated value of  $p = 148,000$  psf is 12.7 to 17.5 times larger than the vertical effective stress. We could conclude that the Lisbon Formation is highly overconsolidated with overconsolidation ratios (OCRs) in the range of 12.7 to 17.5.

If we consider the extreme high measured value of  $PI=70\%$ , and follow the same procedure used for  $PI=25\%$ , we obtain the following:

$$s_v/p = 0.1 + 0.004 \times 70 = 0.38$$

If we use  $s_u = 16,000$  psf and  $s_v/p = 0.38$ , we obtain

$$p = 16,000 / 0.38 \cong 42,000 \text{ psf}$$

Using the vertical effective stress in the Lisbon Formation ranging from 8,478 psf at the top of the layer to 11,634 psf at the bottom of the layer (see our response to RAI 2.5.4-7), the calculated value of  $p = 42,000$  psf is still 3.6 to 5 times larger than the vertical effective stress. We could conclude that the Lisbon Formation is highly overconsolidated with overconsolidation ratios (OCRs) in the range of 3.6 to 5.

We also note that most of the consolidation tests results on thirty eight samples of the Lisbon Formation reported in Bechtel (1974b) showed very flat curves that indicated that the preconsolidation pressure exceeded 64,000 psf. Thus, the 80,000-psf preconsolidation pressure estimated from the empirical correlation is reasonable.

d) As a starting point for this part of the response, we note that the Lisbon Formation is highly overconsolidated, as outlined in part c of this response. There is no evidence (previous or obtained during the ESP subsurface investigation) to suggest that the Lisbon Formation is underconsolidated.

Our conclusion that settlements due to loadings from new structures would be small due to this preconsolidation pressure is based on the fact that heavily overconsolidated soils are known to develop small settlements, and these settlements take place during placement of structural loads, i.e., during construction. This behavior was observed during settlement monitoring for Units 1 and 2, as described in the "VEGP Report on Settlement" prepared by Bechtel in 1986. The same behavior is expected for Units 3 and 4.

**2.5.4-9 SSAR Section 2.5.4.2.5.2 cites Bowles (1982) as the reference for determining the effective angle of internal friction for site soils. It is not clear how the effective angle of internal friction was calculated using this reference. Provide an example of a calculation and justify the accuracy of the results in view of the range of N-values.**

Response:

The angle of shearing resistance,  $\phi$ , of the granular Upper Sand and Lower Sand Strata at the site was estimated from an empirical correlation with SPT N-values (Bowles 1982). Table 3-2 on p. 100 of Bowles (1982) was used. This table provides ranges of  $\phi$ -values as a function of ranges of SPT N-values. A review of Table 3-2 on p. 100 of Bowles (1982) reveals that the ranges of  $\phi$ -values are usually much narrower than the corresponding ranges of SPT N-values, and there is also some overlapping of proposed ranges. Engineering judgment was used in the selection of appropriate  $\phi$ -values, as explained in the next paragraphs.

The average SPT N-value for the Upper Sand Stratum adjusted for hammer efficiency is  $N_{avg} = 25$  bpf, which falls in the range of  $10 \leq N \leq 40$ . The corresponding range of  $\phi$ -values on Table 3-2, p. 100 of Bowles (1982) is  $35^\circ \leq \phi \leq 40^\circ$ . VEGP Unit 1 & 2 FSAR Table 2.5.4-2 recommends  $\phi = 34^\circ$  for the Upper Sand Stratum. We used  $\phi = 34^\circ$ , as shown on SSAR Table 2.5.4-1.

The average SPT N-value for the Lower Sand Stratum adjusted for hammer efficiency is  $N_{avg} = 62$  bpf, which falls in the range of  $20 \leq N \leq 70$ . The corresponding range of  $\phi$ -values on Table 3-2, p. 100 of Bowles (1982) is  $38^\circ \leq \phi \leq 43^\circ$ . VEGP Unit 1 & 2 FSAR Section 2.5.4.2.3 states that SPT N-values for the Lower Sand Stratum ranged from 70 to more than 100 bpf. While  $38^\circ \leq \phi \leq 43^\circ$  would be reasonable to use considering the high SPT N-values, we decided to adopt a more conservative  $\phi = 34^\circ$  for the Lower Sand Stratum. This value is shown on SSAR Table 2.5.4-1 and matches the value for the Compacted Structural Fill contained on VEGP Unit 1 & 2 FSAR Table 2.5.4-8.

**2.5.4-10 Provide relative densities for Blue Bluff Marl.**

Response:

As stated in our response to RAI 2.5.4-14, although the Blue Bluff Marl frequently contains less than 50% of fine material, it has the appearance and characteristics of a calcareous claystone or siltstone and is described as a hard, slightly sandy, cemented, calcareous clay. Its design undrained shear strength is 10 ksf, and its preconsolidation pressure could be as high as 80 ksf, i.e. this is a highly overconsolidated material. Thus, the marl performs as hard clay or soft rock, not as a granular material, and relative density does not apply to these types of materials.

**2.5.4-11 SSAR Section 2.5.4 states that high strain elastic modulus for Upper Sand and Lower Sand Strata were derived based on the Davie and Lewis (1988) relationships. Explain why these relationships are applicable to the ESP soil strata. What is the scientific consensus on Davie and Lewis' relationship between SPT values and elastic modulus, as well as the relationship between undrained shear strength and elastic modulus? How extensively are these relationships used?**

Response:

a) The relationship for sand,  $E = 36N$  ksf, was derived based on elastic modulus  $E$  versus SPT N-value relationships reported in the literature and influenced by a specific case history of measured settlement of a chimney foundation on medium dense to dense quartz sands and gravels described in the paper (Davie

and Lewis 1988). Bechtel's experience has shown that this relationship provides reasonable predictions of settlement when compared to measured settlements for a wide range of foundation sizes on granular materials varying from clean to silty sands and gravels. The Upper Sand Stratum is a medium dense silty sand, and the Lower Sand Stratum is a generally very dense silty sand. Thus, it is anticipated that the relationship can be successfully applied to these sands.

b) *SPT and Elastic Modulus*

Davie and Lewis (1988) provides a summary of various estimates of elastic modulus E for granular soils from SPT N-values in the literature. The table below shows the computed E values based on N = 25 bpf (design value for the Upper Sand Stratum corrected for hammer efficiency), and N = 62 bpf (design value for the Lower Sand Stratum corrected for hammer efficiency).

Reference	Relationship	E, ksf	
		N = 25 bpf	N = 62 bpf
Bowles (1987)	$E = 10(N + 15)$ ksf	400	770
D'Appolonia et al. (1970)	$E = 432 + 21.2N$ ksf	962	1,746
Parry (1971)	$E = 100N$ ksf	2,500	6,200
Schmertman (1970) and Schmertman et al. (1978)	$E = 30N$ to $50N$ ksf	750 to 1,250	1,860 to 3,100
Yoshida and Yoshinaka (1972)	$E = 42N$ ksf	1,050	2,604
<b>Median</b>		<b>1,006</b>	<b>2,232</b>
Davie and Lewis (1988)	$E = 36N$ ksf	900	2,232
Note: The references shown above are cited in Davie and Lewis (1988) and are listed at the end of the response to this RAI.			

As can be seen, the Davie and Lewis (1988) E-value is somewhat lower than the median from the other references for N= 25 bpf and almost identical to the median for N = 62 bpf. Since, as noted in part a) of this response, the  $E = 36N$  ksf relationship has provided reasonable predictions of settlement when compared to measured settlements, and the relationship gives predictions that are close to the median of other E and N relationships, then it is expected that this relationship has reasonable scientific consensus.

*Undrained Shear Strength and Elastic Modulus*

The relationship between a clay's undrained shear strength ( $s_u$ ) and elastic modulus E is widely recognized. As noted in Davie and Lewis (1988), a large range of  $E/s_u$  values have been reported in the literature, from as low as 50 (Skempton 1951-see list of references at the end of the response to this RAI) to as high as 2,500 (D'Appolonia et al. 1971), and thus scientific consensus may be difficult to achieve. To get this wide range of  $E/s_u$  values found in the literature into some context, one can refer to Figure 5 from Duncan and Buchignani (1976-see list of references at the end of the response to this RAI) which shows  $E = Ks_u$  where  $K = E/s_u$  is a function of plasticity index (PI) and overconsolidation ratio (OCR) of the clay. For a normally consolidated clay (OCR = 1), K ranges from about 130 at very high PI to 1,500 at very low PI. For a very heavily overconsolidated clay (OCR = 10), K ranges from about 30 at very high PI to 400 at very low PI. The design PI for the Blue Bluff Marl is 25, and thus the K value will be in the  $PI < 30$  area. Figure 5 of Duncan and Buchignani (1976) shows that  $K = 600$  is comfortably in the range of values in the  $PI < 30$  area. [Bear in mind that the curves on Figure 5 of Duncan and Buchignani (1976) are purely empirical and based on limited data. The figure should be used as a guideline only.]

The  $E/s_u = 600$  used in Davie and Lewis (1988) is in good agreement with values derived by Williams and Focht (1982-see list of references at the end of the response to this RAI) from numerous case histories of mat foundations on Beaumont Clay, the material in the Davie and Lewis paper.

AR-07-0801  
Enclosure 1  
RAI Response

c) These relationships have been used by Bechtel to estimate settlement of major structures for numerous power plant projects both in the US and overseas. These power plants have been founded on a wide range of granular and cohesive materials.

References [All references are cited in Davie and Lewis (1988), except for Duncan and Buchignani (1976)]

Bowles (1987) Bowles, J.E., "Elastic Foundation Settlements on Sand Deposits", *Journal of Geotechnical Engineering*, ASCE, Vol. 113, No. 8, 1987.

D'Appolonia et al. (1970) D'Appolonia, D.J., D'Appolonia, E. and Brissette, R.F., "Settlement of Spread Footings on Sand", Discussion Closure, *Journal of the Soil Mechanics and Foundations Division*, ASCE, Vol. 96, SM2, 1970.

Duncan and Buchignani (1976) Duncan, J.M. and Buchignani, A.L., Engineering Manual for Settlement Studies, CGPR #2, Virginia Tech Center for Geotechnical Practice and Research, Blacksburg, VA, 1987.

Parry (1971) Parry, R.H.G., "A Direct Method of Estimating Settlements in Sands from SPT Values", *Proceedings of the Symposium on Interaction of Structures and Foundations*, Midlands Soil Mechanics and Foundation Engineering Society, Birmingham, England, pp. 29-37, 1971.

Schmertman (1970) Schmertman, J.H., "Static Cone to Compute Static Settlement Over Sand", *Journal of the Soil Mechanics and Foundations Division*, ASCE, Vol. 96, SM3, 1970.

Schmertman et al. (1978) Schmertman, J.H., Hartman, J.P. and Brown, P.R., "Improved Strain Influence Factor Diagrams", *Journal of the Geotechnical Engineering Division*, ASCE, Vol. 104, GT8, 1970.

Skempton, A.W. (1951) Skempton, A.W., "The Bearing Capacity of Clays", *Building Research Congress*, pp. 180-189, 1951.

Williams and Focht (1982) Williams, C.E. and Focht, J.A., "Initial Response of Foundations on Stiff Clay", *ASCE Convention*, New Orleans, LA, 1982.

Yoshida and Yoshinaka (1972) Yoshida, I. and Yoshinaka, R., "A Method to Estimate Modulus of Horizontal Subgrade Reaction for a Pile", *Soils and Foundations*, Japanese Society of Soil Mechanics and Foundation Engineering, Vol. 12, No. 3, 1972.

**2.5.4-12 SSAR Table 2.5.4-1 presents average static engineering properties of the subsurface material. Explain how the value for the unit weights for the different soils were obtained. Based on the discussion in the last paragraph on page 2.5.4-10, the average values are higher than those listed in the table. Also, explain why the plasticity index, liquid limit, and plastic limit values are different from those discussed on page 2.5.4-5 for the Blue Bluff Marl.**

Response:

**Unit Weight** - Unit weight test results for selected soil samples collected during the ESP subsurface investigation are summarized in SSAR Table 2.5.4-4, and are reproduced below. These tests were performed mostly on Lisbon Formation samples, but also on some of the fine-grained samples encountered in the Lower Sand Strata.

Boring Number	Depth (ft)	Formation	$\gamma$ (pcf)	Boring Number	Depth (ft)	Formation	$\gamma$ (pcf)
B-1002	92.0	Lisbon	103.6	B-1004	154.5	Lisbon	117.4
			102.4				119.3
	103.5	Lisbon	114.3		164.5	Lisbon	117.4
			114.5				125.6
	113.5	Lisbon	132.8		177	Lisbon	124.7
			132.9				124.6
	123.5	Lisbon	140.2				188.5
	133.5	Lisbon	118.0		120.4		
			118.1		120.6		
	B-1003	93	Lisbon		115.7	B-1003	198.5
115.8				128.2			
104.7		Lisbon	111.5	<b>Range:</b> <b>Average:</b> <b>Median:</b>	102.4-		
121.7		Lisbon	122.5		140.2		
141.7		Lisbon	126.1		119.7		
B-1004	144.0	Lisbon	105.1	B-1003	165.7	Still	121.7
			105.2		315.7	Congaree	119.4
			114.2		350.7	Snapp	128.3

Additionally, from VEGP Unit 1 & 2 FSAR Table 2.5.4-4 and Sections 2.5.4.10.2 and 3.7.B.1.4, the following moist/saturated unit weight values are recommended for the different layers:

Compacted Structural Fill -  $\gamma_{moist}$  = 123 pcf

$\gamma_{sat}$  = 133 pcf

Upper Sand Stratum –  $\gamma_{moist}$  = 115 pcf

$\gamma_{sat}$  = 115 pcf

Lisbon Formation (Blue Bluff Marl)–  $\gamma_{sat}$  = 115 pcf

Lower Sand Stratum –  $\gamma_{sat}$  = 115 pcf

Considering that the values recommended in the VEGP Unit 1 & 2 FSAR are based on a much larger number of tests, we used the values shown in the VEGP Unit 1 & 2 FSAR. We note that these values will be reassessed during the COL subsurface investigation, where a much larger number of tests will be performed.

**Atterberg Limits** - Natural moisture content ( $\omega_N$ ) and Atterberg limit test results for selected Lisbon Formation samples collected during the ESP subsurface investigation are given in Table 2.5.4-4 and are summarized on the next page. The results indicate average and median values of liquid limit (LL) below 50% which corresponds to low plasticity soils. It's noted that several samples disclosed high plasticity soils. Also, the natural moisture content is mostly near the plastic limit, which corresponds to the hard consistency disclosed by the SPT N-values. Bechtel (1974b) indicates PI-values for the Lisbon Formation ranging from 2 to 70% with an average of 25%. The range of PI-values shown on the table below ( $0 \leq PI \leq 58\%$ ) is similar to that reported in Bechtel (1974b). Considering that the range and average

values reported in Bechtel (1974b) are based on a much larger number of tests, we used  $PI_{avg} = 25\%$ . The values shown on the line of the table below labeled "Use" are the values shown on SSAR Table 2.5.4-1. We note that these values will be reassessed during the COL subsurface investigation, where a much larger number of tests will be performed.

Boring Number	Depth (ft)	Formation	$\omega_N$ (%)	PL (%)	LL (%)	PI (%)	
B-1002	92.0	Lisbon	52.1	37	72	35	
	103.5	Lisbon	56.5	22	34	12	
	113.5	Lisbon	25.5	19	29	10	
	123.5	Lisbon	13.5	17	22	5	
	133.5	Lisbon	28.6	25	32	7	
	153.5	Lisbon	23.3	21	34	13	
B-1003	88	Lisbon	67.4	42	93	51	
	93	Lisbon	30.6	32	54	22	
	104.7	Lisbon	40.6	51	83	32	
	121.7	Lisbon	28.0	NP	NP	NP	
	141.7	Lisbon	25.9	28	46	18	
B-1004	144.0	Lisbon	44.6	38	59	21	
	153.5	Lisbon	30.1	27	43	16	
	163.5	Lisbon	25.1	22	31	9	
	177.0	Lisbon	20.8	22	31	9	
	188.5	Lisbon	29.0	27	34	7	
	198.5	Lisbon	26.2	21	31	10	
B-1006	123.5	Lisbon	53.7	43	99	56	
B-1010	98.5	Lisbon	49.9	36	94	58	
			<b>Range:</b>	<b>13.5-67.4</b>	NP-51	NP-99	NP-58
			<b>Average:</b>	<b>35.3</b>	29	51	22
			<b>Median:</b>	<b>29.0</b>	27	43	16
			<b>Use:</b>	<b>N/A</b>	25	51	26
NOTE: Bechtel (1974b) reports $2 \leq PI \leq 70$ for the Lisbon Formation with average value of 25%.							

**2.5.4-13 SSAR Section 2.5.4.7 states that: "The EPRI curves were extended beyond the 1 percent strain values reported in EPRI (Technical Report (TR)-102293 1993) to 3.3 percent using values provided by Silva (2006)." Provide Silva's values, justification for use of these values, and a detailed description on how the shear modulus and damping curves were extended.**

Response:

Even though the EPRI curves were extended beyond the 1 percent strain values reported in EPRI (1993), the maximum strains calculated during the site amplification analyses remained below 1 percent. The same applies to the SRS curves. SSAR Sections 2.5.2.5.1.5, 2.5.4.7.2.1 and 2.5.4.7.2.2 will be revised in the next revision of the ESP application along with SSAR Tables 2.5.4-12 and 2.5.4-13, and SSAR Figures 2.5.4-9 through 2.5.4-12 to show the degradation curves (EPRI and SRS) stopping at 1% cyclic shear strain.

**2.5.4-14 Since the Blue Bluff Marl has a relatively high variable fines content (24-77 percent) and saturation level (14-67 percent) and since there is also a potentially high ground motion level at the site, justify why liquefaction analyses were not performed.**

Response:

The response is divided into two parts. The first examines whether the Blue Bluff Marl (Lisbon Formation) can be considered potentially liquefiable based on material type and age. The second part assumes that the material is potentially liquefiable based on type and age, and looks at field strength and shear wave velocity results to determine if the marl could liquefy based on these results.

Material Type and Age

*Type:* Soil liquefaction is a process by which loose or medium dense, granular, saturated deposits lose a significant portion of their shear strength due to porewater pressure buildup resulting from cyclic loading, such as that caused by an earthquake. Although the Blue Bluff Marl frequently contains less than 50% of fine material, it has the appearance and characteristics of a calcareous claystone or siltstone and is described as a hard, slightly sandy, cemented, calcareous clay. Its design undrained shear strength is 10 ksf, and its preconsolidation pressure could be as high as 80 ksf, i.e. this is a highly overconsolidated material. Thus, the marl is not loose or medium dense, it performs as hard clay or soft rock, not as a granular material, and although it is saturated since it is below the ground water, its structure is so compressed that it does not have the free water characteristic of a saturated granular material. In short, the Blue Bluff Marl is not a material with liquefaction potential, regardless of the ground motion level.

*Age:* Youd et al. (2001-see list of references at the end of the response to this RAI), “Youd and Hoose (1977-see list of references at the end of the response to this RAI) and Youd and Perkins (1978-see list of references at the end of the response to this RAI) noted that liquefaction resistance increases markedly with geologic age. Sediments deposited within the past few thousand years are generally much more susceptible to liquefaction than older Holocene sediments; Pleistocene sediments are even more resistant; and pre-Pleistocene sediments are generally immune to liquefaction.” Pre-Pleistocene sediments are sediments older than about 2 million years. The Blue Bluff Marl is estimated to be late middle Eocene age, i.e., about 40 to 41 million years old. From the foregoing, even if the marl were potentially liquefiable based on its material characteristics, it should be immune from liquefaction based on its age.

Field Test Results

Youd et al. (2001) describe computation of safety factor against liquefaction based on standard penetration test (SPT) N-values, cone penetrometer test (CPT) tip resistance, and shear wave velocity. For the N-values, tip resistances and shear wave velocities, there are values above which the material is considered non liquefiable, i.e., the computed factor of safety against liquefaction is theoretically infinite, regardless of ground motion level.

*N-Values:* Youd et al. (2001) indicates that, for a sand with 35% or more fines, soils with a corrected N-value of over about 21 are not liquefiable. To correct the N-value, the value measured in the field is corrected for several factors – the two principal correction factors are the overburden stress and the energy efficiency of the SPT hammer. Based on the overburden pressure at the mid-depth of the marl, and the average energy efficiencies of the hammers used for the borings, the corrected N-value will be 40 to 45% of the measured N-value. Thus, the corrected N-value of 21 translates to an uncorrected N-value of about 50. Of the 58 N-values measured in the marl for the ESP investigation, 5 were below 50, ranging from 27 to 46 (SSAR Table 2.5.4-5). Thus, if the marl were a potentially liquefiable material, a liquefaction analysis would be run for these 5 samples. (An initial analysis of these 5 samples show FS values in excess of the accepted 1.35 value in all cases.)

*CPT Values:* All of the CPTs that were able to penetrate to the marl met refusal at or near the top of the stratum. Thus, measured tip resistances showed the material to be non liquefiable.

*Shear Wave Velocities:* The typical shear wave velocities in the marl ranged from 1,400 to 2,650 ft/sec (SSAR Table 2.5.4-6). When corrected for overburden, these values range from about 990 to 1,680 ft/sec. Youd et al. (2001) indicates that, for a sand with 35% or more fines, soils with a corrected shear wave velocity in excess of about 625 ft/sec are non liquefiable.

### Conclusions

Based on material type and age, the Blue Bluff Marl does not have the potential to liquefy. If this conclusion is neglected and the SPT, CPT and shear wave velocity measurements in the marl are analyzed to determine factor of safety against liquefaction, the data show that the CPT and shear wave velocities consistently indicate non-liquefiable materials; the SPT data show that over 90% of the N-values indicate non liquefiable materials, and the remaining N-values show satisfactory factors of safety.

### References

(Youd et al 2001). Youd, T.L., et al., "Liquefaction Resistance of Soils: Summary Report from the 1996 NCEER and 1998 NCEER/NSF Workshops on Evaluation of Liquefaction Resistance of Soils," *Journal of Geotechnical and Environmental Engineering, ASCE*, Vol. 127, No. 10, 2001.

(Youd and Hoose 1977). Youd, T.L. and Hoose, S.N., "Liquefaction Susceptibility and Geologic Setting," *Proceedings, 6<sup>th</sup> World Conference on Earthquake Engineering*, Vol. 3, pp 2189-2193, 1977.

(Youd and Perkins 1978). Youd, T.L and Perkins, D.M., "Mapping of Liquefaction-Induced Ground Failure Potential," *Journal of Geotechnical Engineering, ASCE*, Vol. 104, GT 4, 1978.

**2.5.4-15 SSAR Section 2.5.4.10.2 states that: "For the large mat foundations that support the major power plant structures, general considerations based on geotechnical experience indicate that total settlement should be limited to 2 in., while differential settlement should be limited to ¾ in. (Peck et al. 1974). For footings that support smaller plant components, the total settlement should be limited to 1 in., while the differential settlement should be limited to ½ in. (Peck et al. 1974)."**

- a) Provide justification for adopting the Peck et al. (1974) settlement and differential settlement values as guidelines.
- b) What are the main causes for exceeding these settlement values at the foundation levels for Units 1 and 2? What kind of measures will be taken to prevent settlements and differential settlements for the new units?
- c) Justify the use of an average bearing pressure of 5 ksf for the settlement analyses of compacted fills.

Response:

a) The Peck et al. (1974) total settlement guidelines of 1 inch for column footings and 2 inches for mats are widely accepted and used by the geotechnical community. It is known that when foundation settlements are limited to these values, then differential settlements are minimized, and good structural performance follows. On the other hand, if these limiting settlement values are exceeded, it does not necessarily have adverse effects on structures. This is particularly true for large mat foundations, which

can efficiently distribute structural loads to the soil. A good example is the large mats for Units 1 and 2 where the calculated settlements of the containment buildings ranged from 4 to 4.3 inches.

b) The settlement guidelines based on Peck et al. (1974) were not used for Units 3 and 4. The approach used for Units 3 and 4 consisted of estimating settlements for power-block structures, and using them as design values. A detailed settlement monitoring program was established, and monitored settlements were compared to the design values. The "VEGP Report on Settlement" prepared by Bechtel in 1986 provides comparisons of measured versus calculated settlements, and concludes that the calculated or design values were not exceeded. Reanalysis and/or corrective measures would be employed in the event that monitored settlements exceeded the design values. This same approach will be followed for Units 3 and 4, and Sections 2.5.4.10.2 and 2.5.4.11 will be revised accordingly in the next revision to the ESP application.

c) The value of 5 ksf was used for illustrative purposes as no design value was available during the ESP. The calculation will be revised using design values during the COL.

**2.5.4-16 SSAR Section 2.5.4.10 provides two general scenarios for bearing capacity and settlement analyses. However, in order to meet the requirements of 10 CFR Parts 50 and 100, the stability of all planned safety-related facilities should be analyzed including bearing capacity, rebound, settlement, and differential settlements under deadloads of fills and plant facilities, as well as lateral loading conditions. Please provide justification for not addressing the above information for each planned safety-related structure.**

Response:

This information will be provided as part of the COL application, when more details regarding the bearing capacity, rebound, settlement, and differential settlements etc., are available. This level of detail is not available during the ESP application process.

**2.5.4-17 SSAR Section 2.5.4.7 states that EPRI Procedure TR-102293 was used to develop the shear modulus and damping curves based on the site shear wave velocities and plasticity index values. Please provide a complete description, including sample calculations, to show how the shear modulus and damping curves were developed and how uncertainties in the site parameters were incorporated into their development.**

Response:

The shear wave velocity is used to calculate the low strain dynamic shear modulus ( $G_{max}$ ) only, according to Equation (9) shown in our response to RAI No. 2.5.4-7. The shear modulus reduction curves show the reduction in  $G_{max}$  as the shear strain increases during a seismic event, i.e., the EPRI (1993) curves simply show the ratio  $G/G_{max}$  versus shear strain, regardless of the initial value of  $G_{max}$ .

The shear modulus reduction and damping ratio curves for cohesionless materials were based on confining pressure at depth, or simply depth. The shear modulus reduction and damping ratio curve for the Lisbon Formation was based on the plasticity index (PI).

The next paragraphs contain a summary of how the shear modulus reduction and damping ratio curves shown on SSAR Figures 2.5.4-9 and 2.5.4-11 were derived from the EPRI (1993) curves.

It is noted that shear modulus reduction and damping ratio curves will be obtained using undisturbed samples collected during the COL subsurface investigation.

### Compacted Fill

The compacted backfill extends from the ground surface to a depth of 86 ft. The three EPRI (1993) curves for shear modulus reduction at shallow depths (0-20ft, 20-50ft, and 50-120ft) presented on Figure 7.A-18 of EPRI (1993) were used.

The three EPRI (1993) curves for damping ratio at shallow depths (0-20ft, 20-50ft, and 50-120ft) presented on Figure 7.A-19 of EPRI (1993) were used.

### Lisbon Formation (Blue Bluff Marl)

The shear modulus reduction values were obtained by using  $PI = 25\%$  and interpolating between the curves shown on Figure 7.A-16 of EPRI (1993) for  $PI = 10$  and  $PI = 30$ .

The damping ratio values were obtained by using  $PI = 25\%$  and interpolating between the curves shown on Figure 7.A-17 of EPRI (1993) for  $PI = 10$  and  $PI = 30$ .

### Lower Sand (Still Branch Formation)

The Still Branch Formation extends from a depth of 146 ft to a depth of 213 ft. The curve for depths of 120 ft to 250 ft shown on Figure 7.A-18 of EPRI (1993) was used to obtain the modulus reduction values.

The curve for 120 ft to 250ft shown on Figure 7.A-19 of EPRI (1993) was used to obtain the damping ratio values.

### Lower Sand (Congaree Formation)

The Congaree Formation extends from a depth of 213 ft to a depth of 328 ft. The curve for depths of 250 ft to 500 ft shown on Figure 7.A-18 of EPRI (1993) was used to obtain the modulus reduction values.

The curve for 250 ft to 500 ft shown on Figure 7.A-19 of EPRI (1993) was used to obtain the damping ratio values.

### Lower Sand (Snapp Formation)

The Snapp Formation extends from a depth of 328 ft to a depth of 435 ft. The curve for depths of 250 ft to 500 ft shown on Figure 7.A-18 of EPRI (1993) was used to obtain the modulus reduction values.

The curve for 250 ft to 500 ft shown on Figure 7.A-19 of EPRI (1993) was used to obtain the damping ratio values.

### Lower Sand (Black Mingo Formation)

The Black Mingo Formation extends from a depth of 435 ft to a depth of 474 ft. The curve for depths of 250 ft to 500 ft shown on Figure 7.A-18 of EPRI (1993) was again used to obtain the modulus reduction values.

The curve for 250 ft to 500 ft shown on Figure 7.A-19 of EPRI (1993) was used to obtain the damping ratio values.

### Deep Sands

The 500-1,000 ft curve shown on Figure 7.A-18 of EPRI (1993) was used to obtain the modulus reduction values for soils below 500 ft depth, since the soil extends to just below 1,000 ft depth.

The curve for 500 ft to 1000 ft shown on Figure 7.A-19 of EPRI (1993) was used to obtain the damping ratio values for the deep sands below 500 ft.

### Rock

All rock is assumed to behave elastically and therefore will not degrade with strain. In other words,  $G/G_{\max} = 1$  for all shear strain levels in rock.

For randomization purposes, the shear modulus reduction curves were extended beyond the 1 percent strain values reported in EPRI (1993) to 3.3 percent using values provided by Silva (2006). See our response to RAI 2.5.4-13 for a discussion of Silva (2006).

Based on inspection of SSAR Figure 2.5.4-11, the low strain damping ratio of soils is on the order of 0.5 percent, which generally increases to 0.6 percent to 2 percent for strain compatible conditions. Rock, which would be expected to have lower damping than soil, was assumed to behave as a linearly elastic material with 1 percent damping.

Uncertainties in the site parameters were incorporated during the randomization process. Each layer in the profile is associated with the appropriate base case shear modulus reduction curve and damping ratio curve shown on SSAR Figures 2.5.4-9 through 2.5.4-12. The shear modulus reduction and damping ratios were randomized at one strain level using log-normal distributions with median values given by the values in the corresponding base-case curves and logarithmic standard deviations taken from the statistical summaries obtained by Costantino (1997) for natural soils. For the engineered backfill, these standard deviations were reduced by 1/3 to account for a more homogeneous soil mass. The shear modulus reduction and damping ratios at other strains are generated from the randomized values obtained above, using a hyperbolic parametric form. This approach produces realistic curves with logarithmic standard deviations that approximate the Costantino (1997) values over a wide range of strains. The normal random variables associated with the log-normal shear modulus reduction and damping ratios are taken as having a correlation coefficient of -0.75.

**2.5.4-18 SSAR Section 2.5.4.10.1 provides a brief description of the allowable bearing capacity value, which is based on Terzaghi's bearing capacity equations modified by Vesic (1975). Please provide a more detailed description of how the allowable bearing capacity value was obtained that includes the actual calculations.**

Response:

Following is an explanation of the bearing capacity calculation, a description of the subsurface section used in the bearing capacity calculations, and a typical bearing capacity calculation.

Methodology - The net bearing capacity of shallow foundations, i.e., the bearing capacity beyond the existing overburden pressure, will be calculated according to the following equation (Equation 3.11, p. 128 of Vesic 1975):

$$q_0 = c \cdot N_c \cdot \zeta_c + q \cdot (N_q - 1) \cdot \zeta_q + 0.5 \cdot \gamma \cdot B \cdot N_\gamma \cdot \zeta_\gamma \quad (1)$$

where:  $q_0$  = net ultimate bearing pressure (ksf)

$c$  = soil cohesion (ksf)

AR-07-0801  
Enclosure 1  
RAI Response

- $q$  = effective overburden pressure at bottom of foundation level (ksf)  
 $\gamma$  = unit weight of soil (kcf) – per Equation 2  
 $B$  = foundation width (ft)  
 $L$  = foundation length (ft) – not included in Equation (1).  
 $N_q, N_q, N_q$  = bearing capacity factor from Table 3.1, p. 127 of Vesic (1975)  
 $\zeta_c, \zeta_q, \zeta_\gamma$  = foundation shape factors from Table 3.2, p. 129 of Vesic (1975)

The unit weight of soil to be used in Equation 1 is given by

$$\gamma = \gamma_{sub} + (z_w/B) \cdot (\gamma_m - \gamma_{sub}) \quad (\text{Equation 3.35, p. 138 of Vesic 1975}) \quad (2)$$

- where:  $\gamma_m$  = moist unit weight of soil above the water table (kcf)  
 $\gamma_{sub}$  = submerged unit weight of soil below the water table (kcf)  
 $z_w$  = vertical distance from bottom of foundation to the ground water table (ft)

NOTE: Use  $z_w = 0$  in Equation (2), if the ground water table is above the bottom of foundation.  
If  $z_w > B$ , then use  $z_w = B$  in Equation (2).

The allowable bearing capacity ( $q_a$ ), not considering settlement, is given by

$$q_a = q_o / FS \quad (3)$$

where: FS = factor of safety against bearing failure (FS=3 for static loading, and FS=2 for dynamic loading)

It is noted that Equation (1) applies to a homogeneous profile where the soil thickness is much larger than the width of the foundation. If the foundation is placed on a “strong” layer (compacted granular structural fill) that is underlain by a “weaker” layer (Lisbon Formation or Blue Bluff Marl that acts as a cohesive material), such as is the case for all structures to be analyzed here, the lower “weaker” layer can affect the bearing capacity.

Vesic (1975) gives the following equation (Equation 3.41, p. 142 of Vesic 1975) for the case where the upper layer is cohesionless with  $25^\circ \leq \phi \leq 50^\circ$ , which applies to the compacted structural fill:

$$q_o = q_o'' \cdot \exp\{0.67 \cdot [1 + (B/L)] \cdot (H/B)\} \quad (4)$$

where:

- $q_o''$  = ultimate bearing pressure per Equation (1) of foundation sitting on the surface of the Lisbon Formation (ksf)  
 $H$  = thickness of compacted structural fill between the bottom of the foundation and the top of the Lisbon Formation (ft)

The assumption is still made that  $q_o''$  is calculated for a Lisbon Formation layer that has thickness much larger than the width of the foundation. This assumption will result in conservative  $q_o''$  bearing capacity

values in the case of the foundations for the containment structures, where the thickness of the Lisbon Formation is 63 ft, and the Lower Sand Stratum below is as strong as or stronger than the Lisbon Formation.

It is noted that the bearing capacity value,  $q_o$ , obtained from Equation (4) cannot exceed the value obtained from Equation (1).

Subsurface Section Used in the Bearing Capacity Calculations – The subsurface section and engineering properties used in the bearing capacity calculations is summarized in the table below.

Layer	Shear Strength		Unit Weight (kcf)	
	c (ksf)	$\phi$ (degrees)	Moist ( $\gamma_m$ )	Saturated ( $\gamma_{sat}$ )
Compacted Structural Backfill (0 to 83 ft)	0	34	0.120	0.130
Lisbon Formation (83 to 146 ft)	10	0	N/A	0.115
Lower Sand Stratum (Below 146 ft)	0	34	N/A	0.115

NOTE: The ground water table was taken at a depth of 55 ft below finish grade, i.e., at about El. 165 ft.

Typical Bearing Capacity Calculation – We will look at the bearing capacity of square foundations placed at a depth  $D_f = 4$  ft below finish grade. Consider square foundations with width:  $B = 5$  ft and  $B = 80$  ft. If the Lisbon Formation summarized on the profile in the above table is ignored, and the foundations are placed at a depth  $D_f = 4$  ft below grade on the compacted structural fill with  $c = 0.0$  ksf and  $\phi = 34^\circ$ , then:

$$N_c = 42.16 \qquad N_q = 29.44 \qquad N_\gamma = 41.06$$

$$\zeta_q = 1 + (29.44/42.16) = 1.70 \qquad \zeta_q = 1 + \tan 34^\circ = 1.67 \qquad \zeta_\gamma = 0.60$$

$$q = 4 \cdot 0.130 = 0.52 \text{ ksf}$$

Values of  $\gamma$  according to Equation (2) are as follows:

B (ft)	$D_f$ (ft)	$z_w$ (ft)	$\gamma$ (kcf)
5	4	$z_w = 55 - 4 = 51$ $z_w > B$ Use $z_w = B = 5$	$\gamma = (0.130 - 0.0624) + (5/5) \cdot (0.120 - (0.130 - 0.0624)) = 0.120 \text{ kcf}$
80	4	$z_w = 55 - 4 = 51$ $z_w < B$ Use $z_w = 51$	$\gamma = (0.130 - 0.0624) + (51/80) \cdot (0.120 - (0.130 - 0.0624)) = 0.101 \text{ kcf}$

The ultimate bearing pressure calculated according to Equation 1, ignoring the Lisbon Formation, is

$$q_o' = 0.0 \cdot 42.16 \cdot 1.70 + 0.52 \cdot (29.44 - 1) \cdot 1.67 + 0.5 \cdot 0.130 \cdot 5 \cdot 41.06 \cdot 0.60 \cong 0 + 24.7 + 8.0 = 32.7 \text{ ksf, for } B = 5 \text{ ft}$$

$$q_o' = 0.0 \cdot 42.16 \cdot 1.70 + 0.52 \cdot (29.44 - 1) \cdot 1.67 + 0.5 \cdot 0.101 \cdot 80 \cdot 41.06 \cdot 0.60 \cong 0 + 24.7 + 99.5 = 124.2 \text{ ksf, for } B = 80 \text{ ft}$$

The effect of the Lisbon Formation on this calculated allowable bearing pressure will be considered next.

For square foundations of width  $B = 5$  ft or  $B = 80$  ft placed at the top of the Lisbon Formation with  $c = 10$  ksf and  $\phi = 0^\circ$ :

$$\begin{aligned} N_c &= 5.14 & N_q &= 1.0 & N_\gamma &= 0.0 \\ \zeta_c &= 1+(1.0/5.14) = 1.19 & \zeta_q &= 1+\tan 0^\circ = 1.0 & \zeta_\gamma &= 0.60 \\ q &= 55 \cdot 0.120 + (83-55) \cdot (0.130-0.0624) = 8.49 \text{ ksf} \end{aligned}$$

The ultimate bearing pressure of the foundation resting on top of the Lisbon Formation calculated according to Equation 1 is:

$$q_o'' = 10 \cdot 5.14 \cdot 1.19 + 8.49 \cdot (1.0-1) \cdot 1 = 61.1 + 0 = 61.1 \text{ ksf}$$

and the ultimate bearing pressure calculated according to Equation 4 for the foundation resting at a depth  $D_f = 4$  ft, i.e., at a vertical distance  $H=83-4=79$  ft above the top of the Lisbon Formation is

$$q_o = 61.1 \cdot \exp\{0.67 \cdot [1+(5/5)] \cdot (79/5)\} > 32.7 \text{ ksf, use } 32.7 \text{ ksf for } B = 5 \text{ ft}$$

$$q_o = 61.1 \cdot \exp\{0.67 \cdot [1+(80/80)] \cdot (79/80)\} > 124.2 \text{ ksf, use } 124.2 \text{ ksf for } B = 80 \text{ ft}$$

The results above indicate that the bearing capacity is not affected by the presence of the Lisbon Formation for square foundations with  $B \leq 80$  ft. The static allowable bearing pressures can be taken as

$$(q_a)_{\text{static}} = 32.7/3 = 10.9 \text{ ksf for } B = 5 \text{ ft}$$

$$(q_a)_{\text{static}} = 124.2/3 = 41.4 \text{ ksf for } B = 80 \text{ ft}$$

These allowable bearing pressures do not take into consideration foundation settlements.

**2.5.4-19 SSAR Section 2.5.4.11 does not provide the complete design criteria or actual design methods that will be employed in the geotechnical review. Please provide justification for not providing the above information.**

**SSAR Section 2.5.4.11 provides two factors of safety for slope stability with references to Section 2.5.5.2. Neither of these factors of safety is listed in Section 2.5.5. Please explain their omission.**

Response:

This information will be provided as part of the COL application, when the complete design criteria and actual design methods are available. This level of detail is not available during the ESP application process.

Section 2.5.5 will be revised in the next revision of the ESP application to include the factors of safety for slope stability.

AR-07-0801  
Enclosure 1  
RAI Response

**2.5.4-20 SSAR Section 2.5.4 does not provide the relationship of foundations to the underlying materials in the form of plot plans and profiles. In addition, foundation stability with respect to groundwater conditions is not described, and detailed dewatering plans are also missing. Please provide justification for not providing the above information.**

Response:

This information will be provided as part of the COL application when more details regarding the foundations' interaction with the site including detailed dewatering plans are available. This level of detail is not available during the ESP application process.

**Southern Nuclear Operating Company**

**AR-07-0801**

**Enclosure 2**

**Geologic Data Files**

**on**

**Compact Disc (CD)**

**NOTE:** The following files are contained on Enclosure 2 CD:

1. 252-16\_mmax.xls (Provided electronically as requested in RAI 2.5.2-16)
2. 252-16\_geom.txt (Provided electronically as requested in RAI 2.5.2-16)
3. 252-16\_mmax.pdf (Copy of number "1" above formatted for ADAMS)
4. 252-16\_geom.pdf (Copy of number "2" above formatted for ADAMS)